PROCEEDING OF OCEAN, MECHANICAL AND AEROSPACE

SCIENCE AND ENGINEERING

VOLUME.1

NOVEMBER 19, 2014

ISSN: 2443-1710

PUBLISHED BY ISOMAse

PROCEEDING

The 1st International Conference on Ocean, Mechanical & Aerospace - Scientists & Engineers -

OMASE 2014

19th – 20nd November 2014
Resty Menara Hotel,
Pekanbaru, Indonesia

Organized by:

Universiti Teknologi Malaysia, Malaysia

Universitas Riau, Indonesia

International Society of Ocean, Mechanical, Aerospace
- scientists & engineers -

The 1st Conference on Ocean, Mechanical and Aerospace
-Science and Engineering-
Vol.1: 19-November 2014

Contents

ISOMAse

International Society of Ocean, Mechanical and Aerospace
-Scientists and Engineers-

Section II: Computational Fluid Dynamic

About OMAse

The first Conference on Ocean, Mechanical and Aerospace for Scientists and Engineers is the conference organizes by International Society of Ocean, Mechanical and Aerospace – Scientists and Engineers – (ISOMAse).

The target for this conference is gathered the researchers involved in an area of ocean, mechanical and aerospace to share their findings and discuss the researches issue. We believe interchangeable of idea between researchers from ocean, mechanical and aerospace is important because all of the disciplines are sharing related sciences and engineering theories in their respect area. Therefore, we believe this conference will able to refresh the research experience of the people in these areas and generate impact for the cross discipline research collaboration and knowledge exchange.

Scope of OMAse

The OMAse welcomes participants from academicians, scholars, and practitioners for possible publication from all over the world that meets the general criteria of significance and educational excellence. The scope of the conference is as follows:

- Environment and Safety
- Renewable Energy
- Naval Architecture and Offshore Engineering
- Computational and Experimental Mechanics
- Hydrodynamic and Aerodynamics
- Noise and Vibration
- Aeronautics and Satellite
- Engineering Materials and Corrosion
- Fluids Mechanics Engineering
- Stress and Structural Modeling
- Manufacturing and Industrial Engineering
- Robotics and Control
- Heat Transfer and Thermal
- Power Plant Engineering
- Risk and Reliability
- Case studies and Critical reviews

The International Society of Ocean, Mechanical and Aerospace –science and engineering is inviting you to submit your manuscript(s) to isomase.org@gmail.com for the conference proceeding.

CFD Simulation for Stratified Oil-Water Two-Phase Flow in a Horizontal Pipe

Adib Zulhilmi Mohd Alias,[a] , Jaswar Koto,[a,b,*] and Yasser Mohamed Ahmed,[a]

[a)]*Department of Aeronautics, Automotive and Ocean Engineering, Universiti Teknologi Malaysia, Malaysia*
[b)]*Ocean and Aerospace Research Institute, Indonesia*

*Corresponding author: jaswar,koto@gmail.com

Paper History

Received: 10-October-2014
Accepted: 18-November-2014

ABSTRACT

Oil-water two-phase flow in 0.0254m horizontal pipe is simulated using FLUENT 6.2. The stratified flow regime is modeled using Volume of Fluid (VOF) with turbulent model RNG k-ε. Grid independent study has been conducted to decide mesh size for solution accuracy and optimum computational cost. The simulation is performed in time-dependent simulation where oil and water are initially separated by patching the region base on difference in density. Observation on the effect of velocity to the pressure gradient was also simulated. Flow velocity at 0.2, 0.5, 0.8 and 1.1 m/s with same volume fraction for each phase with appropriate multiphase model and turbulence model are presented.

Keywords: *Stratified oil-water flow; Turbulence flow; CFD*

1.0 INTRODUCTION

Immiscible liquid-liquid flow is a common occurrence encountered in a variety of industrial processes. In oil and gas industry, oil transportation either from reservoir to processing facilities or to onshore refinery are usually transported in multiphase flow condition since water and oil are normally produced together. Fractions of water are usually influenced by its existence within the stratum and also through oil recovery method which used water to enhance the remaining oil in the reservoir.

The presence of water, during the transportation of oil has a significant effect because the flow is no longer can be treated as a single-phase flow. Oil-water has complex interfacial structure which complicates the hydrodynamic prediction of the fluid flow. Changes in water fraction may influence the power required to pump the fluid due to corresponding changes in pipeline pressure drop. Either water-in-oil or oil-in-water dispersions, both can influence the pressure gradient dramatically.

Computational fluid dynamics (CFD) techniques have been used to simulate the stratified pipe flow. One of the early CFD models of turbulent stratified flow in a horizontal pipe was presented by Shoham and Taitel [1] where a 2D simulation for liquid-gas flow was simulated by adopting zero-equation models for the liquid region flow field while the gas region was treated as a bulk flow. Issa [2] numerically simulated the stratified gas-liquid pipe flow, using standard k-ε turbulence model with wall functions for each phase. Newton and Behnia [3] obtained more satisfactory solutions for stratified pipe flow by employing a low Reynolds number turbulent model instead of wall functions.

Hui et al [4] simulated stratified oil-water two-phase turbulent flow in a horizontal tube by applying RNG k-ε model combined with a near-wall low-Re turbulence model to each phase and they adopt continuum surface force approximation for the calculation of surface tension. Their simulation results was compared with Elseth et al [5] who simulated the turbulent stratified flow, however their numerical results are not acceptable when compared with their measured data.

Stratified oil-water two-phase pipe flow was investigated using different type of multiphase model. Awal et al [6] achieved CFD simulation tool to investigate inline oil and water separation characteristics under downhole conditions. They chose the Eulerian-Eulerian model, which is computationally most comprehensive but more suitable for multiphase systems with the dispersed phase exceeding 10% v/v/. Carlos F. [7] developed a 2D model for fully-developed, turbulent-turbulent oil-water stratified flow using finite-volume method in a bipolar

coordinate system and applying a simple mixing-length turbulence model. Hui et al [4] and Al-Yaari et al [8] simulated stratified oil-water two-phase turbulent flow in a horizontal tube numerically using a volume of fluid (VOF) model. They applied RNG k-ε model with enhanced wall function combined with optimum meshes through grid independent study to obtain clearly separated oil layer and optimum computational cost.

In the present paper multiphase model of Volume of Fluid (VOFis used to model the stratified oil-water flow. Optimum number of elements for simulation accuracy has been conducted through grid independent study. Observation on the effect of velocity to the pressure gradient was also simulated at flow velocity 0.2, 0.5, 0.8 and 1.1 m/s with same volume fraction for each phase.

2.0 NUMERICAL SIMULATION

2.1 Geometry and mesh

The domain and the meshes were created using ANSYS Design Modeler. A sketch of the geometry of the calculation domain is shown in Figure 1. The geometry consists of semicircular inlet for oil and water with 1 meter length of the flow domain. The inlet for both phases is at the same inlet face where oil on top and water at the bottom region. This will initially made the flow in stratified condition. In addition, as both inlets also flew with a same velocity with direction almost parallel to each phase makes fewer disturbances to maintain stratified flow. The diameter of the pipe for the present work is 0.0254 m. In order to keep the volume of oil and water are flowing continuously throughout the domain until the outlet, patch file and adapt region is used to declare the top and bottom regions for oil and water. This will avoid insufficient volume of either phase.

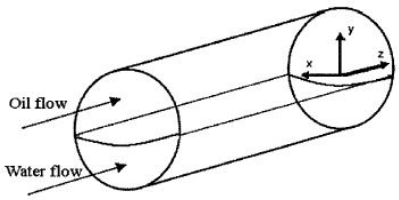

Figure 1: Schematic representation of pipe flow

A block-structured meshing approach was used to create meshes with only tri/tet cells. To obtain fine meshing scheme, sizing was setup with curvature normal angle ll degree, 0.0001 minimum size and 3.0 m maximum size. While to improve the flow near the wall region, two layer inflation with growth rate 1.2 is adapted

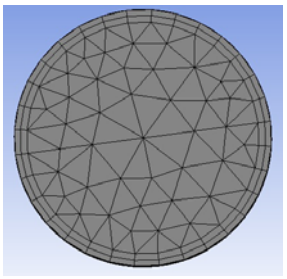

Figure 2: Tri/Tet meshes

2.2 Boundary conditions

There are three faces bounding the calculation domain: the inlet boundary, the wall boundary and the outlet boundary. Flat velocity profile for oil and water were introduced at the inlet of their sections. The outlet boundary condition at the end was set up as a pressure outlet boundary. No slip was used to model liquid velocity at the wall. The main fluid phases' physical properties are reported in Table 1.

Table 1: Fluid phases physical properties

Property	Water Phase	Oil Phase
Density (ρ), kg/m^3	998.2	780
Dynamic Viscosity (μ), Pa.s	0.001003	0.00157
Interfacial Tension, N/m	0.17 m @ 20^{0}C	

2.3 Solution strategy and convergence

Pressure-based solver is chose since it was applicable for wide range of flow regimes from low speed incompressible flow to high speed compressible flow. This solver also requires less memory (storage) and allows flexibility in the solution procedure. Green-gauss Node-Based is elected for higher order discretization scheme since it is more accurate for tri/tet meshes. For pressure, PRESTO! discretization scheme was used for pressure, second order upwind discretization scheme was used for the momentum equation, volume fraction, turbulent, kinetic and turbulent dissipation energy. Second-order upwind is chose rather than First-order upwind because it uses larger stencils for 2nd order accuracy and essential with tri/tet mesh even though the solution to converge may be slower but manageable. In addition, the simulation is time dependent (transient) with 1000 time steps, 0.01 time step size and 200 iterations at each time step size.

3.0 RESULTS

In this section one presents, use of Volume of Fluid multiphase model along with RNG k-ε for turbulent model, grid independent test and sample of pressure drop prediction using this simulation

.

3.1 Grid independent study

A grid independent study is conducted to obtain sufficient mesh density as it was necessary to resolve accurate flow. A grid independent solution exists when the solution does not change when the mesh is refined. The computational grid of 46631,

79488, 104584 and 142374 elements were tested for the mesh independent study to find out the optimum size of the mesh to be used for simulation. Figure 3 shows an oil volume fraction contours at plane z = 0.5 m which indicates the accuracy of the mesh to display the flow pattern. As shown in figure, system increased number of elements shows better prediction for stratified flow pattern with smoothness of the clearly oil and mixed layer. 46631 showing bad prediction on the oil and mixed layer since insufficient amount of elements could not give detail prediction especially on the mixed layer. Both meshes for 104584 and 142374 gave almost similar contours of oil fraction with slight differences in the smoothness of the clearly oil and mixed layer. Therefore, based on the oil volume fraction contours results, 142374 cells are the most optimum number of cells required to predict the oil-water stratified flow in the tested domain and such mesh is going to be used for simulation.

In addition, such decision has been tested by comparing the pressure profiles obtain for every meshes tested (Chart 1). At mesh size 46631, 68204 and 79488, the pressure plot is away from the other plots. The pressure profile starts to unchanged with mesh 92440 until 171393. Before deciding the best meshes size, simulation cost also is required to look at. Since increase num of meshes will increase the amount of time for simulation, the meshes size of 142374 is the most optimum number of elements could be chose.

3.2 Pressure prediction at different flow velocity

By using the simulated oil-water stratified flow, pressure prediction at different flow velocity have been conducted. Flow velocity of 0.2, 0.5, 0.8 and 1.1 m/s with (0.5 input water volume fraction) as a sample flow pattern has been simulated. Volume of fluid (VOF) multiphase model with RNG k-ε model was used for simulation the tested domain containing 142374 cells (the optimum mesh size) based on the decision mentioned earlier in this paper. At such condition, the oil-water flow pattern simulated is seen stratified (see figure 4) with multiple layers of phase density in the middle of the pipe where the oil and water phases met. Figure 5 shows the view of oil volume fraction contours at pipe length (z = 0.5 m) which located in the middle of the pipe length. (Chart 2). Different velocity indicates different inversion point. 0.2 and 0.5 m/s can be considered as slow speed which gives more time for both phases to dispersed within each other. On the view of oil production is not good since avoiding mixing phases will reduce time during separation processes. 0.8 and 1.1 m/s shows better oil and water mixture. From the contours seen the fraction of oil at the upper region shows high fraction of oil. It indicates less water inversion to its phase.

4.0 CONCLUSIONS

The following conclusive remarks result from our analysis. As far as the fluid dynamic analysis is concerned:

1. CFD calculations using Fluent 6.2 were performed to predict the oil-water stratified flow in 0.0254 m horizontal pipe.
2. Volume of Fluid (VOF) multiphase model with RNG k-ε two equations turbulent model was selected among other different multiphase and turbulent models based on the convergence, prediction off the oil-water stratified flow pattern and the smoothness of the interface.
3. Mesh independent study has been achieved to decide on the optimum mesh size to be used in the simulation process.
4. Pressure prediction base on different flow velocity have been observed. It can be seen that as velocity increases, the pressure gradient also increases.
5. The pressure prediction will be extended to examine the effect from different water volume fraction.

ACKNOWLEDGEMENTS

The authors are very grateful to Universiti Teknologi Malaysia, Ocean and Aerospace Research Institute, Indonesia for supporting this study. Authors are also grateful for useful discussions with my family and all my friends.

REFERENCE

1. O.Shoham, Y.Taitel, "*Stratified turbulent-turbulent gas-liquid flow in horizontal and inclined pipes*", AIChE J. 30 (2) (1984) 377-385.
2. R.I, Issa, "*Prediction of turbulent, stratified, two-phase flow in inclined pipes and channels*", Int. J. Multiphase Flow 14 (1) (1988) 141-154.
3. C.H. Newton, M. Behnia, "*Numerical calculation of turbulent stratified gas-liquid pipe flows*", Int. J. Multiphase Flow 24 (5) (1998) 141-154.
4. Hui gao, Han-Yang Gu and Lie-Jin Guo, "*Numerical study of stratified oil-water two-phase turbulent flow in a horizontal tube*", Int. J. heat and mass transfer, (46) (2003) 749-754
5. G. Elseth, H.K. Kvandal, M.C. Melaaen, "Measurement of velocity and phase fraction in stratified oil-water flow", *International Symposium on Multiphase Flow and Transport Phenomena*, Antalya, Turkey, pp.206-210, 2000
6. Awal, Mohammad R., Zughbi, Habib D., Razzak, Shaikh A., Al-Majed, Abdulaziz A., and Al-Yousef, hasan Y., "*Liquids phase holdup and separation characteristics as a function of well inclination and flowrate*", SPE SA, 2005, 14-16 May.
7. Carlos F. "*Modelling of oil-water flow in horizontal and near horizontal pipes*", PhD Thesis, Tulsa University, 2006.
8. Al-Yaari, M., and Abu-Sharkh, "*CFD Prediction of stratified oil-water flow in a horizontal pipe*", Asian Transactions on Engineering Volume 01 Issue 05, November 2011.

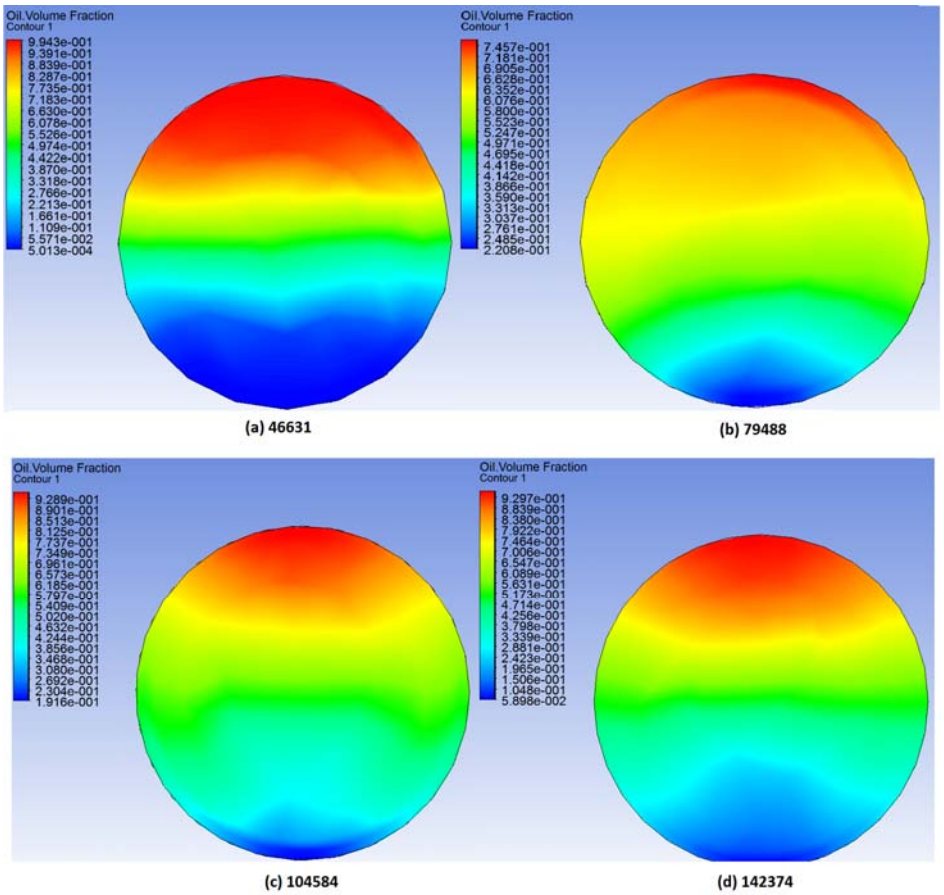

Figure 3: Oil volume fraction contours at pipe length (z = 0.5 m)

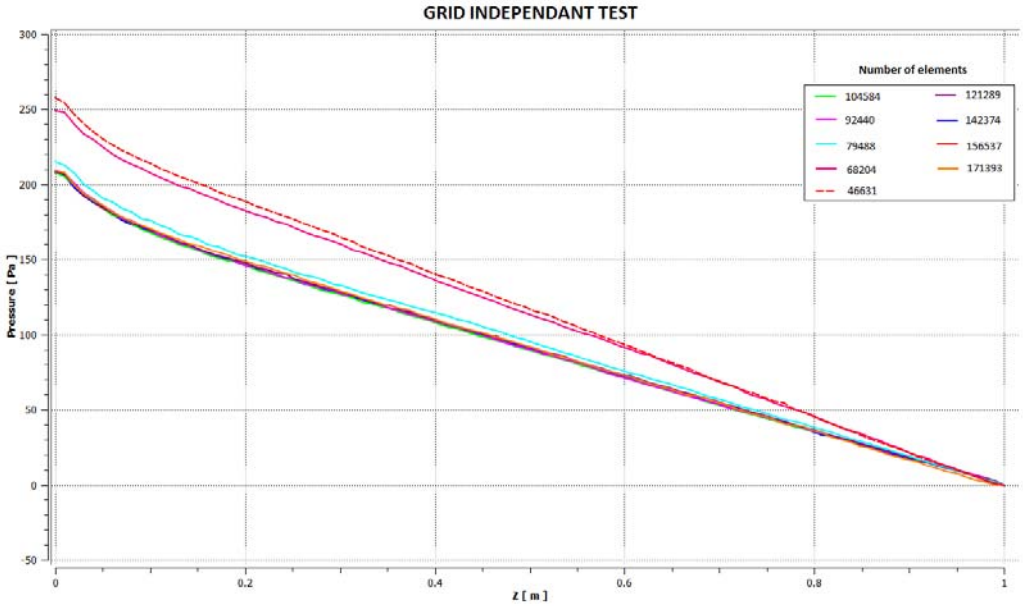

Chart 1: Optimum mesh size at unchanged pressure profile

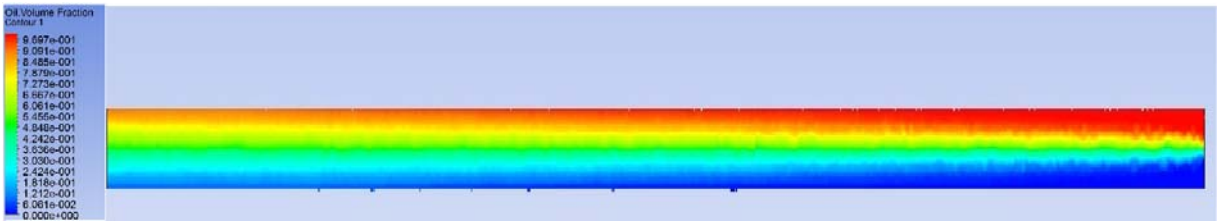

Figure 4: Stratified Oil-water flow simulation

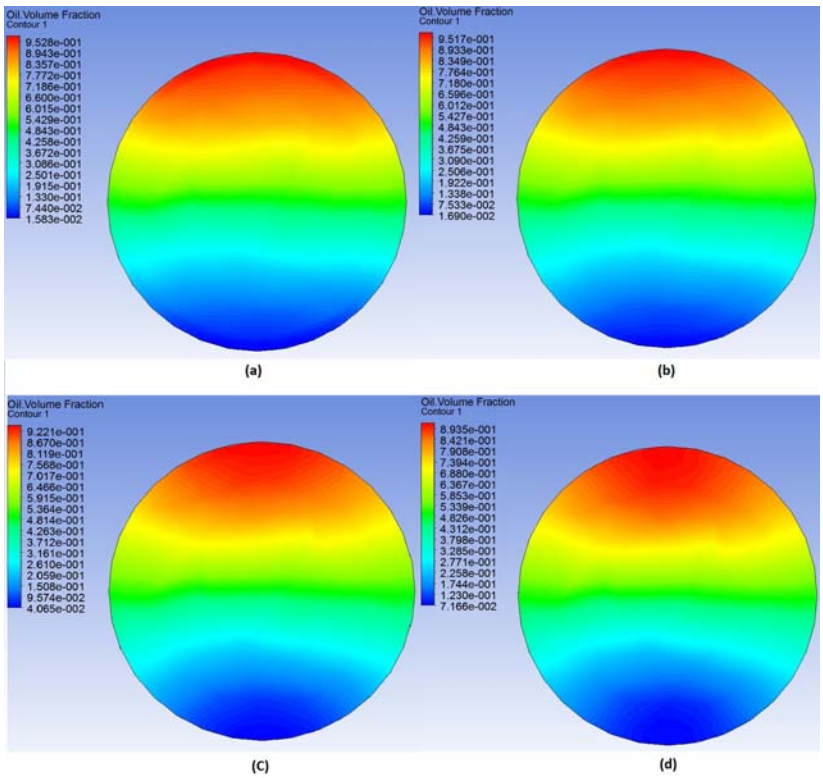

Figure 5: Oil volume fraction contours at pipe length (z = 0.5 m); (a) 1.1 m/s (b) 0.8 m/s (c) 0.5 m/s (d) 0.2 m/s

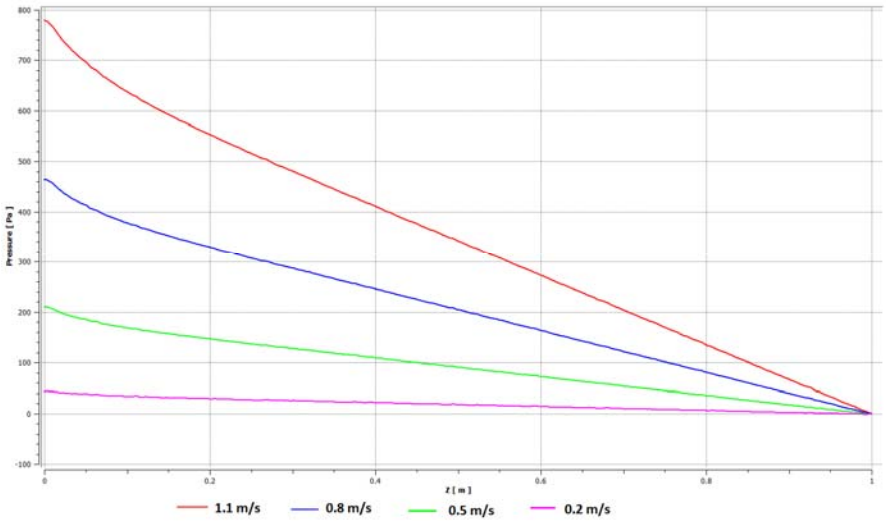

Chart 2: Pressure profile at each flow velocity

Dynamic Performance Simulation of Hydraulic Transmission for Low Speed Vertical Axis Marine Current Turbine Using Simulink Mat-Lab

Adi Maimun, [a,*] and Atef Salem Souf Aljen, [b]

[a)] *Marine Technology Centre, Faculty of Mechanical Engineering, Universiti Teknologi Malaysia*
[b)] *Postgraduate student,Faculty of Mechanical Engineering, Universiti Teknologi Malaysia*

* Corresponding author adi@fkm.utm.my

Paper History

Received: 25-October-2014
Accepted: 11-November-2014

ABSTRACT

For Malaysia, ocean energy can be the best resource of green marine renewable energy, because the generation of the electricity by burning of fossil fuels produces undesired greenhouse gases, moreover the reserves of fossil fuels are being depleted and there is no accurate way to determine how much remains. Turbines using hydraulic drive are being used for generating electricity by some manufacturers in the wind industry as an alternative to gearbox drive-trains because of reliability issues. Likewise in marine renewable sector hydraulic-drive is an attractive option in terms of improved system efficiency, reliability and robustness. This paper presents a time domain simulationof hydraulic transmissions forLow Speed Vertical Axis Marine Current Turbines using Simulink software. These turbines are applied to harness marine current energy because of their relative simplicity and represent a promising technology to exploit low speed currents due to their small plants with reduced installation and maintenance costs.

KEYWORDS:*Renewable energy, Low Speed Vertical Axis Marine Current Turbines, hydraulic transmissions, Simulink, Time domain simulation*

NOMENCLATURE

A_S	Turbine swept area (m^2)
C_P	Performance coefficient
T	Torque (Nm)
Q	Flowrate (m^3/s)
P	Pressure (Pa)
D_P	Rotor Diameter, (m)
d	Paddle Diameter, (m)
r	arm, (m)
H	Rotor Height, (m)
P_P	PeakPower (Watt)
n	Rotation rate (RPM - Revolutions per minute)
U_∞	Current velocity (m/s)
ω	Angular velocity (rad)
λ	Tip speed ratio -TSR
ρ	water density (Kg/m^2)

INTRODUCTION

Ocean energy can be the best resource of green marine renewable energy, because the generation of the electricity by burning of fossil fuels produces undesired greenhouse gases. As known the forms of these resources of marine energy especially the ocean energy can be categorized into tidal, wave, current, thermal gradient and salinity gradient [1, 2]. To harness energy from marine current, there are two kinds of hydro-turbines; vertical-axis and horizontal-axis turbines that can be used as power generation devices as stated in [3]. Many studies and researches are carried out to demonstrate the feasibility and advantages of power generation plants. Horizontal-axis turbines are complex system and they are suitable only for large size plants where high installation and maintenance costs are balanced by large energy produced. In other hand, the vertical-axis turbines are relatively simple and represent a promising technology to exploit marine currents due to their small plants with reduced installation and maintenance costs and they are suitable for deployment in remote areas. One of the vertical-axis turbine types is a conventional Savonius turbine which has good potentials and suitable for the Malaysia's waters requirement; low speed current and shallow water depth [4, 5]. But this turbine has a main drawback which is low tip speed ratio TSR (λ) and difficult to integrate it with a generator.

Recently, large wind turbines are using speed-increasing gearboxes to connect the high speed RPMs of generator to the slow motion rotors. However, these gearboxes are heavy and got a lot of mechanical problems. Also their maintenance work and replacement process is costly and very expensive. Other wind/marine turbines use direct drive low-speed generators which is connected direct to the generator. But these machines are expensive and very heavy even they are efficient and reliable. In another hand they need full-power electronic frequency and voltage converters to condition their power to

supply the grid to avoid the network instability. Convictional hydraulic transmission systems have long been considered for wind turbines and to make them attractive some companies and researchers have developed new high efficient hydraulic pumps and drive motors such as variable displacement and digital displacement machines. So a continuously variable transmission ratio allows the rotor to be operated at the best speed for optimal power capture, while the synchronous generator is driven at a much higher constant speed. Besides, short-term storage in hydraulic reservoirs (accumulators) can smooth out wind/current turbulence. So this is a good motivation to use these new solutions and developed technologies for marine current turbines due to the important features of the hydraulic system which are:-

- Continuously variable transmission ratio.
- A save and reliable operation.
- Good damping characteristics

For Malaysian sea which has low current speed and shallow depth, researchers had proposed a Savonius vertical-axis turbine to harness current energy [4, 5]. But this type of turbine has a main drawback which is low tip speed ratio TSR (λ) and difficult to integrate it with a generator. So, this paper presents a dynamic performance simulation of matching the Low Speed Vertical Axis Marine Current Turbine with synchronic generator using the hydraulic transmission system.

1.0 HYDRAULIC TRANSMISSIONS SYSTEM

Currently power transmission systems used are heavy with high cost of components moreover theConcept of the energy transfer systemexperiences dynamic loads and requires high maintenance, hence using hydraulic power transmission is the solution. Moreover the hydraulic transmission has a steeples gear ratio which enables the rotor to change speed independent of the generator.To illustrate that, a functional principal sketch of the hydraulic drive train system for current turbine is shown in fig.1.

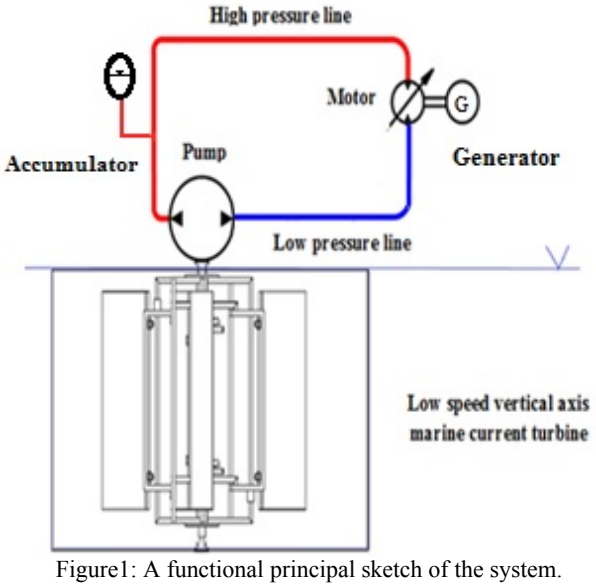

Figure1: A functional principal sketch of the system.

Concept of the Energy Transfer System

Recently, there are many projects under different countries such as Scotland, Norway, USA, Germany and Netherlandsas stated in [6] and Japanare developed and adopted this technology. In all of this technology the concept is that the main shaft connects the rotor of the turbine to the positive displacement hydraulic pump. This pump converts the torque and speed of the turbine into a pressure flow. This fluid power is transferred in a circuit to hydraulic motor where the pressure flow is again converted into torque and speed (mechanical energy) to run and drive a generator at constant speed to produce the electrical energy. The Schematic diagram of the concept is shown in the figure 2.

A gearless hydraulic marine current energy transfer system utilizes the hydraulic power transmission principles to harvest the energy from current flow. The gearless marine current power transfer technology may replace the current energy harvesting system to reduce the cost of operation and increase the reliability of current power generation.

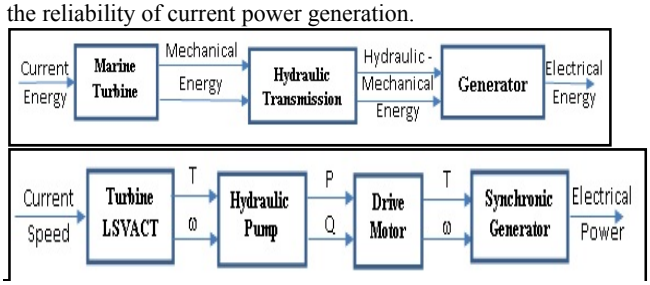

Figure 2. Concept of energy transfer

From the literature, the HTS is widelyused in the wind energy and summary of some important findings are:
A hydrostatic transmission for wind turbines which offers good characteristics in controlling rotor RPM and damping torque impulses becomes apparent due to the overall efficiency of the system which was reached to 86% and its development is presented in the reference [7].Enhancement of efficiency is gained by adding another wind-driven fixed displacement hydraulic gear pump to the wind turbine hydraulic power plant. So, increasing efficiency and energy generation of the wind power plant can be achieved by collecting the energy from more wind turbines [8].

In reference [9] reported that solution to overcome the uncertainties with off-the-shelf high pressure oil pumps and motors for hydraulic transfer system such as low efficiency to combine power from different sources and the type of hydraulic machine described in his paper which is the design of the variable-displacement machine [9].Efficiency of the hydraulic machine, variable hydraulic pump and the variable hydraulic motor are function of pressure, rotating speed, densitydynamicviscosity of the fluid and control angle as stated in [8, 10]. Also the optimized control comparing with traditional control (control the hydraulic machines in sequence) is saving up to 1.5 KW for his HTS size used in simulations and found that the best accessible improvements are at low torques (low loads).But, the traditional control still operating well on most working points [10].A continuously variable transmission (CVT) is required to capture the wind marine energy more efficiently. This system in the form of a hydrostatic transmission (HST) can be a viable solution for a mid-sized wind turbine. A hydrostatic transmission allows to use a synchronous generator, hence the generator speed is decoupled from the rotor speed [11].

Using the technology based on Digital Displacement^{TM} machine for hydraulic transmission system maintains the generator to operate at the constant RPM even a tidal current turbine operates at variable rotor speeds. So, the generator power output remains uniform and unaffected until the system does not exceed the rated capacity, besides the generator does not show any fluctuation even the incoming power from the pump to the drive motor varies, due to the absorptions of the fluctuations by the accumulator [12].

Advantages of the Marine Turbine System with the Hydraulic Transmission
The main advantages of the system are:

- Gearless transmission.
- More robust than mechanical gearboxes.
- High power-to-weight ratio.
- Inherently less stiff than mechanical equivalent.
- Damping of dynamic loads.
- Mature technology with High reliability/low maintenance

2.0 THE SYSTEM USED IN THIS SIMULATION

The principal particular of the Low Speed VAMCT:
This turbine is based on the full scale prototype of the conventionalSavonius turbine with a rotor height 15 m height which is suitable for the Malaysia's waters requirement; low speed current and water depth [4, 14]. The parameters of the prototype used in this simulation are based on the experimental and simulated results of model tests which scaled up to obtain prototype estimated parameters [13]. The main particular of the Savonius prototype specifications and estimated parameters will be used for marine current application and its model are presented in the following table.1 below. The current velocity of the prototype is 0.56 m/s and it is regarding the actual averaged current speed in the location of the research [15].

Table 1: Prototype and model specifications

No	Description	Model	Prototype VAMCT
1	Height, H [m]	1.5	15
2	Rotor Diameter, D_P [m]	0.375	3.75
3	Flow velocity U_∞ [m/s]	0.17	0.56
4	Torque, T [Nm]	0.36	3600
5	Angular speed n [RPM]	11.97	3.79
6	Angular speed ω [rad/s]	1.25	0.4
7	Peak Power, P_P [Watt]	0.45	1426.28

Simply in this simulation, the performance characteristic of the Low Speed VAMCT can be quantified by a generic performance coefficient curve or by using the lock-up table. The performance coefficient, C_P, expresses the ability of the turbine to extract kinetic energy from the stream flow. It is equal to the ratio of the mechanical power available from the turbine shaft to the power conveyed by the current stream through the swept area of the turbine rotor

$$C_P = \textit{Shaft mechanical power avail.}/0.5\,\rho\,A\,U_\infty^3 \qquad (1)$$

Where ρ is the water density, A- the turbine swept area, and U_∞ the free stream velocity [12].
The performance coefficient is typically expressed as a function of the tip speed ratio λ, which is the ratio of the blade tip speed V to the free stream velocity U_∞. Figure 3 shows the power coefficient C_P curve used for this study from experimental results done by [13].The curvecan be defined by a fifth-order polynomial as shown below:

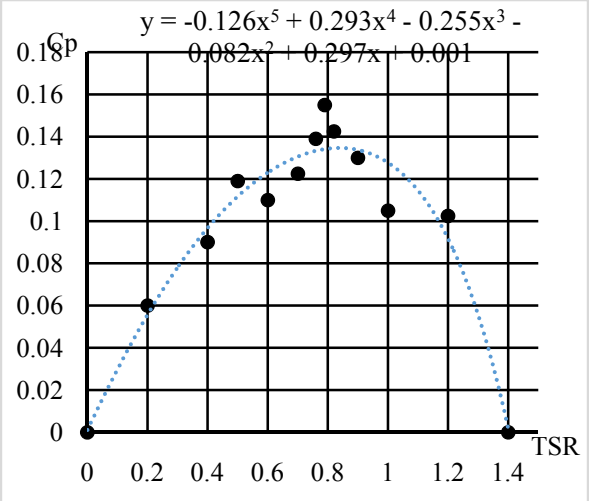

Figure3: Power coefficient (C_P) Vs TSR (λ)curve

The principal particular of modified LS-VAMCT:

This modified turbineas shown in figure 4 a new novel concept of vertical axis water current turbine based on modified Savonius rotor proposed by [17] called self-rotating vertical axis current turbine SR-VACT.

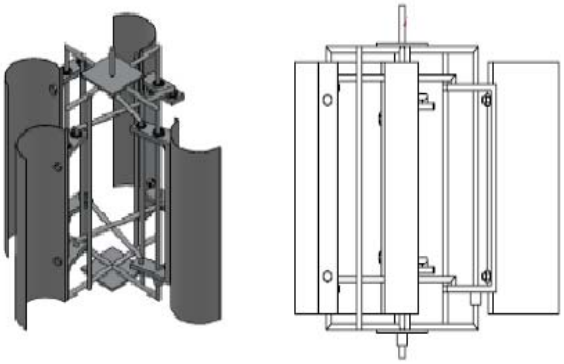

Figure 4: Representation of SR-VACT

In this designa self-movement or self-rotating four blades technique is applied for increasing the hydrodynamic pressure loads and at the same time, to decrease the hydrodynamic resistance and drag forces which leads to enhance performance and efficiency of this type of turbine. Table 2 below illustrates the main estimated parameters of modified design.

Table 2: Prototype and model specifications

No	Description	VAMCT	SR-VACT
1	Height, H [m]	15	15
2	Paddle Diameter, d [m]	1.85	1.85
4	Arm, r (m)	-	0.542
5	Torque, T [Nm]	3600	4914
6	Angular speed n [RPM]	3.79	3.137
7	Angular speed ω [rad/s]	0.4	0.3285
8	Peak Power, P_P [Watt]	1426.28	1614.48

The performance coefficient of this turbine is typically expressed as a function of the tip speed ratio λ and torque

coefficient Cm. Figure 5 shows the torque coefficient C_m curve used for this study from simulation results done by [17].The curvecan be defined by a second-order polynomial as shown:

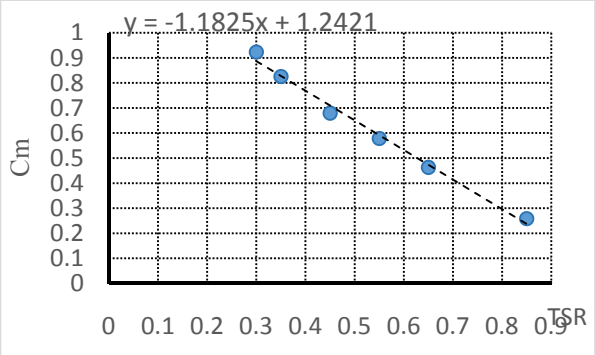

Figure5: Torque coefficient (C_m) Vs TSR (λ)curve

The principal particular of the Hydraulic Transmission System (HTS)

Marine Current Turbine is driving a hydraulic system based upon oil using axial displacement pumping fluid around the system to drive a hydraulic motor, which is then coupled to a conventional induction machine. Accumulators provide energy storage to compensate for the variations in power [12]. The efficiency of a HTS is dependent on several parameters including volumetric flow rate, rotational speed and torque at the pump shaft, and the pressure difference across the inlet and outlet of the hydraulic pump and motor[10].The main components of the system and the specificationsof theAccumulatorare shown below in the table 3.

Table 3:Hydraulic transmission components

Hydraulic Pump	
Working Pressure (Pa)	350 x10^5
Peak Pressure (Pa)	400 x10^5
Volumetric Efficiency	0.97
Hydraulic Motor Drive	
Working Pressure (Pa)	350 x10^5
Peak Pressure (Pa)	400 x10^5
Volumetric Efficiency	0.97
Hydraulic Reservoir(Accumulator)	
Hydraulic Reservoir Max Volume (m^3)	0.5
Max Pressure (Pa)	400 x10^5
Pre-charge Gas Pressure (Pa)	350x10^5
Gas Index	1.25

The conventional hydraulic pumps and motors have good efficiency at full displacement but their performance drops significantly at partial displacement [16].In practice more efficient and better performance of the system is achieved when both machines used have variable displacement capabilities [12]. There is also a digital displacement technology is developed specifically for avoiding the higher losses in the transmission when the input power from the turbine is lower as stated in [12].

In this simulation study, Simulink Hydraulics library is used to model a hydraulic system and to describe the physical phenomena of it.The conceptive easiest way to model a hydraulic system is to identify all important components, e. g. pump, valves, orifices, motors, etc. as shown in figure 4 below.Connect the models according to the circuit diagram and place a lumped volume at each node (no need to do so if the placement of lumped volumes can be done automatically by the simulation program), the connection of two or more components. This leads to a set of differential equations where the through variable, flow rate, can be easily calculated from the known state variables, i. e. the across variables, which are the pressures in the volumes.

The specifications of the generator

The main electrical characteristics of the generator are presented in the following table 4.

To simulate this generator in this study a Simulink electric library is used to model a synchronic generator and the load on it.

Table 4: The specifications of the synchronic generator

Synchronous Generator	
Nominal Power (KW)	2.25
Rated Rotation (RPM)	1725
Rated voltage (V)	220
Frequency (Hz)	60
Number of Poles (pcs)	2

3.0 Dynamic Performance simulation

Mat-lab simulation program is developed to simulate LS-VAMCT with the hydraulic transmission system. In this program the energy is harvested by a low speed-high torque marine current turbine connected to a fixed-displacement hydraulic pump, which is connected to variable-displacement hydraulic motor. This drive motor will provide and maintain constant RPM to the loaded synchronic generator which is integrated to it. In this computer program as mentioned above the turbine is presented by using a block diagram where the turbine is simulated by gating the power from C_P curve of a fifth-order polynomial using the equation (1) to power the pump in terms of torque and RPM.

4.0 RESULTS AND DISCUSSION

Simulation Results for low Speed VAMCT

The current speed used in this simulation is 0.56 m/s and that based on the annual average currentvelocityof Malaysian sea as reported in [15]. The dynamic simulation results as illustrated in table 5 and infigures 7 below show that the RPM remains constant and total power obtained from a synchronic generator is1675(Watts).

Table 5: VAMCT simulation results

Parameter	Value
Hydraulic Pump	
Pump Displacement (m^3/rad)	9.1543x10^{-5}
Torque at shaft (N.m)	3614
Power rating at 3.75 r/min (KW)	1.445
Hydraulic Motor	
Motor Displacement (m^3/rad)	1.123x10^{-7}
Power rating at 1500 r/min (KW)	1.211
Torque at generator shaft (N.m)	11.15
Hydraulic transmission System with the Generator	
Generator Power P_G (Kw)	1.675
Total Efficiency	~ 85 %

Simulation Results for modified LS-VAMCT

The same current speed used in this simulation which is 0.56 m/s and dynamic simulation results are shown in table 5andin figures 6, 7 below show that the velocity remains constant and

total power obtained from a synchronic generator is 1728(Watts).

Table 6: LS-VAMCT simulation results

Parameter	Value
Hydraulic Pump	
Pump Displacement (m^3/rad)	$0.1375x10^{-3}$
Torque at shaft (N.m)	4914
Power rating at 1.57 r/min (KW)	1.6142
Hydraulic Motor	
Motor Displacement (m^3/rad)	$1.904x10^{-7}$
Power rating at 1500 r/min (KW)	2.227
Torque at generator shaft (N.m)	12.33
Hydraulic transmission System with the Generator	
Generator Power P_G (Kw)	1728
Total Efficiency	~ 85 %

Using Math-lab block signal builder as shown if figure8 below the current speed is changed and stepped from 0.56 to 1 m/s and generator power for both simulations remain without changes and any fluctuations.Thesefluctuations are absorbed by the accumulator.

As result, the LS-VACT has been integrated with synchronous generator. In addition, a hydraulic transmission system can transfer amounts of power and has more flexibility than a mechanical and electrical (direct drive) system. Moreover the efficiency of a HTS is dependent on several parameters including volumetric flow rate, rotational speed and torque at the pump shaft, and the pressure difference across the inlet and outlet of the hydraulic pump and motor. Through dynamic performance simulation of the system, an enhanced understanding of the HTS through simulation was gained that lead to an efficient hydraulic energy transmission system forlow speed vertical axis marine turbine in this case a Savonius rotor.

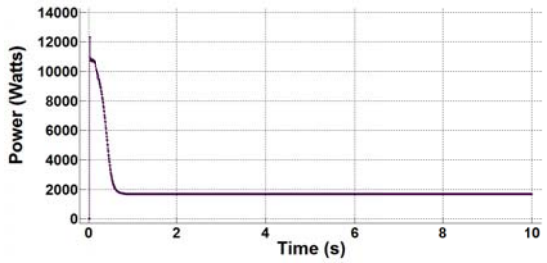

Figure 6: Generator Power RS-VACT

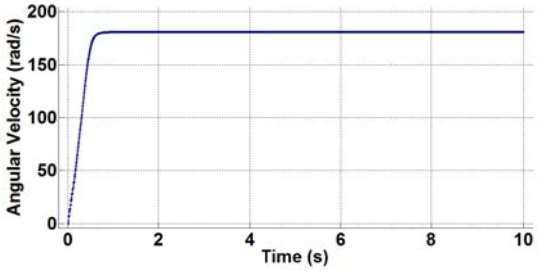

Figure 7: Generator angular velocity

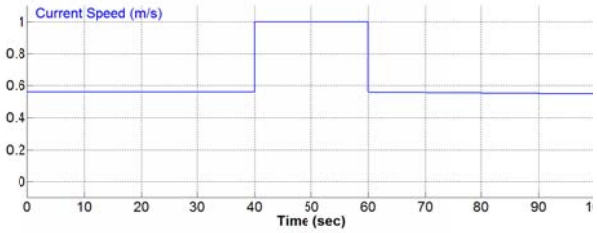

Figure 8: Current speed steps 0.56 to 1 m/s

5.0 CONCLUSION

The time domain dynamic performance simulation program for low speed marine current turbine with the hydraulic transmission has been developed.

Electricity generation from low speed current and high torque can be possible with hydraulics transmission and has decent performance under constant and variable current speed conditions.

A gearless hydraulic marine current energy transfer system utilizes the hydraulic power transmission principles to harvest the energy from current flow. The gearless marine current power transfer technology may replace the current energy harvesting system to reduce the cost of operation, increase the efficiency and the reliability of current power generation.

In the future, this simulation can be upgraded for the purpose of further analysis in dynamics and control. Moreover the Simulation is not supported by experimental results of the whole system, so for future work a small system prototype can be built and comparison between the results obtained from tests conducted and simulations can be demonstrated and validated.

REFERENCES

1. Bedard, R.; Jacobson, P.T.; Previsic, M.; Musial, W.; Varley, R. An overview of ocean renewable energy technologies. *Oceanography* 2010,, 22–23.
2. *Review and Analysis of Ocean Energy Systems Development and Supporting Policies*. OES-IA: Ireland. June 2006. Available online
3. Khan M, Bhuyan G, Iqbal M, Quaicoe J. Hydrokinetic energy conversion systems and assessment of horizontal and vertical axis turbines for river and tidal applications: a technology status review. Applied Energy 2009; 86 (10):1823-35.
4. Yaakob, O.B., Yasser M. Ahmed, M. Arif Ismail, "*Validation Study for Savonius Vertical Axis Marine Current Turbine using CFD Simulation*",Asia-Pasific Workshop on Marine Hydrodynamics, Vol.6, 2012, pp.327-332.
5. Yaakob, O., Tawi, K. B., and Suprayogi, D. T., "Development of Vertical Axis Marine Current Turbine Rotor" International Conference Marine Renewable Energy, RINA, London, U.K., (2008), 77-83.
6. N.F.B. Diepeveen and A. Jarquin Laguna 'Dynamic Modelling of Fluid Power Transmissions for Wind Turbines' EWEA Offshore 2011
7. Schmitz J. Vatheuer N. And Murrenhoff H. 'Hydrostatic drive train in Wind Energy Plants'RWTH Aachen, Aachen, Germany, 2009
8. Ayana Pusha, Majid Deldar and Afshin Izadian. 'Efficiency Analysis of Hydraulic Wind Power Transfer

System' in *IEEE Transactions on Industrial Electronics*, 2013.
9. Stephen Salter (2005) 'Digital Hydraulics for Renewable Energy': World Renewable Energy Conference Aberdeen 2005. Available on the web.
10. Mika Ijas and Esa Mäkinen. 'Improvement of Total Efficiency of Hydrostatic Transmission by Using Optimized Control' Proceedings of the 7th JFPS International Symposium on Fluid Power, Toyama 2008, pp.271-274
11. Feng Wang and Kim A. Stelson. 'Model Predictive Control for Power Optimization in a Hydrostatic Wind Turbine'. *The 13th Scandinavian International Conference on Fluid Power, SICFP2013, June 3-5, 2013, Linköping, Sweden*.
12. G. S. Payne, A. E. Kiprakis, M. Ehsan, W. H. S. Rampen, J. P. Chick1, and A. R. Wallace 'Efficiency and dynamic performance of Digital Displacement ™ hydraulic transmission in tidal current energy converters' Proc. IMechE Vol. 221 Part A: J. Power and Energy2007, pp. 207–218
13. Yaakob, O., Suprayogi, D. T., Abdul Ghani K.B. and Tawi, K. B., "*Experimental Studies on Savonius-type Vertical Axis Turbine for Low Marine Current Velocity*"International Journal of Engineering, IJE Transactions A: Basics,Vol. 26-1, (2013) pp 91- 98.
14. Yaakob, O., Tawi, K. B., and Suprayogi, D. T., "Computer Simulation Studies on the Effect Overlap Ratio for Savonius Type Vertical Axis Marine Current Turbine" ***IJE Transaction A: Basic,*** Vol. 23, (2010), 79-88
15. Royal Malaysian Navy. *Tide Tables Malaysia 2005*. Kuala Lumpur: The Hydrographic Department, Royal Navy Malaysia. 2005.
16. Payne, G. S., Stein, U. B. P., Ehsan, M., Caldwell, N. J. and Rampen, W. H. S. Potential of Digital Displacement™ hydraulics for wave energy conversion. Sixth European Wave and Tidal Energy Conference, Glasgow,UK, 29 August–2 September 2005, pp. 365–371.
17. Adi Maimun et al. (2014). An Innovative Vertical Axis Current Turbine Design for Low Current Speed. *Jurnal Teknologi (Sciences & Engineering) 66:2 (2014), 177–182*

Mathematical Model for the Inclusion of Livability Items in Conceptual General Arrangement Design of Long Term Habitable of Mega Floats

A. Z. N. Hanani[a], Mohd Zamani[a], and J. Koto[b]

[a] *The Institute of Sultan Iskandar, Universiti Teknologi Malaysia, Malaysia*
[b] *Department of Aeronautics, Automotive and Ocean Engineering, Faculty of Mechanical Engineering, Universiti Teknologi Malaysia*

*Corresponding author: nhanani4@gmail.com

Paper History

Received: 26-October-2014
Accepted: 14-November-2014

ABSTRACT

Mega-floats are designed for offshore exploration and as floating cities for human habitation. Therefore, livability items are one of the most important design factors such as recreation area, environment system, safety and etc. Many design concepts have been proposed, but the inclusion of livability – related components is not well explained. Livability criteria have not been defined. Basic descriptions and design specifications have not been provided either. The paper proposes an approach for systematic incorporation of livability items into mega-float design concepts. Based on a selected set of livability criteria a list of livability items for the mega-float has been drawn. Area requirement for each livability items has been systematically estimated based on a set of benchmark values. Gross and individual area requirement for livability item on each of the mega-float modules could be estimated. Generic expressions have been proposed and could be applied for non- modular type mega-float design concepts.

KEY WORDS: *Liveability;Megafloat; Concept Design*.

1.0 INTRODUCTION

Megafloats are concepts more advanced than current offshore structures. Megafloats suitable for long term human habitation are intended to be self –sufficient in all aspect including supply of energy and resources for their inhabitants and governance. Advanced megafloats are still at conceptual design stage. Several ideas have been proposed with various concept on floatation, distribution of functional spaces, elements on living conditions and primary facilities.

As highlighted by Zamani at el. [1], Darren [2] describes the Lilypad floating city which has three marinas and three mountains which surround a centrally submerged artificial lagoon below the water line. The function of three mountains and marinas divided as work, shopping and entertainment for the comfortable social environment of city population. The whole set of mountains planted with a suspended garden for producing their own food through and aquaculture farming technique. A centrally submerged artificial lagoon collects rainwater and purifies the rain water further also act as ballast of the city. Vincent [3] describes the application of renewable energy as power generation, such as solar, thermal and photovoltaic energies, wind energy, hydraulic, tidal power station, osmotic energies, photopurification and biomass to create a positive energy balance with zero carbon emission.

As highlighted by Zamani at el.[1], Shimizu [4] reports that Green Float has a diameter of 3000m and uses the 1000m concept of vertical sky in the city. The concept introduced by Green Float is terraced community in the sky. It deploys tower characteristic featuring community housing, shop, restaurant and medical facilities. The tower concept provides an elevator of seven hundred meters and walking scale between workplace and residence. In the middle of the tower is a plant factory that is self-sufficient in food production. On the water side, facilities that build provide such marine city, airport, jogging zone, aquatic leisure zone a paddy agriculture area and field agriculture area. In addition, the conversion of drifting "garbage island" into the energy source concept and a waste recycling system have also been introduced. Bio business introduced, offer pharmaceutical market, food and cosmetic market, beauty and health market. OTEC is used as power generation that generates 30MW of electric power that need by 100,000 people. Other power sources are wave power and a solar power satellite in geosynchronous orbit that transmit energy to Earth in the form of microwaves. Fundamental safety from events such as strong wind countermeasure, wave countermeasures, earthquake countermeasure and lightning are taken care of using countermeasure systems.

As highlighted by Zamani at el [1], DeltaSync [5] describes a Seastanding mega-float as a combined concept of aquaculture and hydroponics to create a self–contained ecosystem in food production. An integrated multi-tropic aquaculture was introduced as the new concept for saltwater fish production that complete the metabolism chain of living population cities. For efficient water management strategy, rainwater collected and stored, seawater is desalinated and grey water is reused. The building's roof and the floating platform are used to collect rainwater and stored in flexible tanks. The power sources that

supply electricity for resident are Ocean Thermal Energy Conversation , wind energy and solar energy. Breakwater structure and a hinged connection for the floating structures is used concept as an element for the safety aspect against natural disaster.

Different between current concept designs are quite large. For a given set of mission, for example deep sea-exploration , differences on the five conceptual elements are noticeable. Details on design philosophies are not easily recognized. Primary functional facilities differs. Technical specifications not provided or sketchy. Method of estimating spaces and volumes provided not given or easily traceable to widely accepted standards. The research aims to establish an approach such that the design concept would serve as reference.

2.0 LITERATURE REVIEW

2.1 Megafloat and Liveability Issue

As propose by Zamani at el. [6], megafloat is an extended version of the conventional very large floating structure which Wang et al. (2007) correctly claims of having "many advantages including (i) cost effectiveness when the water depth is large and the seabed is soft,(ii) environmental friendliness as they do not damage the marine eco-system, or silt-up deep harbours or disrupt the tidal/ocean currents, (iii) their shorter construction time, (iv) easily removal, reconfiguration and reusing, (v) not affected by earthquakes as they are inherently base isolated, (vi) they provide scenic 360^0 view of the water body, (vii) their interior spaces may be used for offices, car parks and storage rooms and(viii) their constant position with respect to the water level make them ideal for use as piers and berths for ships." While conventional VLFS has been proposed for various near-shore uses such as floating airports,bridges, breakwaters, piers and docks, fuel storage facilities, emergency bases, entertainment facilities,recreation parks and mobile offshore structures (Watanabe et al., 2004b) Megafloat removed very large floating structure's dependency on shore-based supply thus creating total readiness for sustainable habitation. The immediate application of megafloat concept is of course to all potential OTEC installations for the 99 nations identified by Takahashi and Trenka (1996). He has included in his list countries where sites could be established for shore-based OTEC installations 10 km from shore so that installations are within the states territorial waters of 12 nautical miles. Applying megafloat's concept to current OTEC platform design is quite straight forward for the OPeCS configuration could be coupled to the awaiting OTEC platform byengineering means.

As highlighted by Zamani at el. [1], Leby [7] describes factors that represent the quality of living and comfort which are sustainable in neigborhoods. Liveability dimensions that are crucial for neighborhoods include social, physical, functional and safety. Factors that influence liveability dimension are community life and social contact, environment quality, accessibility, feeling of safety, numbers of crime and accident, and maintenance of built environments. Lee [8] evaluates conditions that provide environmental liveability and benefit to the community by preventing disasters and sustainable subsistence. To evaluate liveability in the community, one must consider health, convenience, comfortable, secure and socioeconomic. Other criteria of environment livability can be availability of water, density of public facility, growth and development of the population, and agriculture resources.

2.2 General Arrangement Items on Megafloat

Naceur [9] describes the characteristics of shared outdoor spaces in housing estates influence residents to interact with one another. The facilities provide in housing estate are a primary school, a college, administrative buildings (bank, insurance company, police station, soccer field) and bus stations. Desley [10] describes household activities influence the perceived dimension of the neighbourhood: for example, how far people are willing to walk to public transport, banks, health facilities, shops and recreational facilities. Reiko [11] reports facility that availables in the Silver Peer Housing that make resident feel comfortable housing and a communal space open to public such as a bus stop or train station, clinic or hospital, post office, bank, grocery, and so on. Eziyi [12] analyzed the factor of resident satisfaction with the housing environment by location of housing estates, housing service, and social environment. The housing service criteria provide good facilities such as public infrastructure, health facilities, education facilities, sporting facilities, business, security and safety service. Lisa [13] compared three suburbs of different street network design: traditional, conventional and hybrid in term of useful amenities and daily need such as petrol station, post office, child care centre, and market.

MacDonald [14] considers a commercial building for specialized service and enterprise management exist in United State. The example of commercial building are bank, courthouse, shopping mall, fire station, police station, jail, laboratory, post office, vacant, convention center and religious organization. Buck [15] groups the building type of commercial sector includes a retail store, public admin, public hall and indoor entertainment and recreation. Ricardo [16] give example of the spatial structure of the Canadian in commercial sector are pharmacies, community centre and religious facilities. Matthew [17] classified commercial building types are financial service, manufacturing, retail and medical service. Nuri [18] categorized commercial building as office building include medical building, warehouse and financial building. Schleich [19] describes the sub –sector in the German commercial sector, such as bakeries, butcheries, car repair industry, laundries and dry cleaner, metal industry and bank. Mortimer [20] defines building consists in the commercial sector by reference to Standard Industrial Classification (SIC) for instance, hotel, air transport, postal service, sanitary service and banking.

Zhu [21] groups the industry sector for Chinese economy through agriculture, manufacturing, and service that include the farming, fishery, textile manufacturing, transportation service and telecommunication service. Zafer [22] analyzed the performance of energy for industrial modes such as chemical-petrochemical, cement, fertilizer and sugar . Raul [23] classified a large sized industries in city are food and beverage industry, cement and ceramic industry, glass and plastic industry, textile manufacturing,manufacturing of metal product and chemical – pharmacy industry. In addition, Pierre [24] analyzed the sector that covered in the industrial category are ICT service, transportation service and natural resources service. Jiansu [25] exploitation the industry that engaged in natural resources such as extraction of petroleum and natural gas, mining and processing of

ferrous metal ores and non-ferrous metal, and manufacture of paper and paper product. Bujold [26] give example of industrial land based on printing and publishing and medical device such as pharmaceutical and medical manufacturing, newpaper and directly publisher industry, and motion picture and video industry.

Myriam [27] state sustainability of city sometime is being synonymous with having a public mission such as education, health , security and safety to work done by government. Anthony [28] asses innovation activities within national government through public administration, public service provider and publicly- owned commercial corporations. The example of public administration are fire protection, police, waste management, environment and health. Bogdan [29] also evaluate the performance indicator derived from the role of the government in providing opportunities to give benefits of public activities and public sector efficiency throughout public administration, education, health –care and public infrastructure. Ashley [30] describes government agencies responsibility to serve the public good to ensure lasting sustainability such as department of park and recreation, department of youth and community development and food department. Bernard [31] classification five cases of basic attributes by governance are education, healthcare, transportation, defense and justice. Ida [32] state that welfare service and water supply need to be recognized as a particular type of public service to the complexity of governmentally in considering the increase of development of the citizen.

Falin [33] groups the assessment of renewable energies includes, solar energy, wind power, wave energy, which are all commercialized and matured in terms of current technologies while other renewable energies, which have not proven as matured as the aforementioned ones such as ocean thermal energy conversion. Rodrigo [34] describes two basic ocean thermal energy conversion designs are closed cycle plants using an expanding working fluid to drive a turbine-generator system, and open cycle plants using vaporized seawater to drive the turbine. Young [35] describes the development concepts of the floating type photovoltaic energy generation system that designed, fabricated, and installed successfully at the sea site in Korea. Oriol [36]describes the offshore wind power plants can be connected by means of high voltage direct current system require a power converter at the entrance of the wind farms, allowing a centralized control for the whole wind farm like some offshore wind farms employ only this central power converter with squirrel cage induction generators or synchronous generators , while others combine a central power converter with individual converters and doubly fed induction generators in each wind turbine.

3.0 METHOD

Let total area inclusive of livability items is A_T. A_T is made up of sub area on the megafloat such as residential space, commercial space and etc. Hence,

$$A_T = \sum_{i=1}^{t} A_i \quad (1)$$

Where ,

A_T = Total area of all main systems on that particular megafloat

A_i = Sum of main system area on that particular megafloat

i = Megafloat's main system or module such as residential space, commercial space, industrial space, government space , power generation space and etc

t = The number of main systems on that particular megafloat

For each A_i,

$$A_i = \sum_{j=1}^{u} a_j \quad (2)$$

Where ,

a_j = Sum area of sub- component of main system on that particular megafloat

j = A sub – component of main system such as housing area, education area, security of life and property area, connected community area, public infrastructure and urban service area, business area, sport facilities and recreation for residential space.

u = Number of sub- system on that particular megafloat

But □ is the m of its own sub-component ā . Hence,

$$a_j = \sum_{k=1}^{m} \bar{a}_k \quad (3)$$

Where ,

$\bar{a}_k$ = Sum area of sub- component of system a on that particular megafloat

k = Sub –component of system a such as housing estate, water supply area, electrical area and sanitary service area for housing area

m = Number of sub- component of system a on that particular megafloat

i.e

$$\bar{a} = \bar{a}_b x \beta \quad (4)$$

$$\bar{a}_b = (a_c) x\ p\ x \beta \quad (5)$$

i.e if demand factors is number of population (P), where $0 \leq \beta \leq 1.0$

$\bar{a}_b$ = Area benchmark value of sub- component of system a on that particular megafloat

a_c = Area per demand factor

p = Total demand by population

β = Liveability index

4.0 APPLICATION

When the formula (1) is applied expression in all space in megafloat it become:

$$A_T = \sum_{n=1}^{5} A_R + A_{CM} + A_I + A_{GV} + A_{PG} \quad (6)$$

A_R = Area for residential space
A_{CM} = Area for commercial space
A_I = Area for industrial space
A_{GV} = Area for government space
A_{PG} = Area for power generation space

When the formula (2) is applied expression in residential space it become:

$$A_L = \sum_{j=1}^{7} a_H + a_E + a_S + a_C + a_{PU} + a_B + a_{SR} \quad (7)$$

a_H = Area for housing space
a_E = Area for education space
a_{SF} = Area for security of life and property
a_C = Area for connected community space
a_{PU} = Area for public infrastructure and urban service
a_B = Area for business
a_{SR} = Area for sport facilities and recreation

When the formula (3 and 4) is applied expression in residential space at housing space it become:

$$a_H = \sum_{n=1}^{m} \bar{a}_{HE} + \bar{a}_{WS} + \bar{a}_{ES} + \bar{a}_{SS} \quad (8)$$

Where,
$\bar{a}_{HE}$ = Area for housing estate
$\bar{a}_{WS}$ = Area for water supply storage
$\bar{a}_{ES}$ = Area for electrical service
$\bar{a}_{SS}$ = Area for sanitary service

$\bar{a}_{HE}$ = Area per house x number of houses according to population
$\bar{a}_{WS}$ = Area storage water demand per house x number of houses according to population
$\bar{a}_{ES}$ = Area electricity demand per house x number of houses according to population
$\bar{a}_{SS}$ = Area treatment waste product per house x number of house according to population

When the formula (3 and 4) is applied expression in residential space in education space it become:

$$a_E = \sum_{n=1}^{m} \bar{a}_{CS} + \bar{a}_{PS} + \bar{a}_{CL} + \bar{a}_{MS} \quad (9)$$

$\bar{a}_{CS}$ = Area for children school
$\bar{a}_{PS}$ = Area for primary school
$\bar{a}_{CL}$ = Area for college
$\bar{a}_{MS}$ = Area for middle school

$\bar{a}_{CS}$ = Area school per student x number of students
$\bar{a}_{PS}$ = Area school per student x number of students
$\bar{a}_{CL}$ = Area college per student x number of students
$\bar{a}_{MS}$ = Area school per student x number of students

When the formula (3 and 4) is applied expression in residential space at security of life and property space it become:

$$a_{SS} = \sum_{n=1}^{m} \bar{a}_{PS} + \bar{a}_{FS} \quad (10)$$

$\bar{a}_{PS}$ = Area for police station
$\bar{a}_{FS}$ = Area for fire station

$\bar{a}_{PS}$ = Area of police station per police x police according to area coverage
$\bar{a}_{FS}$ = Area of fire station per fireman x fireman according to area coverage

When the formula (3 and 4) is applied expression in residential space at connected community space it become:

$$a_C = \sum_{n=1}^{m} \bar{a}_P + \bar{a}_L + \bar{a}_M \quad (11)$$

$\bar{a}_P$ = Area for postal service
$\bar{a}_L$ = Area for library
$\bar{a}_M$ = Area for mosque

$\bar{a}_P$ = Area of post office per postman x postman according to area coverage
$\bar{a}_L$ = Area of libary per population x number of population
$\bar{a}_M$ = Area of mosque per population x number of Muslim population

When the formula (3 and 4) is applied expression in residential space at public infrastructure and urban service space it become:

$$a_{PU} = \sum_{n=1}^{m} \bar{a}_T + \bar{a}_{TS} + \bar{a}_N + \bar{a}_{PS} \quad (12)$$

$\bar{a}_T$ = Area for public transport
$\bar{a}_{TS}$ = Area for train station
$\bar{a}_N$ = Area for nurseries and child care centres
$\bar{a}_{PS}$ = Area for petrol station

$\bar{a}_T$ = Area of public station x number of stations according to area coverage
$\bar{a}_{TS}$ = Area of train station x number of stations according to area coverage

$\bar{a}_N$ = Area per nurseries x number of nurseries according to population and

$\bar{a}_{PS}$ = Area of petrol station x petrol station according to area coverage

When the formula (3 and 4) is applied expression in residential space at business space it become:

$$a_{BS} = \sum_{n=1}^{m} \bar{a}_{HC} + \bar{a}_{MT} + \bar{a}_{BK} + \bar{a}_{RS} \quad (13)$$

$\bar{a}_{HC}$ = Area for health care
$\bar{a}_{MT}$ = Area for market
$\bar{a}_{BK}$ = Area for bank
$\bar{a}_{RS}$ = Area for retail shop

$\bar{a}_{HC}$ = Area of clinic x number of clinic according to population
$\bar{a}_{MT}$ = Area of market x number of markets according to population
$\bar{a}_{BK}$ = Area of bank branch x number of bank branch according to population
$\bar{a}_{RS}$ = Area of retail shop x number of retail shop according to population

When the formula (3 and 4) is applied expression in residential space at sport facilities and recreation space it become:

$$a_{SR} = \sum_{n=1}^{m} \bar{a}_{PK} + \bar{a}_{LF} + \bar{a}_{SF} + \bar{a}_{S} \quad (14)$$

$\bar{a}_{PK}$ = Area for park
$\bar{a}_{LF}$ = Area for leisure facilities
$\bar{a}_{SF}$ = Area for sport facilities
$\bar{a}_{S}$ = Area for soccer field

$\bar{a}_{PK}$ = Area of park per population x number of population
$\bar{a}_{LF}$ = Level of sports facility provision per person x number of population
$\bar{a}_{SF}$ = Level of sports facility provision per person x number of population
$\bar{a}_{S}$ = Level of sports facility provision per person x number of population

Most unknown for ā will be obtained from standard value used for land base application.

5.0 DISCUSSION

The whole idea of this research is to establish a reference on how conceptual designing of megafloat should incorporate livability elements. It has been considered as an issue because providing livability items in the form of space and facilities on megafloats involve high cost since space as scarce. Additionally, current concept designs did not indicate how quantity for livability items such as space are estimated and incorporated into the concept design. The difference in livability items indicated if any, on the current conceptual designed poses questions about the consistency of its fundamental.

The approach proposed has been based on strong fundamentals set by MohdZamani [37] . He established eight livability element affecting conceptual designs of megafloats, ranked according to degree of importance and supplied with proposed types of livability items. Quantity for space area, for a livability item has been estimated based, for example, on benchmark values and proportioned according to its degree of importance reflected by the value of β.

As far as the estimation is concerned uncertainties are on the selection of benchmark values and the value of the degree of importance β. Current values considered as standards for similar but land – based projects could be used. Even so, a wide range of values exists for one particular livability item. Furthermore, standard used by countries around the world are different.The values are ethnic and culture related. Furthermore, there is always the possibility of mixing values from a different set of standard since certain values may be missing from the set of standard taken as the principal act. The biggest problem is to source the dynamic nature of livability itself. Lately livability has been defined around abstract concepts such as safe living, green, sustainable etc. Hence, a set of benchmark values considered as excellent could be the lowest livability standard 5 years from now. Those uncertainties should be taken care of appropriately.

Another issue is on choosing the values of β. This factor has been introduced to shrink the land –based benchmark values. The underlying argument is space on megafloat is scarce and costly. Since that a livability item by type or similar must be made available β will take effect on its quantity. What then should be the value of β for each livability items? Should the value of β be set hierarchically by group of livability items and later by elements in each group? Current observation seems to indicate that the most important livability element should be given the highest β value. If $0 \leq \beta \leq 1.0$ should the height β value be 1.0? If the limit for β between 0 to 1.0 is true which livability items qualifies for $\beta = 0$? It is quite easy to determine β arbitrarily. What then is the practical method of determining β? Should designer's chose on β be questioned?Answer to these fundamental questions will affect the quantity to be allocated for the livability items..

6.0 CONCLUSION

In an effort to solve the problem of lack of reference on method of identifying types and quantity of livability items to be provided on long term habitable megafloats the researcher has proposed an approach where values provided for similar land based applications are utilized after being resized by factors that correspond to the items' degree of importance. The approach proposed is found a mentally sound when applied in creating concept designs of megafloat it is expected to produce results with traceable argument and justifications.

Further works are required while current effort is focused on completing the formula for different module of the megafloat including benchmark and β values. The new research focus

should be on addressing uncertainties in those values. The possibility of reducing uncertainties using fuzzy method should be explored. At the advanced stage the research should produce design specifications for livability items on megafloats after megafloat livability indexes have been establish.

ACKNOWLEDGEMENTS

The study has been initially funded by Institut Sultan Iskandar, Universiti Teknologi Malaysia and later by Ministry of Education (MOHE), vote no (4F295), Malaysia managed by Universiti Teknologi Malaysia. The authors acknowledge the great contribution by these organizations.

REFERENCE

1. Mohd Zamani , A., Hanani ,A. A., Daniel. M. R, *Liveability Elements On Current Cocepts Of Megafloat– A Review*. 2014.
2. Darren. , Q. *Lilypad Floating City Concept*. 2011 [cited 23 April 2014; Available from: http://www.gizmag.com/lilypad-floating-city-concept/17697/.
3. Vincent. *Lilypad A Floating Ecopolis for Climate Refugees*. 2008 [cited 23 October 2013; Available from: http://vincent.callebaut.org/page1-img-lilypad.html.
4. Report, S.C., *The Environmental Island Green Island*. 2010, Environment & Techinal Solution Division Corporation Planning Division.
5. DeltaSyncBV, *Final Report Seasteading Implementation Plan*. 2013.
6. A. MohdZamani, D.M.R., J. Koto, Sunarsih, A. Azman, *Large offshore remote terminal - First step towards offshore community settlement*, in *International Seminar on Blue Economy in the 21st Century on the Pacific Rim: Challenges and Opportunities University of Abdul Rachman Saleh*. 2013: Indonesia.
7. Leby, J.L., Hashim,A. H. , *Liveability dimension and attributes Their relative importance in the eyes of neighbourhood residents.* Journal of construction in developing countries 2007. **15**: p. 67–91.
8. Lee, Y.F., Chi,Y.Y., *Using the analytic network process to establish a new evaluation model of environment livability*, in *40th International Conference on Computers and Industrial Engineering (CIE)*. 2010.
9. Naceur, F., *Effects of outdoor shared spaces on social interaction in a housing estate in Algeria* Frontiers of Architectural Research, 2013. **2**: p. 457-467.
10. Desley, V., Laurie, B., Rosemary,A., *The use of amenities in high density neighbourhoods by older urban Australian residents.* Landscape and Urban Planning, 2012. **107**: p. 159-171.
11. Reiko, M., Hisako, Y., Shigeo, T., *Factors affecting the mental health of residents in a communal-housing project for seniors in Japan.* Archives of Gerontology and Geriatrics, 2005. **41**: p. 1-14.
12. Eziyi , O.I., Egidario, B. A., *Assessment of residential satisfaction in public housing in Ogun State, Nigeria.* Habitat International, 2013. **40**: p. 163-175.
13. Lisa, W., Tya, S., Max, B., Terri ,P.,Gavin, M.C, Billie ,G.C, *The anatomy of the safe and social suburb: An exploratory study of the built environment, social capital and residents' perceptions of safety.* Health & Place, 2008. **14**: p. 15-31.
14. Macdonald, J.M., *Commercial Sector and Energy Use.* Encyclopedia of Energy, 2004. **1**: p. 605- 616.
15. Buck, J., Young, D., *The potential for energy efficiency gains in the Canadian commercial building sector: A stochastic frontier study.* Energy, 2007. **32**: p. 1769 –1780.
16. Ricardo, G.I., *The spatial structure of the Canadian business/commercial sector: a study in supply-side segmentation.* Progress in Planning, 2003. **60**: p. 13-34.
17. Matthew , E.K., Nils, K., John,M. Q., *Carbon emissions from the commercial building sector: The role of climate, quality, and incentives.* Journal of Public Economics, 2014. **113**: p. 1-12.
18. Nuri, O.C., Kucukvar,M., Tatari,O., *Scope-based carbon footprint analysis of U.S. residential and commercial buildings: An inputeoutput hybrid life cycle assessment approach.* Building and Environment, 2014. **72**: p. 53-62.
19. Schleich, J., *Analysis Barriers to energy efficiency: A comparison across the German commercial and services sector.* Ecological Economics, 2009. **68**: p. 2150–2159.
20. Mortimer, N.D., Ashley,A ., Mood,C. A. C, Rix,J. H. R.,Moss,S. A . *Carbon dioxide savings in the commercial building sector.* Energy Policy, 1998. **26**(8): p. 615Ð 624.
21. Zhu, L., Yong ,G., Soeren, L. , Hongyan, Z., Tsuyoshi, F., Dabo, G., *Embodied energy use in China's industrial sectors.* Energy Policy, 2012. **49**: p. 751–758.
22. Zafer , U., Arif, H., *Energetic and exergetic assessment of the industrial sector at varying dead (reference) state temperatures:A review with an illustrative example.* Renewable and Sustainable Energy Reviews, 2008. **12**: p. 1277–1301.
23. Raul, G.P., Silvia, A.N., *The potential of natural gas use including cogeneration in large-sized industry and commercial sector in Peru.* Energy Policy, 2012. **50**: p. 192-206.
24. Pierre, T., David, D., Tyler, C., *Innovationnoveltyand(commercial)performanceintheservice sector: ACanadianfirm-levelanalysis.* Technovation, 2011. **31**: p. 655-665.
25. Jiansu , M., , Yanchun, D.U. , Hong, C, Pan, J., *Energy Efficiencies of Industrial Sectors for China's Major Cities.* Procedia Environmental Sciences, 2010. **2**: p. 781–791.
26. Bujold, M., Martin, G., Spector, M., *Industrial Land Use Study and Employment Policy Plan*. 2006, Minneapolis City Council.
27. Myriam, M., Nicolas, D., Frédéric, M., *A pragmatic way of achieving Highly Sustainable Organisation: Governance and organisational learning in action in the public French sector.* Safety Science, 2014. **69**: p. 18-28.
28. Anthony, A., Dorothea ,H., *From too little to too much innovation? Issues in measuringinnovation in the public sector.* Structural Change and Economic Dynamics, 2013. **27**: p. 146– 159.
29. Bogdan, G.Z., Anca,S.S, *Recent changes in public sector efficiency in Romania: determinants and implications.* Procedia - Social and Behavioral Sciences, 2012. **58**: p. 423 – 433.
30. Ashley , L., MS, Christine, J. C., Lynn, D. S., Sonia, Y. A., ,

Toward a Healthier City Nutrition Standards for New York City Government. American Journal of Preventive Medicine, 2014. **46** (4): p. 423–428.
31. Bernard, A., , Nigel ,J. S.,Denise, B., *What risks are common to or amplified in programmes: Evidence from UK public sector infrastructure schemes.* International Journal of Project Management, 2011. **29**: p. 303–312.
32. Ida, L., Gabriella, J., *Electronic services in the public sector: A conceptual framework.* Government Information Quarterly, 2013. **30**: p. 163–172.
33. Falin , C., Shyi,M.L, Kuo,T.T, Si,C.L,, Eric, W., *Assessment of renewable energy reserves in Taiwan.* Renewable and Sustainable Energy Reviews, 2010. **14**: p. 2511–2528.
34. Rodrigo, S., Julio, V., *Thermal power plant efficiency enhancement with Ocean Thermal Energy Conversion.* Applied Thermal Engineering, 2014. **62**: p. 105-112.
35. Young, G.L., Hyung,J.J, Soon-,J.Y, *Design and installation of floating type photovoltaic energy generation system using FRP members.* Solar Energy, 2014. **108**: p. 13-27.
36. Oriol, G.B., Adrià,J.F, Andreas, S., Samuel ,G.A, *Maximum generation power evaluation of variable frequency offshore wind farms when connected to a single power converter.* Applied Energy, 2010. **87**: p. 3103–3109.
37. Mohd Zamani, A., Idris. , J., Sunarsih, Loke.,K.B., Hanani.,A. Z. N. , *Liveability Factors For Long Term Habitable Offshore Megafloats.* Hindawi Publishing Corporation, 2014. **in submitted**.

Study on Subsea Petroleum Pipeline Design in Deepwater

Abd Khair Junaidi,[a] and Jaswar Koto,[a,b,*]

[a)]*Department of Aeronautics, Automotive and Ocean Engineering, Mechanical Engineering, Universiti Teknologi Malaysia, Malaysia*
[b)]*Ocean and Aerospace Research Institute, Indonesia*

*Corresponding author: jaswar,koto@gmail.com

Paper History

Received: 25-October-2014
Accepted: 13-November-2014

ABSTRACT

Developments of offshore pipeline projects in Malaysia waters are showing general trend towards deeper water, such as KIKEH in 2200 meter water depth. As the exploration is getting into deeper water or crossing a deep water section. The different design issues may become governing compared to shallow water. Several number of issues are needed to be taken onto account in the design of pipelines in deep water such as aspect related to high external pressure, limitation for installation and geo-hazards are addressed. In order to give an early insight for designer to measure the reliability for a deep water project to current technology capabilities, a simulation program is required to achieve the objective.

KEYWORDS: *Design; Deep Water; Subsea Pipeline*.

1.0 INTRODUCTION

Demands on petroleum as the main source of energy with the maturity of established oil reserved in onshore and shallow water has influenced for many oil and gas companies to extend their operation further into deep water as fact that most shallow water oil basin has been almost fully utilized. As a result of this shifting of offshore oil and gas production further away from shore, the pipelines have to be laid in deeper waters and over longer distances. During last 30 years, significant reserves have been located offshore in places like North Sea, the Gulf of Mexico, the Persian Gulf, offshore Brazil, West Africa, Malaysia, Indonesia, Northwest, Australia and other places.

In this study we will discuss on conceptual design for deep water. Design issues associated with deep water pipelines are pressure containment, hydrostatic collapse, local buckling, propagation buckling, on-bottom stability, plastic strain limits, free spanning as well as fatigue and fracture aspects. The effects of fabrication tolerances such as ovalisation and wall thickness variation on hydrostatic collapse and the design of buckle arrestors also need to be considered. Manufacturing capabilities for large diameter pipe also taking consider design reliability.

2.0 LITERATURE REVIEW

The ocean covers 70% of our planet and is a huge bank of energy waiting to be extracted. This makes the prospect of the ocean as an alternative energy source immense. Marine renewable energy comes in various forms, namely ocean thermal gradient, tidal range, ocean currents, ocean waves and ocean salinity gradient. For each form, there are a number of ways to convert the energy into a useful form such as electricity.

2.1 Hydrostatic Collapse Pressure Buckling

Pipeline wall thickness design is one of the most critical design considerations that have to be done before pipeline construction. This will affect the pipes resistance against internal- and external pressure, the allowed corrosion, and the influence of longitudinal stress, bending and indentation, as well as the cost aspect.

As the pipeline is installed deeper into the sea by lay barge, the pipelines are typically subjected to external pressure due to hydrodynamic pressure. The pipelines are designed to withstand external pressure at possibility when there is no fluid in pipeline (no internal pressure. This differential pressure between external and internal pressure acting on the pipe wall due to hydrostatic head can cause pipe to collapse.

The collapse pressure predicted by these formulas should be compared to the hydrostatic pressure due to pipeline depth at seabed, in order to choose the most adequate and feasible diameter and wall thickness for particular range of depth.

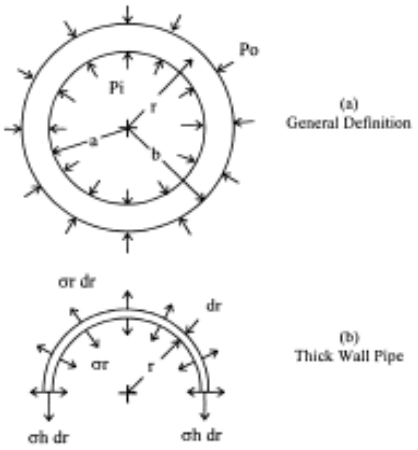

Fig.1 Pressurized Pipe System [2].

2.2 Buckle Propagation

A buckle resulting from excessive bending during installation or any other cause may propagate along the pipe due to presence of hydrostatic pressure by the seawater acting on the pipeline. For deep water pipelines, since the hydrostatic pressure is the major force that cause failure mode of pipeline, it is essential to estimate buckle propagation. Buckle arrestors may be used to stop such propagating buckles by confining a buckle/collapse failure to the interval between arrestors. Buckle arrestors may be designed as devices attached to or welded to the pipe or they may be joints of thicker pipe. Buckle arrestors will normally be spaced at suitable intervals along the pipeline for water depths where the external pressure exceeds the propagating pressure level. The following are types of buckle arrestors;

- Integral Thick Wall Arrestors which consist of suitable length of thick walled joints.
- Integral Ring Arrestors which comprise forged or machined rings that are welded in between pipe joints.

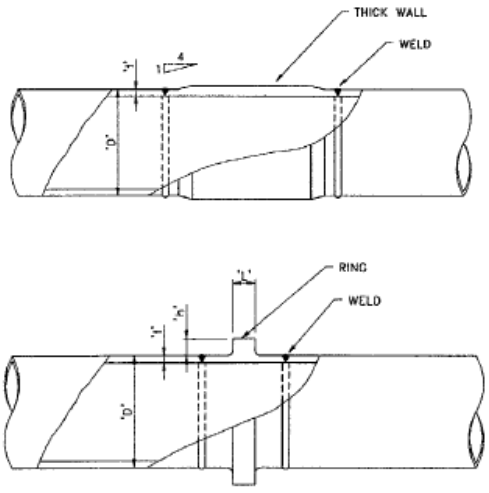

Fig.2 Integral Thick Wall and Integral Ring Type Buckle Arrestors [3].

2.3 Pipe-laying Limitation

In recent years, offshore oil and gas exploration and production activities have increased dramatically in deep waters. The offshore pipelines have to be laid to the seabed of corresponding water depth to gathering and transporting the products. The safety of offshore pipelines in complicated loading conditions such as high ambient pressure, axial tension and bending moment during deep water installation has drawn more attentions than shallow waters.

There are two common methods applied for installing offshore pipelines;

- S-Lay
- J-Lay

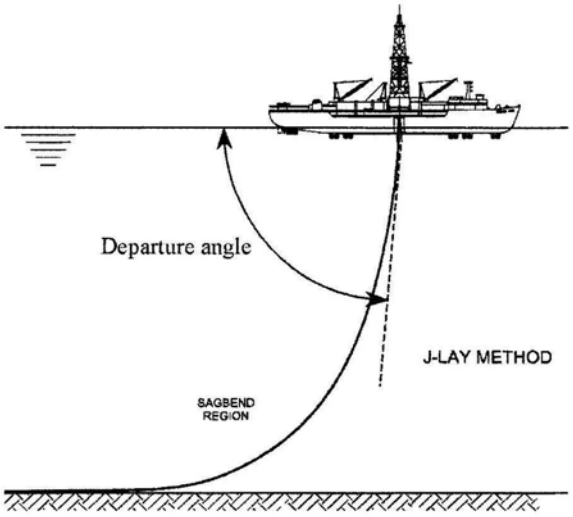

Figure 3: Schematic of J-Lay method for pipe laying.

J-Lay is one of method applied for deep water pipeline installation. As name implies, J-Lay laid the pipeline from the vessel nearly vertical position forming characteristic of J-shape. The J like shape of the pipeline segment during installation has been found to have advantages for laying deep waters, as there is no over bend region (only sag bend at lower curvature) and less tension required than for the S-Lay.

2.4 Geo-Hazards for Route Selection

Ultra deep water routes descend the continental slope into water depth in excess of 2000m.These slope areas are the main paths of sediment transfer from the continental shelves to the deep ocean basin. Hazard that can impact on the pipeline originate from fault rupture and slope failures that may cause long term processes such as landslides, turbidity flow and gravity flow, soil liquefaction and combination of these events.

Free span can result in failure of pipelines due to excessive yielding and fatigue. It may also cause interference with human activities such as fishing. Free span can occur due to unsupported

weight of the pipeline section and dynamic loads from waves and currents. When a fluid flows across a pipeline the flow separates, vortices are shed and periodic wake is formed. Each time a vortex is shed it alters the local pressure distribution and the pipeline experiences a time-varying force at the frequency of vortex shedding. Under resonant conditions, sustained oscillations can be excited and the pipeline can eventually lead to catastrophic failure. The oscillations are normally in-line with the flow direction but can be transverse (cross-flow) depending on current velocity and span length.

3.0 METHODOLOGY

In this study, a simulation program that functioned to perform FEED design for pipeline is developed using Microsoft Visual Studio 2012. The algorithm used in this program is based on classification standards such as DNV, API and ABS. The program also verified based on published journal and design reports. The following are steps in methodology.

- Identify problem statement, objectives and literature review.
- Discuss challenges involves for deep water pipeline design.
- Code development (C-Deep) and perform simulation based on case study on wall thickness selection, buckle arrestor design and free spanning and installation configuration
- Results, Discussion and Conclusion

3.1 Code Development for Conceptual Design

Microsoft Visual Basic 2012 was selected as the main tools in orders to develop the simulation program. Microsoft Visual Studio is an integrated development environment (IDE) from Microsoft. It is used to develop console and graphical user interface application along with Windows Forms which is making it very user friendly to the programmer as well to the program user compared to others code developer program such as Fortran and Matlab which required the users to understand at least few commands to run the codes.

Table 1: Pipeline Design Simulation Program Developed (C-Deep).

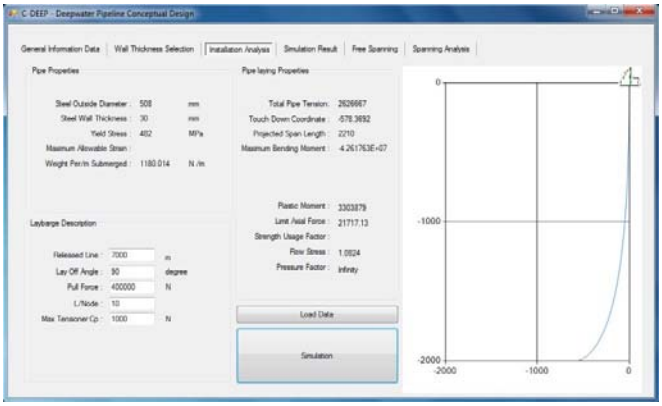

3.2 Programming Flow Chart

Before developing the simulation program, a programming flow chart was outlined systematically in order to achieve the objectives of this study. This step is very essential for any code development works as its provide a systematic and clear on flow of the program as well to prevent any unhandled exception due to unstructured flow.

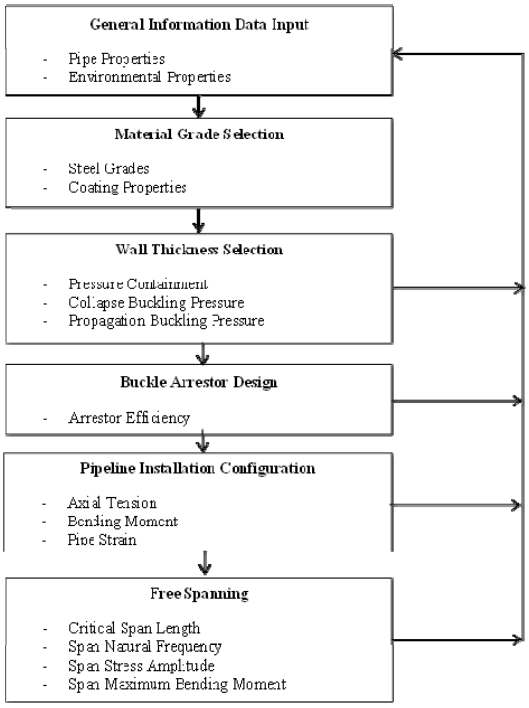

Figure 4: Programming Flow Chart for the Overall Simulation Program

4.0 RESULTS AND DISCUSSION

4.1 Wall Thickness Selection

Wall thickness selection due to collapse buckling pressure is obtained by using three different high strength steel grades namely X60, X65 and X70. The output of collapse pressure obtained from the simulation and plotted as show in Figure.5. By using higher strength steel grade has a higher effect on wall thickness requirements especially for deeper water compared to shallow water. Wall thickness generally will affect both cost and weight and by using higher steel grade these both parameters can be greatly reduced especially when involving high external pressure. Wall thickness reduction as a result of increased steel grades is depending of pipe diameter when using pipe collapse requirement. The percentage increment of collapse pressure among the steel grades is increasing to respective wall thickness.

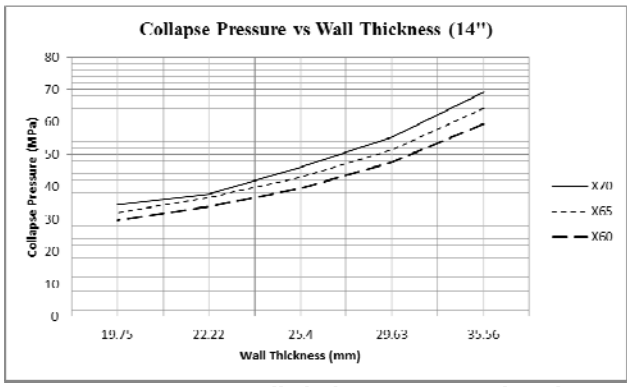

Figure 5: 14" Pipe: Wall Thickness against Steel Grade.

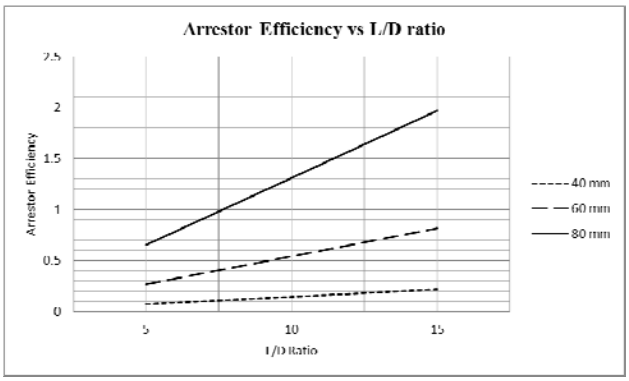

Figure 6: Integral Arrestor Efficiency versus L/D ratio of Buckle Arrestor.

4.2 Buckle Arrestor Design

Integral ring arrestor is used in this study as it is known for its good efficiency buckle arrestors by most. These arrestors directly increase wall strength by welding it to pipe and hereby increasing thickness of one section of pipe. The plotted results for the arrestor efficiency show in Figure.6. From Figure.6 we observe that the arrestor efficiency can be increased significantly by increasing its thickness. Therefore, we can conclude that arrestor efficiency is greatly affected by increasing thickness compared to length.

4.3 Installation Configuration

The results obtained from static installation analysis for J-Lay from the simulation program based on general information data input. Results presented in the following are provided to prove lay ability of the given pipelines with existing lay vessels as shown in Table.2. The installation configuration for 90^{o} was setup with 400kN horizontal force as shown in Figure.7. The result from the simulation is based on simple catenary equation not including flexural stiffness on sag bend. The seabed is assumed as rigid and plane and no hydrodynamic loads acting on the pipe with water depth of 2000 meter. The following conclusion were achieved,

- Top tension required for pipeline installation were found to be within the tension capacities of existing vessels at 2000 meter water depths.
- Sag bend bending moment were inside the allowable bending moments at 2000 meter water depth
- Departure angles required are within the vessels ability

Table 2: J-Lay Pipe Installation Results

Lay-off angle	Horizontal Pull Force (kN)	Projected Span length (m)	Touchdown point along axis from vessel (m)	Top tension load (kN)	Sag bend bending moment (kNm)
80	400	2360	978	2639.5	372004
90	400	2260	602	2529.80	370260
90	1000	2310	830	2742.32	314019

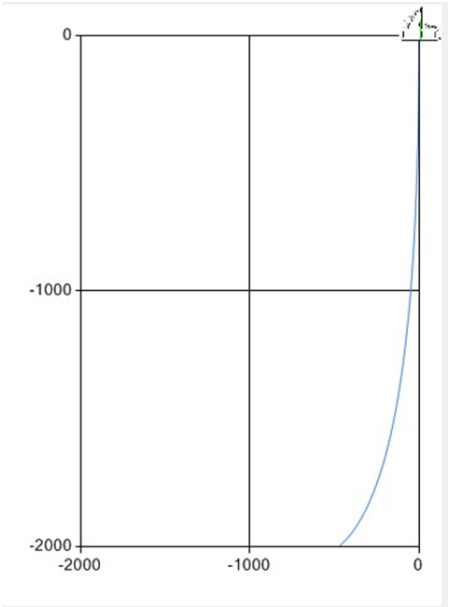

Figure 7: Static Pipe-Lay Configuration for (a) 90o angle 400 kN force.

4.4 Free Spanning

The results obtained from the free spanning section of the simulation program. The simulation is based on 20" diameter pipeline with 25.4 mm wall thickness. The pipe weight is based on flooded condition which is the most risky condition for free span. The plotted results obtained as shown in Figure.8

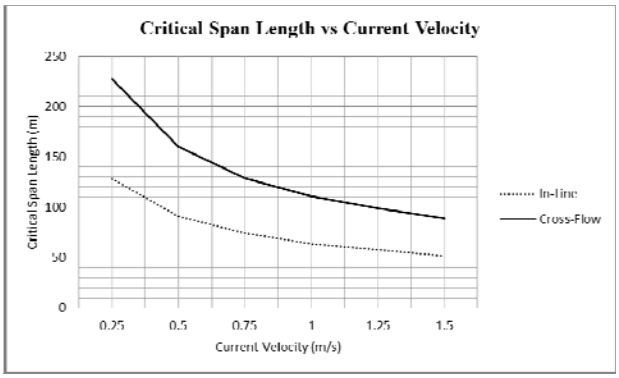

Figure 8: Graph for the Critical Span Length against the C urrent Velocity.

5.0 CONCLUSION

As conclusion from this study, numbers of issues associated in designing deep-water pipeline are was delivered in this paper and to put into application a simulation program was developed that function to perform preliminary design for deep water pipeline. The program developed was verified based on published journals and a simulation based on case study was performed.

ACKNOWLEDGMENTS

The authors are very grateful to Universiti Teknologi Malaysia and Ocean and Aerospace Research Institute, Indonesia for supporting this study.

REFERENCES

1. Det Norske Veritas, DNV 2007, Offshore standard DNV-OS-F101, Submarine Pipeline Systems, Hovik Norwat, Det Norske Veritas, DNV
2. API Recommended Practice 1111 (1999) 'Design, Construction,Operation, and Maintenance of Offshore Hyrdocarbon Pipelines (Limit State Deign)', American Petroleum Institute.
3. S. Braskoro, T.D.T. Dronkers, M. van Driel (2004). From Shallow to Deep: Implications for Offshore Pipeline Design. Journal of the Indonesian Oil and Gas Community, pp.1-9, 2004
4. Mohd Nazree Mohmed. Design, Fabrication and Testing of Wave Energy Float. B. Eng. Thesis. Universiti Teknologi Malaysia; 2009
5. T. Sriskandarajah, P. Ragupathy, G. Anurudran and R. Wilkins (2001), Design and Installation Aspects in the Use of High Strength Steels for Deep and Ultra-Deep water Pipelines, The International Society of Offshore and Polar Engineers, 2001
6. Yong Bai, Ragnar 19land and Torgeir Moan(1992), Collapse of Thick Tubes Under Pressure, Tension, Bending and Their Combinations, The International Society of Offshore and Polar Engineers (1992)Heights Data in South China Sea ", International Conference on Marine Technology MTP-21
7. T.G Johns, R.E Nesloh and J.E Sorenson (1976), Propagating Buckle Arrestors for Offshore Pipelines, Battelle Columbus Laboratories (1980)
8. S.A Karamanos and J.L Tassoulas (1991) Stability of Deep water Pipelines Under Combined Loading, 1991
9. Z.G Li (2010), Configuration of Submarine Pipeline for Deep water S-Lay Technique, The International Society of Offshore and Polar Engineers (ISOPE)(2010)
10. Guarracino, F. V., Mallardo (1999), "A refined analysis of submerged pipelines in seabed laying", Applied Ocean Research, vol. 21, 1999.

Application of Quasi-Continuous Vortex Lattice Method to Determine Aerodynamic Characteristics of Helicopter Tail Rotor Propeller

Firdaus,[a], Jaswar Koto,[a,b,*], M.S Ammoo, [a], and Iskandar Shah Bin Ishak,[a]

[a)]*Department of Aeronautical, Automotive and Ocean Engineering, Faculty of Mechanical Engineering, Universiti Teknologi Malaysia*
[b)]*Ocean and Aerospace Engineering Research Institute, Indonesia*

*Corresponding author:jaswar@fkm.utm.my and jaswar.koto@gmail.com

Paper History

Received: 15-October-2014
Accepted: 16-November-2014

ABSTRACT

Application of Quasi-Continuous Vortex Lattice Method (QCVLM) was widely used to predict the performance of propeller in open water and behind the hull of ships. In other hand, the application the QCVLM in aeronautics is less than in marine. This paper reviews on application of quasi continuous vortex lattice method for determining the performance of helicopter tail rotor propeller. Tail rotor blade for Bell B206 of one seat helicopter is used. The prototype helicopter was manufactured in the Aeronautics Laboratory, Universiti Teknologi Malaysia.

KEY WORDS: *Helicopter Tail Rotor Propeller; Quasi Continuous Vortex Lattice Method; Bell B206*.

NOMENCLATURE

VLM	Vortex Lattice Method
MFM	Mode Function Method
QCM	Quasi Continuous Method
SSPM	Simple Surface Panel Method
CFD	Computational Fluid Dynamic

1.0 INTRODUCTION

The propeller is the device that mainly used as propulsive for marine vehicles, airplanes and rotorcraft. As it is a crucial part, it has to be designed to meet power requirement at the indicated speed with optimum efficiency. Now days, with growing demands for of higher speed and greater power, the propeller is becoming increasingly larger in size and its geometry shape become more complicated. Due this complicated geometry, the propeller should be optimally designed for increased propulsion efficiency.

To predict the steady and unsteady propeller characteristics, many numerical models and propeller theories were proposed. One of them and will be used in this study is based on lifting surface theory. The lifting surface theory also plays as important role in the hydrodynamics analysis of marine propeller. The theory has been developed for a long time in the field of aeronautics. While almost all of the applications of the theory are to wings of airplanes, there is an old application to screw propellers (Kondo, 1942).

A number of methods based on lifting surface theory to estimate the propeller characteristics have been published. They can be classified into two groups. One group is based on the continuous loading method such as Mode Function Method (MFM) and the other the discrete loading method such as Vortex Lattice Method (VLM). Due to the complexity in numerical calculation using MFM, its application to unconventional

propellers is not easy. VLM, however, also has some room to be improved; in the neighborhood of leading edge, vortex strength predicted by VLM is always lower compared with analytical solutions. Owing to the discrete and concentrated loading distribution, pressure distribution is not estimated straightforwardly. Leading edge suction force is not estimated straightforwardly either. A large number of elements are necessary to get converged solutions (Naoto Nakamura, 1985).

Taking the above circumstances into consideration, a numerical method to estimate aerodynamics characteristics of helicopter tail propeller based on Quasi-Continuous Method (QCM) will be developed. QCM has both advantages of continuous loading method and discrete loading method; loading distribution is assumed to be continuous in chord-wise direction and stepwise constant in span-wise direction. Simplicity and flexibility of discrete loading method are also retained.

2.0 LITERATURE REVIEW

2.1 Quasi Continuous Method Theory

C. Edward LAN (1974) has developed a quasi-continuous method for solving the thin wing problem. In his study, the spanwise vortex distribution is assumed to be stepwise constant while the chordwise vortex integral is reduced to a finite sum through a modified trapezoidal rule and the theory of Chebychev polynomials, in order to satisfying the boundary condition. Wing edge and Cauchy singularities are accounted for, based on two-dimensional theory; that contain the conventional Vortex Lattice Method and the present analysis. Based on his conclusions, the wing square-root singularities and the Cauchy singularity has been properly accounted for in this method, compared to the conventional vortex lattice method. The total aerodynamic characteristics are obtained by an appropriate quadrature integration. The two-dimensional results for airfoil without flap deflection reproduce the exact solutions in lift and pitching moment coefficients, the leading edge suction, and the pressure difference at a finite number of points. For a flapped airfoil, the present results are more accurate than those given by the vortex lattice method. The three dimensional results also show an improvement over the results of the vortex lattice method.

Naoto Nakamura (1985) has conducted research on estimation of propeller open- water characteristics base on Quasi – Continuous Method. This study show that comparisons of propeller open-water calculated by this method with measured data showed good agreement for a wide variety of propellers. This method is promising for the improvement of numerical methods in propeller lifting surface theory. However, for propeller with extremely large skew, the estimation accuracy was not so good. Nakamura recommended for improvement, a more realistic wake model should be formulated based on the geometry of slipstream such as contraction, variation of pitch etc. Force acting on source distribution and leading edge suction force should be properly accounted for. And lastly, more exact treatment of blade thickness is necessary for the improvement in the calculation accuracy of pressure distribution on blade surface.

J.Ando and KuniharuNakatake (1999) have conducted a calculation method for the three – dimensional unsteady sheet cavitation hydrofoil problem. This method is based on simple surface panel method “SQCM” which satisfied easily the Kutta condition even in the unsteady condition problem. This method uses source distribution (Hess and Smith, 1964) on the hydrofoil surface and discrete vortex distribution arranged on the mean chamber surface according to QCM (Quasi-Continuous vortex lattice Method) (Lan, 1974). These singularities should satisfied the boundary condition that the normal velocity is zero on the hydrofoil and the mean camber surface. The partially cavitation hydrofoil was treated in heaving motion and both partially cavitation and super cavitation was in sinusoidal gust. The calculated results ware compared with other calculated results and the accuracy of the present result is confirmed.

J. Ando and K. Nakatake (2000) have conducted research on a new surface panel method to predict steady and unsteady characteristic of marine propeller. These methods represent the flow field around a wing by the source and the doublet distributions on the wing surface, and are applied successfully to calculation of the pressure distribution on the propeller blade. But it is not easy to satisfy the Kutta condition at the tailing edge and many discussions were raised about it (Koyama, 1989). A reasonable expression of the Kutta condition is that the pressure becomes equal on the upper and lower wing surfaces at the tailing edge. In order to satisfy the above condition, it is need to solve iteratively the quadratics simultaneous equations for singularity distributions. They have developed a new surface panel method which is a kind of singularity method. This method uses source distributions (Hess and Smith, 1964) on the wing surface and discrete vortex distribution arranged on the chamber surface according to quasi-continuous method vortex lattice method (QCM) (Lan,1974). Then these singularities both the wing surface and the camber surface condition that the normal velocity should be zero in case of the steady problem. Since these singularities satisfy automatically Kutta condition, they not need use any iterative procedure. In case of the unsteady problem, they introduce the normal velocity to the chamber surface at the trailing edge in order to make the pressure difference between the upper and the lower wing surface zero. Even though the iterative procedure to satisfy the Kutta condition is necessary, the convergence is quite fast. They named this simple surface panel method SQCM (source and QCM). In SQCM, the upper and the lower surface of the propeller blades are divided into the same numbers of source panels, respectively. Then the ring vortices are located on the mean chamber according to the unsteady QCM (Hoshino, 1985) (Murakami et al., 1992). The hub surface is also divide into source panels. The trailing vortices flow out as ring vortices from the trailing edge every time step. They assume that the trailing vortices leave the trailing edge in tangential to the

mean chamber surface and the pitch of trailing edge vortices reach an ultimate value, which is the mean of geometrical pitch distribution of the propeller blade, within a haft revolution. They solved the boundary conditions every time step Δt. The source distributions on propeller blades and hub surface and the vortex distributions on the chamber surface are obtained for each time step from the boundary conditions at the center of the source panels and control points on chamber surfaces whose positions are determined by the QCM theory. Here the pressure Kutta condition is considered simultaneously. The perturbation potentials and velocity distributions on the blade surfaces are obtained from the singularity distributions. The pressure distributions are calculated by the unsteady Bernoulli's equation. Then the force acting on propeller blades are obtained by pressure integration on the propeller blade.

J.Ando (2009) has done the numerical analysis of steady and unsteady sheet cavitation on a marine propeller using a Simple Surface Panel Method (SSPM). This SSSPM uses source distribution on propeller blade surface from Hess & Smith (1964) and discrete vortex distributions arranged on the camber surface according to QCM (Quasi-Continuous vortex lattice Method) by Lan (1974). The singularities satisfy the boundary condition that the normal velocity is zero on the propeller blade and mean chamber surface. From this analysis Jun Ando concluded that present method can predict the thrust and the torque in extensive advance coefficients and cavitation numbers. For unsteady case, this method can express the variations of the cavity area and cavity volume. And the cross flow effect on the cavity surface gives reasonable cavity shapes and variations of cavity area and volume especially in HSP.

2.2 Lifting Surface Theory

Research on application of the lifting surface theory to marine propeller was carried out by Koichi Koyama (2012). In this research they use three methods, named here Method 1, Method 2, and Method 3, of propeller lifting surface theory proposed by Hanoaka (1969). Method 1 and Method 3 in this research belong to mode function method group, and Method 2 belongs to discrete function method group. Method 1 may be called series expansion method. Two – dimensional integral equation for lifting surface is converted into simultaneous one-dimensional integral equations, in expanding the two-variable integral equation in power series of one- variable by Taylor' theorem and equating the coefficient functions of successive powers to zero. The method is equivalent to Flax's method on condition that the mode function is orthogonal series. The method, however, is distinguished by easy calculation of coefficients of simultaneous equations in comparison with Flax's method. The method can deal with the simple mean chamber line accurately without many chordwise control points in contrast to the collocation method. The method reduces the labour for numerical integration along the helical surface to the minimum. Especially for the case of unsteady condition, the machine running time for calculation not long. In Method 2, existing integral equation is solved by the doublet-lattice method. The blade is divide into many blade element by cylindrical surface, and each blade element is divided into many boxes. Surface distribution of doublet in the pressure field is replaced by line doublets with constant strength and direction in every box. The chordwise arrangement is determined by Lan's method, which is devised so as to give the accurate solution near the leading edge. Method 1 yields valid circulation density in wide range near the tip and yields valid circulation of blade section in all range for the usual broad bladed propeller. The method is useful for the calculation of propeller forces. Method 2 gives the converged chordwise distribution of circulation density. It is supposed to give the accurate solution near the leading edge and to be useful for the calculation cavitation. Method 3 yield the accurate solutions for the circulation density near the blade tip as well, even though the blades are highly broad. The method is considered useful for the calculation of cavitation. There are many possibilities of application of the propeller lifting surface theory to the propeller design. The following are some examples of the application method to be employed in the design procedure. The blade outline is adjusted according to the inflow variation of hull wake from the view point of vibratory propeller forces, when Method 1 is useful. If the blade outline is given, the relation between upwash and loading is controlled by the lifting surface theory. If the pitch of the helical surface is assumed to fix, single calculation of the matrix of coefficient corresponding to the integral equation, make it possible to obtain upwash distribution and to obtain loading distribution by the upwash distribution with ease. In this case, Method 2 and Method 3can control accurately the pitch correction or chamber correction in the design method, from the cavitation point of view.

Koichi Koyama (2012) has conducted relation between the lifting surface theory and the lifting line theory in the design of an optimum screw propeller. This research is based on the propeller lifting surface theory. Circulation density (lift density) of the blade is determined by the lifting surface theory on a specified condition in general. However, it is shown that, in the case of optimum condition, the circulation density is not determined by the lifting surface theory, although the circulation distribution which is the chordwise integral of the circulation density is determined. The reason is that the governing equation of the optimization by the lifting surface theory is reduced to that by the lifting line theory.

2.3 Propeller

Davide Grassi has done numerical for analysis of the dynamics characteristics propeller in uniform and stationary inflow by lifting surface theory where this lifting surface analysis method based upon Kerwin (1978) theory. These procedures employs a simplified defined shape for representing propeller wake geometry which given good results for moderately skewed blade geometries not too far from their design point, while tend to overestimate thrust and torque at low advance coefficient. To

overcome this difficulties, DavideGrassi was employed this analysis fully numerical wake adaption method. The present tool employs a discrete vortex line representation of the blade, with elements located at the exact mean surface. The leading edge suction and tip vortex separation was consider in an accurate and efficient way. The propeller was assumed to work in an inflow with radially varying axial and tangential component, while the presents of the hull hub and free surface is discounted. The blade force calculation was separated into three components, force acting on vortex sheet elements that determined by using Kutta – Joukowski theorem, force acting on source singularity determined by using Lagally's theorem, and viscous drag forces are calculated at each radial position using a global frictional coefficient experimentally. Tip separation effect has been considered based on the Kerwin's formulation. These segment with the local velocity vector is necessary to align, since chordwise vortex element are to be force free. Vortex ring corner points placed at bladed tip are all shifted in a direction normal to the mean surface by a quality linearly proportional to its position on the tip chord. The effect of tip vortex separation is in the logically to increase propeller thrust and torque at low advance coefficient, while its effect is negligible around the design advance coefficient.

A. Brocklehurst (2012) has make the review of helicopter tip shapes to discussed the evolution of helicopter blade designs and tip shapes, and the development of methods for their analysis and evaluation. The review has identified three main types of helicopter tip designs: the parabolic tip, the swept (tapered) tip, and the BERP tip. In addition there are several tip shapes intended to alleviate BVI noise by splitting, or diffusing the tip vortex. The literature review has identified some overlap with fixed-wing aircraft, particularly with regard to tip aerodynamics and the details of vortex formation. While there are some obvious fundamental differences, both fixed-wing and rotary-wing con-figurations require accurate resolution of the flow-field if the results are to be useful in tip design studies. The nature of the helicopter problem is, however, much more complex than fixed-wing and is much more demanding from a modelling point of view due to the need to preserve wake vortices, take into account variations in incidence and sideslip (in cruising flight), and also include unsteady effects. The design must also work within much tighter moment constraints. Nevertheless, much can be learnt from validating the methods against fixed-wing tests, and there is considerable carry-over in some of the detailed design thinking. In particular, the work of Hoerner and K¨uchemann has provided a basis for generating improved tip shapes. The review has also covered the development of computational methods. Analysis techniques have developed from rotor models based on lifting-line and lifting-surface theory, with a prescribed or free wake, to the application of sophisticated CFD methods. Initially the numerical approach required some of the world's largest computers, but these modern methods are now becoming available in industry, and offer greater insight and higher resolution than traditional design methods. Two main features of the computational approach would appear to require further development for helicopter applications. One is that it is important to fully capture the wake in order to determine the correct flow-field around the rotor blade, and the other is that the solver needs to include boundary layer transition in both steady and unsteady (3D) conditions, if accurate overall performance and the effects of retreating blade stall are to be predicted. Much effort has been expended on coupling wake models with near-field Navier–Stokes solutions in an effort to obtain the desired accuracy at acceptable computational cost. It is also clear that rotor trim and blade deflections are important aspects of helicopter simulation. Often, the rotating and pitching blades may operate in proximity to a stationary fuselage, or fin, and this presents challenges in grid generation, requiring the use of sliding grids, or Chimera overset grid techniques. From the literature there appears to be a preference toward structured grids to resolve the flow features, but some developers favor the Chimera approach. It is also clear that CFD methods are maturing quickly and through rapidly growing computer resources will soon be universally accepted and indispensable for rotor blade design evaluations. Recent research effort on CFD has been directed towards tackling the challenging problems of whole helicopter simulations. Coupling of CFD with structural dynamics to take into account blade deflections has also been a focus of attention, and offers to greatly improve the fidelity of the simulation. Most recently, fast harmonic-balance methods have begun to emerge which promise further run-time reductions for forward flight simulations. However, while CFD has been applied to a range of rotors problems, including investigations of tilt-rotors, little new work has been found on the use of CFD for the design of new tip shapes, particularly for tail rotors.

3.0 UTM ONE SEATED HELICOPTER

One of the very first problems helicopter designers encountered when they tried to create a machine that could hover was the problem of torque reaction (Guo-HuaXu, 2001). Newton's third law of motion requires that for every action there is an equal and opposite action. A typical single main rotor helicopter has a rotor system mounted on a rotor mast. The helicopter engine supplies power so that the helicopter can turn the mast, and thus the rotor system connected to it. When the helicopter applies torque to the mast to spin it, there is an equal-and-opposite torque reaction which tries to turn the helicopter in the opposite direction as shown in Figure 1.

Igor Sikorsky seems to be the first to settle on using a single rotor mounted at the rear of the helicopter as a way to counter the torque. This is the most popular arrangement today. Sikorsky actually experimented with many different arrangements before selecting a single tail mounted rotor. It seems strange that the majority of helicopters produced use this method of countering

torque, given that there are several major problems with this method which are not encountered with counter-rotating rotor systems (J. Gordon Leishman, 2002).

One major problem with tail rotors is that they rob an enormous amount of power. As a rule of thumb, tail rotors consume up to 30% of the engine power (C. Young, 1976).Still another problem with tail rotors is that they are fairly difficult to control accurately. Turbulence and crosswinds make it extremely difficult to hold a constant heading in a tail rotor equipped helicopter. The workload is very high, and good results are difficult to achieve. Many larger helicopters end up being designed with a yaw stabilization system, which is essentially an autopilot for the tail rotor.In the study, one seat helicopter is used as a case study as shown in Figure.2

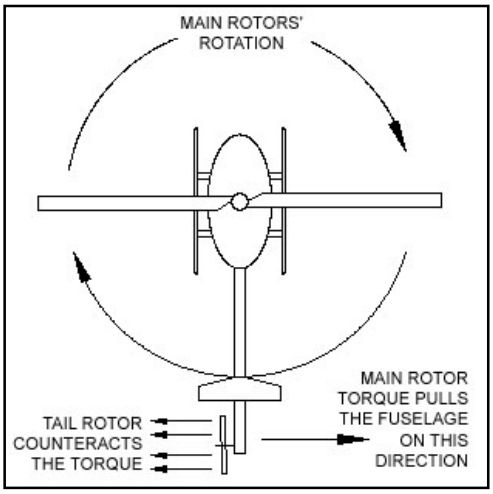

Figure 1: Tail rotor function

Figure.2: One seated helicopter.

3.1 Tail Helicopter Rotor Blade

In this study, offsets coordinate from tail rotor blade for Bell B206 helicopterwill be used as simulation data to calculatethe air forces and other performance characteristics on the rotor blade. Experimental will be done to make comparison with the data from simulation to ensure that data will be valid for both simulation and experimental.

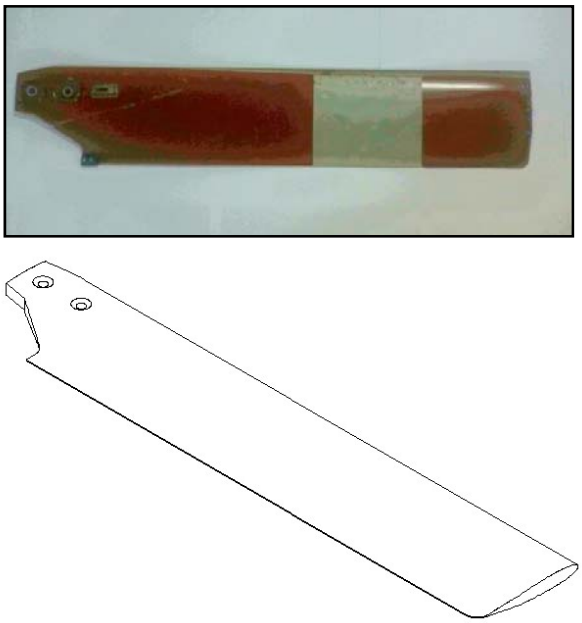

Figure 3: The real model of tail rotor blade for Bell B206.

4.0 QUASI-CONTINUOUS VORTEX LATTICE METHOD

4.1 Outline of QCM

The propeller blade is divided into M panels in the spanwise direction. The face and back surfaces of the blade section are divide into N panels in the chordwise direction, respectively. Therefore, the total number of source panels becomes*(M × 2N) × K* and constant m is distributed in each panel. The total *(M × 2N) × K* horse shoe vortices are located on the mean chamber surface according to Eq. 1 as illustrated in Figure 5.

$$\xi_{\mu\nu}^{LP} = \xi_L(r_\mu) + \frac{\xi_T(r_\mu)-\xi_L(r_\mu)}{2}\left(1 - cos\frac{2\nu-1}{2N_\gamma}\pi\right) \quad (1)$$

$$\xi_{\mu\nu}^{CP} = \xi_L(\bar{r}_\mu) + \frac{\xi_T(\bar{r}_\mu - \xi_L(\bar{r}_\mu)}{2}\left(1 - cos\frac{\nu}{2N_\gamma}\pi\right)$$

where,

$$\bar{r}_\mu = \frac{1}{2}(r_\mu + r_{\mu+1}) \quad (2)$$

μ and ν are numbers in the spanwise and chordwise directions.

$\xi_L(r_\mu)$ and $\xi_T(r_\mu)$ are the positions of the leading edge (LE) and trailing edge (TE), respectively.

The induced velocity vector due to ν-th ring vortex of unit strength which start from the μ-th strip and ones due to the ℓ-th ring vortex of unit strength located in trailing wake defined as $\vec{v}^{\gamma}_{k\mu\nu}$ and $\vec{v}^{w}_{k\mu\ell}$. These induced velocity vectors are expressed as

$$\vec{v}^{\gamma}_{k\mu\nu} = \vec{v}^{B}_{k\mu\nu} + \sum_{\nu'=\nu}^{N_\gamma}\left(\vec{v}^{F}_{k\mu+1\nu'} - \vec{v}^{F}_{k\mu\nu'}\right) - \vec{v}^{ws}_{k\mu\ell}|_{\ell=1} \quad (3)$$

$$\vec{v}^{w}_{k\mu\ell} = \vec{v}^{ws}_{k\mu\ell} - \vec{v}^{ws}_{k\mu\ell+1} + \vec{v}^{wc}_{k\mu+1\ell} - \vec{v}^{wc}_{k\mu\ell}$$

where, $\vec{v}^{B}_{k\mu\nu}$ is the induced velocity vector due to the bound vortex of unit strength on the mean camber surface, $\vec{v}^{F}_{k\mu\nu}$ the induced velocity vector due to the free vortex of unit strength on the mean camber surface, $\vec{v}^{ws}_{k\mu\ell}$ the induced velocity vector due to the spanwise shed vortex of unit strength in the trailing wake and $\vec{v}^{wc}_{k\mu\ell}$ is the induced velocity vector due to the streamwise trailing vortex of unit strength in the trailing edge.

The induced velocity vector $\vec{V}$ due to each line segment of vortex is calculated by the Biot-Savart law. The segment of the ring vortex on the mean chamber surface at time t_L and the ring vortex in the trailing edge wake defined as $\gamma_{k\mu\nu}(t_L)$ and $\Gamma_{k\mu}(t_L)$, the induced velocity vector due to the vortex model of the QCM theory in given by the following equation.

$$\vec{V} = \sum_{k=1}^{K}\sum_{\mu=1}^{M}\sum_{\nu=1}^{N_\gamma}\gamma_{k\mu\nu}(t_L)\vec{v}^{\gamma}_{k\mu\nu}\Delta\xi_L + \sum_{k=1}^{K}\sum_{\mu=1}^{M}\sum_{\ell=1}^{L-1}\Gamma_{k\mu}(t_{L-\ell})\vec{v}^{\gamma}_{k\mu\nu}\Delta\xi_L\vec{v}^{w}_{k\mu\ell} \quad (4)$$

where

$$\Delta\xi_{\mu\nu} = \frac{\pi c(\bar{r}_\mu)}{2N_\gamma}\sin\frac{2\nu-1}{2N_\gamma}\pi, \qquad \Gamma_{k\mu}(t_L) = \sum_{\nu=1}^{N_\gamma}\gamma_{k\mu\nu}(t_L)\Delta\xi_{\mu\nu},$$

and $c(\bar{r}_\mu)$ is the chord length of μ section.

This Equation (4) is used when the control points are on the mean camber surface (J. Ando, 2012). When the control points are on the blade surface, the ring vortices are close to the control points especially for the thin wing. For this case, the ring vortices on the mean camber surface and shed vortex nearest to T.E. treat as the vortex surface in order to avoid numerical error. This is called the "thin wing treatment" (S. Maita, 2000).

J. Ando and T. Kanemaru (2012) has been modify the vortex model of the QCM theory (Fig. 5b) as follows:

For first step, the ring vortex on the mean camber surface at T.E. is close and locate the ring vortices ABCH, HCDG and GDEF downstream from T.E. as shown in (Fig. 5b).

After that the ν-th ring vortex replace with a set of ring vortices distribution along $\Delta\xi_{\mu\nu}(\xi^{CP}_{\mu\nu-1}\sim\xi^{CP}_{\mu\nu})$ on the mean camber surface as illustrated in the middle of Fig. 5b. Then the ring vortex ABCH just downstream from T.E. and ring vortex HCDG are replaced with a set of ring vortices distribution along $\Delta\xi^{w}_{\mu}$ in the trailing wake. The other ring vortices form $\Delta\xi^{w}_{\mu}$ are calculated as discrete ring vortices.

Figure 4: Tail propeller blade of helicopter.

For this case, the induced velocity vectors due to the vortex systems on the mean camber surface and trailing wake are expressed as

$$\overrightarrow{V_\gamma} = \sum_{k=1}^{K}\sum_{\mu=1}^{M}\sum_{\nu=1}^{N_\gamma}\gamma_{k\mu\nu}(t_L)\int_{\xi^{CP}_{k\mu\nu-1}}^{\xi^{CP}_{k\mu\nu}}\vec{v}^{\gamma}_{k\mu}(\xi)d\xi + \sum_{k=1}^{K}\sum_{\mu=1}^{M}\sum_{\nu=1}^{N_\gamma}\gamma_{k\mu\nu}(t_L)\frac{\Delta\xi_{\mu\nu}}{\Delta\xi^{w}_{\mu}}\int_{\xi_T(\bar{r}_\mu)}^{\xi_T(\bar{r}_\mu)+\Delta^{w}_{\mu}}\vec{v}^{ABCH}_{k\nu}(\xi)d\xi + \sum_{k=1}^{K}\sum_{\mu=1}^{M}\Gamma_{k\mu}(t_L-1)\frac{1}{\Delta\xi^{w}_{\mu}}\int_{\xi_T(\bar{r}_\mu)}^{\xi_T(\bar{r}_\mu)+\Delta^{w}_{\mu}}\vec{v}^{HCDG}_{k\mu}(\xi)d\xi + \sum_{k=1}^{K}\sum_{\mu=1}^{M}\Gamma_{k\mu}(t_L-1)\vec{v}^{GDEF}_{k\mu} + \sum_{k=1}^{K}\sum_{\mu=1}^{M}\sum_{\ell=2}^{L-1}\Gamma_{k\mu}(t_L-\ell)\vec{v}^{w}_{k\mu\ell} \quad (5)$$

where

$$\vec{v}^{\gamma}_{k\mu\nu}(\xi) = \vec{v}^{B}_{k\mu}(\xi) + \left(\vec{v}^{F}_{k\mu+1}(\xi) - \vec{v}^{F}_{k\mu}(\xi)\right) + \sum_{\nu'=\nu+1}^{N_\gamma}\left(\vec{v}^{F}_{k\mu+1\nu'} - \vec{v}^{F}_{k\mu\nu'}\right) - \vec{v}^{AB}_{k\mu}$$

$$\vec{v}_{k\mu}^{ABCH}(\xi) = \vec{v}_{k\mu}^{AB} + \vec{v}_{k\mu+1}^{BC}(\xi) - \vec{v}_{k\mu}^{AH}(\xi) - \vec{v}_{k\mu}^{HC}(\xi)$$
$$\vec{v}_{k\mu}^{HCDG}(\xi) = \vec{v}_{k\mu}^{HC}(\xi) + \vec{v}_{k\mu+1}^{CD}(\xi) - \vec{v}_{k\mu}^{HG}(\xi) - \vec{v}_{k\mu}^{GD}$$
$$\vec{v}_{k\mu}^{GDEF} = \vec{v}_{k\mu}^{GD} + \vec{v}_{k\mu+1}^{DE} - \vec{v}_{k\mu}^{GF} - \vec{v}_{k\mu}^{FE}$$

The velocity vector V → around a propeller in the propeller-fixed coordinate system is expressed as

$$\vec{V} = \vec{V}_I + \vec{V}_\gamma + \vec{V}_m, \quad (6)$$

where $\vec{V}_I$, $\vec{V}_\gamma$ and $\vec{V}_m$ are inflow, induced velocity vectors due to vortex and source distributions, respectively.

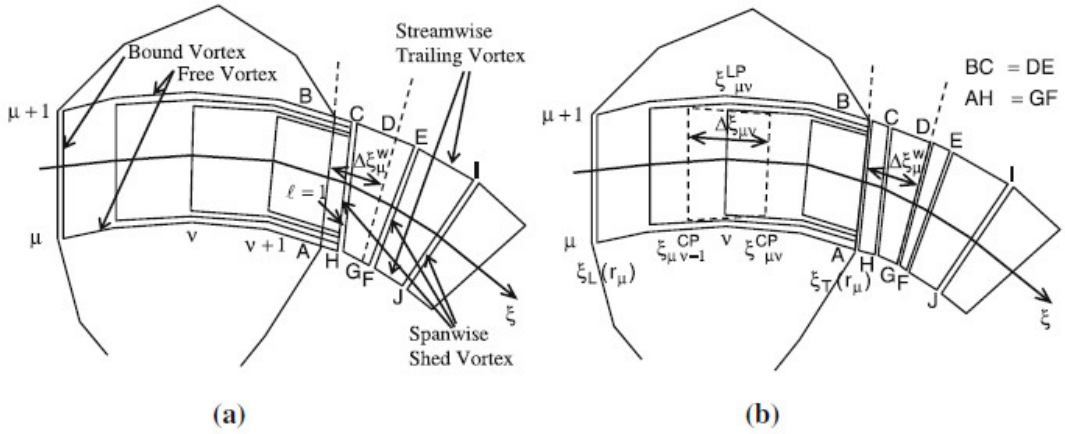

Figure 5: Arrangement of vortex system. a) From QCM. b) Thin wing treatment.

4.2 Boundary Condition and Numerical Procedure

The boundary condition of the control points on the rotor blade and mean camber are that there is no flow across the surface. But, to satisfy the Kutta condition as expressed by Equation (7), there exists at T.E the normal velocity which was introduced. So, the equation for the boundary condition as expressed by Equation (8).

$$\Delta p = \rho \frac{\partial}{\partial t}(\phi_+ - \phi_-) + \frac{1}{2}\rho(V_+^2 - V_-^2) \quad (7)$$

$V \cdot n = 0$ on wing and camber surfaces (except T.E)

$$V \cdot n = V_N \quad \text{at T.E} \quad (8)$$

Where *n* is the normal vector on the blade and mean camber.

The unknown value are the vortex strength on the mean camber surface, source strength on the blade and normal velocity $\vec{V}_N$ at T.E. $\vec{V}_N$ is expressed by the following equation and determined so as to satisfy the Kutta condition iteratively.

$$V_N^{(i+1)} = \frac{\Delta p^{(i)}\beta}{\rho|V_I|} + V_N^{(i)} \quad (9)$$

Where *i* is the number iteration. From the Equation (7), ϕ_+ and ϕ_- or V_- and V_+ are the mean of the magnitude or perturbation potential of the velocity at the control point on the upper and the lower surface blade, where it is close to T.E. This iteration is move on until Δp is small enough. According to J. Ando (2012), in this calculation $\beta = 1$ and β means the accelerations factor. In the unsteady of QCM, the Kutta condition is when $\Delta p = 0$ .The first term in the right hand side in Equation (9) means the corrector for the value of the previous step $V_N^{(i)}$ which is proportional to the pressure difference $\Delta p^{(i)}$. The iteration is continued until the pressure difference becomes small ($\Delta C_p < 0.5 \times 10^{-3}$). Assuming the normal velocity V_N at T.E. at each iterative step, Equation (8) can be solved as the linear simultaneous equations for singularity distributions.

4.3 Unsteady Pressure and Propeller Forces

The unsteady pressure distribution on the propeller blade is calculated by the unsteady Bernoulli equation expressed as

$$p(t) - p_0 = -\frac{1}{2}\rho(|V|^2 - |V_I|^2) - \rho\frac{\partial\phi}{\partial t} \quad (10)$$

Where; p_0 is the static pressure in the undisturbed inflow, p is the density of the fluid and ϕ is the perturbation potential in the propeller coordinate system The time derivative term of ϕ in Equation (10) is obtained numerically by two points upstream difference scheme with respect to time.

The blade pressure of the propeller is expressed as the pressure coefficient C_p in order to compare the calculate results with the experimental data. The pressure coefficient is defined by

$$C_p = \frac{p(t)-p_0}{\frac{1}{2}\rho n^2 D^2} \quad (11)$$

where*n*is the rate of the revolutions of the propeller and D is the diameter of the propeller.

The lift, drag and moment coefficients are given by the relationships

$$C_L = \frac{L}{\frac{1}{2}\rho AV^2}, C_D = \frac{D}{\frac{1}{2}\rho AV^2}, \text{and} C_M = \frac{M}{\frac{1}{2}\rho AlV^2} \quad (12)$$

in which A is the propeller area, l is a reference length, $V$is the free stream incident velocity,ρ the density of thefluid, L and $D$are the lift and drag forces, perpendicularand parallel respectively to the incident flow, and M isthe pitching moment defined about a convenient point.

For analysis purposes, the sectional lift, drag and moment coefficients are given by the relationships

$$c_L = \frac{L}{\frac{1}{2}\rho cV^2}, C_D = \frac{D}{\frac{1}{2}\rho cV^2}, \text{ and } C_M = \frac{M}{\frac{1}{2}\rho c^2V^2} \quad (13)$$

in which c is the section chord length and L', D' and M' are the forces and moments per unit span.

The thrust T and the torque Q of the propeller are calculated by pressure integration. Denoting the x-, y- ad z- components of the normal vector on the blade surface by n_x, n_y and n_z, respectively, the thrust and the torque are expressed by

$$T(t) = \int\int_{S_B+S_H}(p(t)-p_0)n_x ds \quad , \quad Q(t) = \int\int_{S_B+S_H}(p(t)-p_0)(n_y z - n_z y)ds \quad (14)$$

According to Naoto Nakamura (1985), in the steady calculation the viscous components of the thrust and the torque are considered approximately using the viscous drag coefficient of blade element C_d at the radius r. these component T_D and Q_D are expressed as

$$T_D = -K\frac{1}{2}\rho\int_{r_H}^{r_0} C_d(r)\bar{W}(r)\bar{V}_x(r)c(r)dr$$

$$Q_D = K\frac{1}{2}\rho\int_{r_H}^{r_0} C_d(r)\bar{W}(r)\bar{V_\theta}(r)c(r)dr$$

$$C_d(r) = \begin{cases} 0.0084 + 0.016\left(\frac{t}{c}\right) & for\ C_l < 0.2 \\ 0.0084 + 0.016\left(\frac{t}{c}\right) + 0.03(C_l - 0.2) & for\ C_l \geq 0.2 \end{cases} \quad (15)$$

where

c_l = sectional lift coefficient

$\bar{W}(r) = \sqrt{\bar{V_x}(r)^2 + \bar{V_\theta}(r)^2}$

$\bar{V_x}(r)$ = x- component of resultant flow velocity averaged in the chord wise direction

$\bar{V_\theta}(r)$ = θ- component of resultant flow velocity averaged in the chord wise direction

$c(r)$ = chord length of the rotor blade

r_0 = propeller radius

r_H = hub radius

t/c = thickness ratio

The force F_X, F_Y, F_Z and moments M_X, M_Y, M_Z is acting on the propeller in the X, Y, Z directions of the space coordinate system are expressed as

$$F_X(t) = -T(t) = \int\int_{S_B+S_H}(p(t)-p_0)n_x ds$$

$$F_Y(t) = \int\int_{S_B+S_H}(p(t)-p_0)(n_y\cos(\Omega t) + n_Z\sin(\Omega t))\ ds$$

$$F_Z(t) = \int\int_{S_B+S_H}(p(t)-p_0)(n_z\cos(\Omega t) - n_y\sin(\Omega t))\ ds$$

$$M_X(t) = Q(t) = -\int\int_{S_B+S_H}(p(t)-p_0)(n_y z - n_z y)ds$$

$$M_y(t) = -\int\int_{S_B+S_H}(p(t)-p_0)[(n_z x - n_x z)\cos(\Omega t) + [(n_x y - n_y x)\sin(\Omega t)]ds$$

$$M_z(t) = -\int\int_{S_B+S_H}(p(t)-p_0)[(n_x y - n_y x)\cos(\Omega t) + [(n_x z - n_z x)\sin(\Omega t)]ds \quad (15)$$

For the force and moments are non-dimensionalized as below:

$$K_{FX}(t) = \frac{F_X(t)}{\rho n^2 D^4} \quad , \quad K_{FY}(t) = \frac{F_Y(t)}{\rho n^2 D^4}$$

$$K_{FZ}(t) = \frac{F_Z(t)}{\rho n^2 D^4} \quad , \quad K_{MX}(t) = \frac{M_X(t)}{\rho n^2 D^5}$$

$$K_{MY}(t) = \frac{M_Y(t)}{\rho n^2 D^5} \quad , \quad M_{MZ}(t) = \frac{M_Z(t)}{\rho n^2 D^5} \quad (16)$$

And finally the advance J, the torque and the thrust coefficientK_Q, K_T and the propeller efficiency η_p are expressed as follows:

$$J = \frac{V_A}{nD} \quad , \quad K_T = \frac{T}{\rho n^2 D^4}\ K_Q = \frac{Q}{\rho n^2 D^5} \quad , \quad \eta_p = \frac{J}{2\pi}\frac{K_T}{K_Q} \quad (17)$$

5.0 CONCLUSION

In conclusion, this paper reviewed on prediction of performance of helicopter tail propeller using quasi continuous vortex lattice method. As a case study, tail rotor blade for Bell B206 for one seat helicopter is used.

ACKNOWLEDGEMENTS

The authors are very grateful to Universiti Teknologi Malaysia and Ocean and Aerospace Research Institute, Indonesia for supporting this study.

REFERENCES

1. C. Edward Lan. 1974. *A Quasi-Vortex-Lattice Method in*

Thin Wing Theory. The University of Kansas, Lawrence, Kan.
2. Naoto Nakamura. 1985. *Estimation of Propeller Open-Water Characteristics Based on Quasi-Continuous Method*. Spring Meeting of The Society of Naval Architects of Japan.
3. Twenty-Second Symposiums on Naval Hydrodynamics .1999. *Propulsor Hydrodynamics/Hydro acoustics*. Commission on Physical Sciences, Mathematics, and Applications (CPSMA). Page: 110-238.
4. J. Gordon Leishman. 2002. *Principles Of HelicopterAerodynamics.* Cambridge University Press. Page: 28-40
5. Jun Ando and KuniharuNakatake. 2001. *Calculation of Three-Dimensional Unsteady Sheet Cavitation by a Simple Surface Panel Method "SQCM"*. Kyushu University, Fukuoka 812-8581, Japan.
6. Jun Ando, S. Maita and K. Nakatake. 2000. *A New Surface Panel Method to Predict Steady and Unsteady Characteristics of Marine Propeller*. Twenty-Second Symposiums on Naval Hydrodynamics.
7. Koichi Koyama,*on application of the Lifting Surface Theory of Marine Propeller*. Ship Research Institute Tokyo. Japan
8. Takashi Kanemaru and Jun Ando. 2009. *Numerical Analysis of Steady and Unsteady Sheet Cavitation on a Marine Propeller Using a Simple Surface Panel Method "SQCM*". First International Symposium on Marine Propulsors smp'09. Norway.
9. Koichi Koyama. 2012. *Relation between the lifting surface theory and the lifting line theory in the design of an optimum screw propeller*. National Maritime Institute, Japan.
10. T. Kanemaru and Jun Ando. 2012. *Numerical Analysis Of Cavitating Propeller And Pressure Fluctuation On Ship Stern Using A Simple Surface Panel Method ''SQCM''*. Faculty of Engineering, Kyushu University, Fukuoka, Japan.
11. DavideGrassi and Stefano Brizzolara. . *Numerical Analysis of Propeller Performance by Lifting Surface Theory.* Universityof Genoa, Department of Naval Architecture and Marine Engineering, Genova, Italy.
12. Anders Smærup Olsen. 2001. *Optimization of Propeller Using the Vortex-Lattice Method*. PhD Thesis, Technical University of Denmark. Page: 17-50.
13. Anders Smærup Olsen. 2003. *Energy Coefficients for a Propeller Series*. Department of Mechanical Engineering, Technical University of Denmark, Denmark.
14. Hajime Yuasa and Norio Ishii. . *Practical Application of Discrete Vortex Element Method for Calculation of Propeller Induced Excitation Forces.* Mitsui Engineering & Shipbuilding Co., Ltd. Japan.
15. Brocklehurst and G.N.Barakos. 2012. *A Review of Helicopter Rotor Blade Tip Shapes*. CFD Laboratory, Department of Engineering, University of Liverpool, Liverpool L633GH, United Kingdom.
16. JosebaMurua. 2012. *Applications of the Unsteady Vortex-Lattice Method in Aircraft Aeroelasticity and Flight Dynamics*. Department of Aeronautics, Imperial College, London SW72AZ, United Kingdom.
17. A.R.S. Bramwell, George Done, David Balford. 2001. *Helicopter Dynamics Second Edition*. Butterworth-Heinemann, Oxford.
18. Guo-Hua Xu, Shi-Cun Wang. 2001. *Effects ofthe Shroud on Aerodynamic Performance in Helicopter Shrouded Tail Rotor System*. Aircraft Engineering and Aerospace Technology, Vol. 73 Iss: 6, pp.568 – 573.
19. C. Young. 1976. *The Prediction of Helicopter Rotor Hover Performance using a Prescribed Wake Analysis.* Aerodynamics Dept., R.A.E., Farnborough, London.

Prediction of Open Water Propeller Performance Using Steady Quasi-Continuous Method

Hao Rui,[a] and Jaswar Koto,[a,b,*]

[a)]*Department of Aeronautics, Automotive and Ocean Engineering, Universiti Teknologi Malaysia, Malaysia*
[b)]*Ocean and Aerospace Research Institute, Indonesia*

*Corresponding author: jaswar,koto@gmail.com

Paper History

Received: 25-October-2014
Accepted: 13-November-2014

ABSTRACT

This research is targeted to apply the numerical method in the ship's propeller design and analysis. In this thesis, the Quasi Continuous Method developed based on lifting surface theory is applied to predict the performance of propeller in open water condition. To fulfill the desire of industry to obtain an accurate, fast and low cost solution in propeller design, this design and analysis process is proposed made by computer programming software. This is because fast development on computer technology provided the possibility to carry propeller design task by using numerical software. In this research, the Quasi Continuous Method for propeller performance evaluation is applied. This method allows the fast propeller prediction process and low computer cost required. In this research, the VLCC ship model and it propulsion system is preselected. The propeller of the VLCC ship is designed and analyzed using the propeller database system in the numerical software OCARI S-Power. Next, the function of Quasi Continuous Method in the software is applied to predict the open water performance of the designed propeller. Finally, the appropriate propeller model and it dimension is determined in this research. In conclusion, application of numerical software in propeller design is an advance solution where this solution is relatively high efficient compare to the traditional method.

KEY WORDS: *Propeller Blade Design; Quasi Continuous Method; Lifting Surface Theory*

1.0 INTRODUCTION

Ship propulsion system is the important system to ensure the designed ship to sail with requires speed. The system is consisted with several important sub-systems such as the powering system like marine engine, power delivering system like shaft, reduction gear and power extraction system like the propeller. To able the ship sail with determined condition, the propeller play an important role to generate the thrust to push the ship. The function of propeller in the propulsion system is converting the power from engine to thrust where the thrust is worked as the pushing force for ship to move in desire speed.

Due to the interaction between ship hull and propeller, typically the propeller of the ship is custom made to ensure it can work with the optimum performance once install on the ship model. The designed propeller also will test in model scale to confirm the accuracy of the estimated result before it is constructed in the actual scale. However, due to the complexity of the fluid flow phenomena and cavitation effect, the propeller design and analysis task is become very complicated.

The complexity of the propeller working behavior become a main problem in estimate it performance. In current industry development, the propeller design is mostly depended on the empirical method which developed base on the previous experience gain by the company in previous design.

To improve the overall efficiency of the ship propulsion system, more suitable propeller of ship is required. Due to this requirement, many of ship design firms are searching an effective method to optimize the propeller design in the effective way. Besides, the more effective propeller evaluation method can be contributed to improve the propeller design process. Due to the limitation on the evaluation on propeller, most of the propeller evaluation required to have a model scale experiment test.

The objective of this study is to design geometry of propeller of ship, and apply the Quasi Continuous Method to predict open water performance of the designed propeller. The computational method to optimum propeller of the ship was introduced in the research, after that, the Quasi Continuous Method applied in this

research to study the performance of the propeller. This research was investigate the possibility of design the ship propeller by fully computational approach where the approach is more time and cost efficient approach in the design process compared to the experimental approach.

2.0 LITERATURE REVIEW

This chapter is proposed to study the related research achieved by the previous researchers. Besides, this chapter also presented the relate information and finding of QCM method on propeller analysis.

Naoto Nakamura (1985) has conducted research on estimation of propeller open-water characteristics base on QCM. QCM was originally developed by Lan (1974) for solving planar thin wing problems. QCM has both advantages of continuous loading method and discrete loading method; loading distribution is assumed to be continuous in chordwise discrete loading method are also retained [1].

The Propulsor Hydrodynamics (1999) shows the design system of marine propeller ,the basic equations and process of design with a new blade sections based on the lifting-line method and lifting surface method, such as the QCM. In order to improve the cavitations performance, the new blade sections with the prescribed three-dimensional pressure distribution over blade surface are design by the numerical optimization technique [2].

Jun Ando (2009) conducted a calculation method which based on a simple surface panel method “SQCM” which satisfies the Kutta condition easily. For the method, there is some descriptions of how to apply SQCM to the calculation of non-linear cavitations on propeller and show some calculated results about cavitations patterns, cavity shapes and cavity volumes in steady and unsteady flow [5].

3.0 METHODOLOGY

The process of research is show in the Figure 1. To start the research, firstly the objective should be identified and then learn about propeller design and QCM by read literatures. Besides, the ship power test need to do before propeller design because the requirement of power result is necessary for blade design, then apply design and calculations to QCM and study the code. Finally collect the calculation result and analysis the performance.

Besides, due to the limited on the experimental data and propeller model data, this design research only can be using the internal propeller data from the provided propeller design software OcARI S-Power.

To able the performance of the propeller can be analysis by the Quasi Continuous Method and achieve the objective of this research, the dimension of the propeller and it geometry must be determined and obtained from the OcARI S-Power first.

The data analysis process can be separated into two main stage where the first stage of data analysis is propose to study the geometry of the designed propeller and how the propeller include the overall propulsion system performance. While, the second stage of data analysis is the study of performance of the propeller in open water condition.

In the first stage of data analysis, this research will highlight the designed dimension of the propeller.

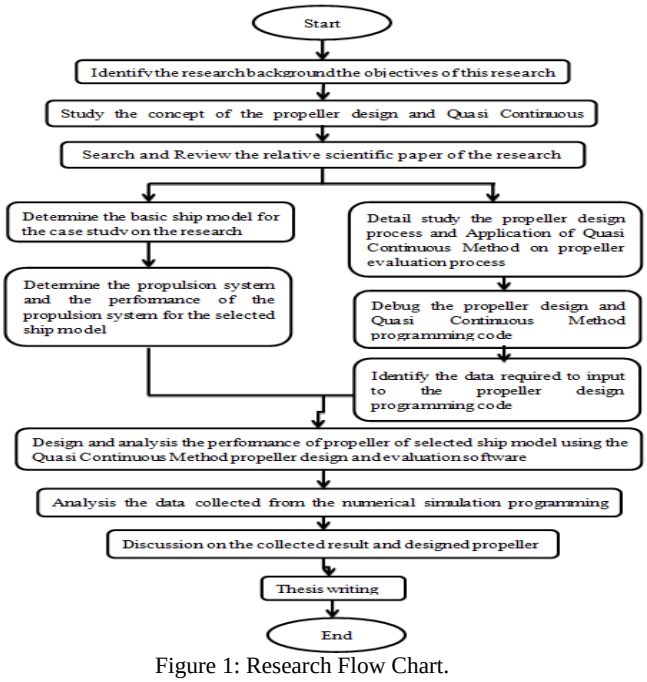

Figure 1: Research Flow Chart.

The second stage of the data analysis is focused in the study of designed propeller open water performance; the data collected from the numerical software provided the information to analysis the distribution force loading on propeller surface.

Besides, the performance of the propeller can be analysis through the open water chart estimate by the Quasi Continuous Method. From the collected open water chart of the designed propeller, the efficiency of the propeller in the selected operating speed range can be identifying.

The performance on the propeller to generate the thrust to the in different engine speed can be analyzed from the open water chart data. This analysis can estimate the overall performance of the ship in different speed due to different operation condition such as voyage and maneuvering during the design.

4.0 MATHEMATICAL MODEL

4.1 Lifting Surface Theory

$$\xi_{\mu\nu}^{CP} = \xi_L(\bar{r}_\mu) + \frac{\xi_T(\bar{r}_\mu)-\xi_L(\bar{r}_\mu)}{2}\left(1-\cos\frac{v}{N_\gamma}\pi\right) \quad (1)$$

$$v_{k\mu l}^{w} = v_{k\mu l}^{ws} + v_{k\mu+1 l}^{wc} - v_{k\mu l}^{wc} - v_{k\mu l+1}^{ws} \quad (2)$$

$$\vec{F}_{\mu\nu} = \rho\vec{V}_{\mu\nu} \times \vec{\gamma}_{\mu\nu} - \rho\vec{V}_{\mu\nu}\sigma_{\mu\nu}\left|\vec{l}_{\mu\nu}\right| \quad (3)$$

$$Fs = \frac{1}{4}\pi pcCs^2 \quad (4)$$

$$\vec{V}_{ij\pm} = \vec{V}_{ij}^{G} + \vec{V}_{ij}^{S} + \vec{V}_{ij}^{I} \pm \frac{1}{2}(\gamma_{ij}\cdot\vec{\tau}_{ij} + \sigma_{ij}\cdot\vec{n}_{ij}) \quad (5)$$

$$Cpij(+-) = \frac{Pij(\pm)-Po}{\frac{1}{2}\rho Wo^2} = 1 - \frac{|Vij\pm|^2}{Wo^2} \quad (6)$$

$$Wo = \sqrt{Va^2 + (\gamma ci\Omega)^2} \quad (7)$$

$$T=To +Ts +Td, \quad (8)$$

$$Q=Qo +Qs +Qd \quad (9)$$

$$Kt=\frac{T}{\rho n^2 D^4}, \quad (10)$$

$$Kq = \frac{Q}{\rho n^2 D^5} \quad (11)$$

$$\eta_p = \frac{J.Kt}{2\Pi Kq} \quad (12)$$

$$T_o = -K\int_{r_B}^{r_o} dr' \int_{S_L}^{S_T} F_x ds' = -K\sum_{\mu=1}^{M} \frac{\pi c_\mu^*}{2N} \sum_{\nu=1}^{N} (F_x)_{\mu\nu} \sin \alpha_\nu \quad (13)$$

$$Q_o = K\int_{r_B}^{r_o} dr' \int_{S_L}^{S_T} (-F_{y\cdot z} + F_{z\cdot y}) ds' = K\sum_{\mu=1}^{M} \frac{\pi c_\mu^*}{2N} \sum_{\nu=1}^{N} [-(F_y)_{\mu\nu} z_{\mu\nu} + (F_z)_{\mu\nu} y_{\mu\nu}] \sin \alpha_\nu \quad (14)$$

$$T_s = K\int_{r_B}^{r_o} F_s(\gamma') \sin \varphi(\gamma') dr' = K\frac{\pi(\gamma_o - \gamma_B)}{2M} \sum_{i=1}^{M} F_s(\gamma_{ci}) \sin \varphi(\gamma_{ci}) \sin \beta_i \quad (15)$$

$$T_s = K\int_{r_B}^{r_o} F_s(\gamma') \sin \varphi(\gamma') dr' = K\frac{\pi(\gamma_o - \gamma_B)}{2M} \sum_{i=1}^{M} F_s(\gamma_{ci}) \sin \varphi(\gamma_{ci}) \sin \beta_i \quad (16)$$

$$Q_s = -K\int_{r_B}^{r_o} F_s(\gamma') \cos \varphi(\gamma') \gamma' dr' = -K\frac{\pi(\gamma_o - \gamma_B)}{2M} \sum_{i=1}^{M} F_s(\gamma_{ci}) \cos \varphi(\gamma_{ci}) \gamma_{ci} \sin \beta_i \quad (17)$$

$$T_D = -K\frac{1}{2}\rho \int_{r_B}^{r_o} C_{D(\gamma')} \bar{W}_{(\gamma')} \bar{V}_{x(\gamma')c(\gamma')} d\gamma' = -K\rho\frac{\pi(\gamma_o - \gamma_B)}{4M} \sum_{i=1}^{M} C_D(\gamma_{ci}) \bar{W}(\gamma_{ci}) \cdot \bar{V}_x(\gamma_{ci}) c(\gamma_{ci}) \sin \beta_i \quad (18)$$

$$Q_D = K\frac{1}{2}\rho \int_{r_B}^{r_o} C_{D(\gamma')} \bar{W}_{(\gamma')} \bar{V}_{\theta(\gamma')c(\gamma')} d\gamma' = K\rho\frac{\pi(\gamma_o - \gamma_B)}{4M} \sum_{i=1}^{M} C_D(\gamma_{ci}) \bar{W}(\gamma_{ci}) \cdot \bar{V}_\theta(\gamma_{ci}) c(\gamma_{ci}) \sin \beta_i \quad (19)$$

5.0 SHIP PARTICULAR AND HYDROSTATIC DATA

In this research, the selected VLCC ship has the overall length of 335.115 meter and breadth of 58 meters. Principle dimension, hydrostatic data and full load operation condition of selected ship as shown in Table 1 to Table 3 as follow.

Table 1: Principle dimension

Length over all (Loa)	335.115
Length water line (Lwl)	326.85
Length between perpendicular (Lpp)	320
Length between perpendicular model (Lppm)	3.5
Breadth molded (Bm)	58
Depth molded (Dm)	30

Table 2: Hydrostatic Data

Block Coefficient (Cb)	0.8045
Prismatic coefficient (Cp)	0.8084
Prismatic Coefficient at after (Cpa)	0.7557
Prismatic Coefficient at fore (Cpf)	0.8611
Midship Coefficient (Cm)	0.9952
Water plane coefficient (Cwp)	0.8878
LCB (% LPP)	-2.45

Table 3: Operation Condition

Draft molded (dm)	19.3
Wetted Surface (m2)	26330
Displacement (m3)	288175

Table 4: Propulsion factor

Form Factor (K)	0.23

6.0 DESIGNED PROPELLER GEOMETRY AND PERFORMANCE

By using the empirical equation from the OcARI S-Power software, the propeller of selected ship is designed. The diameter of the designed propeller is 9.13 meter in full scale. The detail information of this propeller and cross section dimension of the propeller is presented in Table 5 and Table 6 respectively. While, the cross section design of this propeller is showed in Figure 2.

Table 5: Propeller data output (design input)

Propeller diameter	9.13
Propeller pitch ratio	0.714
Propeller expanded ratio	0.473
Propeller working condition (J)	0.4612

Table 6: Propeller Blade Geometry and Cross Section Dimension

Radi(mm)	Chord	CE	Pitch(mm)	Rake	LER	Skew	T-max	Camber	P/D	r/R	P-tang
821.700	1275.328	462.218	6518.820	71.889	0.000	-175.446	374.061	187.031	0.714	0.180	75.851
913.000	1312.190	484.080	6518.820	79.877	0.000	-172.014	366.398	183.199	0.714	0.200	74.352
1141.250	1403.441	541.106	6518.820	99.846	0.000	-160.615	345.670	172.835	0.714	0.250	70.703
1369.500	1492.885	601.126	6518.820	119.816	0.000	-145.317	323.040	161.520	0.714	0.300	67.209
1826.000	1663.768	727.644	6518.820	159.754	0.000	-104.240	273.769	136.884	0.714	0.400	60.741
2282.500	1819.670	857.383	6518.820	199.693	0.000	-52.452	221.973	110.987	0.714	0.500	54.997
2739.000	1955.425	982.306	6518.820	239.632	0.000	4.593	171.045	85.523	0.714	0.600	49.958
3195.500	2065.866	1092.995	6518.820	279.570	0.000	60.062	124.375	62.188	0.714	0.700	45.567
3652.000	2145.826	1179.246	6518.820	319.509	0.000	106.333	85.355	42.677	0.714	0.800	41.749
4108.500	2190.137	1230.844	6518.820	359.447	0.000	135.776	57.374	28.687	0.714	0.900	38.426
4336.750	2197.311	1240.687	6518.820	379.417	0.000	142.031	48.583	24.292	0.714	0.950	36.928
4565.000	2193.634	1238.526	6518.820	399.386	0.000	141.709	43.824	21.912	0.714	1.000	35.527

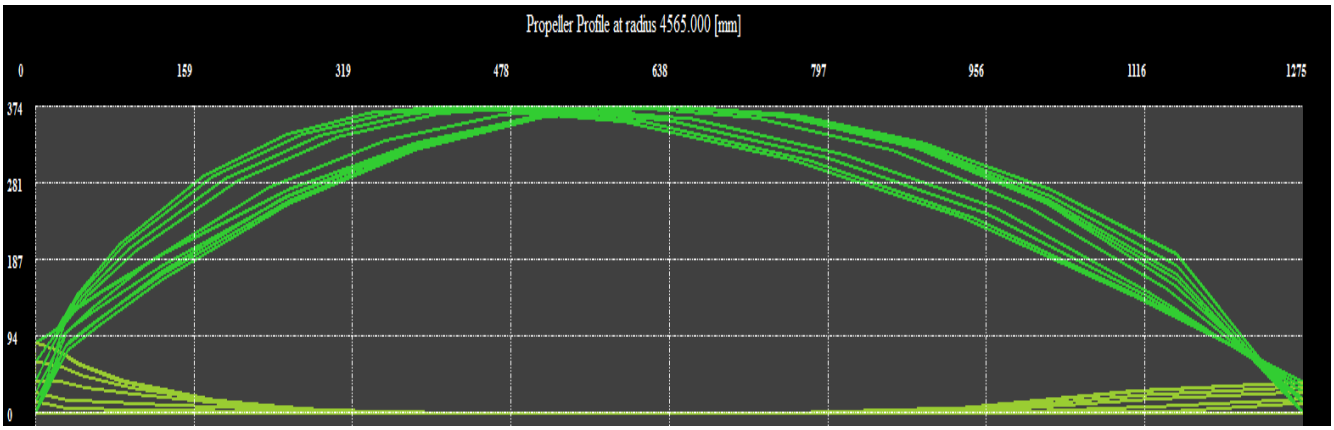

Figure 2: Geometry of blade.

The figure 2 shows geometry after combines these 12 cut surfaces of sections of blade. Every point in these two line design depend on these data in table 6. The propeller blade cross section is having the aerofoil design and the maximum blade thickness is around 374 mm.

By using the Quasi Continuous Method which applied the Lifting Surface Theory and the mathematical model as showed from equation 1 to 19, the pressure distribution on the propeller surface was determined. The suction side pressure and pressure side pressure calculated by the mathematical model is showed in Table 7. In the figure 3, the green line is for suction loading pressure and the red line is pressure surface pushing. The blade is divided into 10 section on lengthways be marketed with cj/Cj. The total pressure distribution is D-value of these two pressures on opposite surfaces. The change tendency of total pressure every point on blade directly can be predicted.

In this figure 4, the yellow line shows Kt, green line shows Kq, red line shows efficiency. Efficiency of our ship working at J = 0.4612 with is not the maximum, but it's appropriate. Maybe the condition of J more than 0.5 has more higher efficiency, but the effectives of cavitation around blade on thrust and stability will increase with the efficiency. The efficiency in the area shows in graph must be chosen with considering cavitation.

From the figure 5, it is also observed that the different pressure on the blade surface is negative for r/R=0.8799. The reason for the negative difference pressure on this cross section is due to the change of the pressure direction between pressure side and suction side pressure line. There will be 10 same graph which can combine to discusses the whole blade.

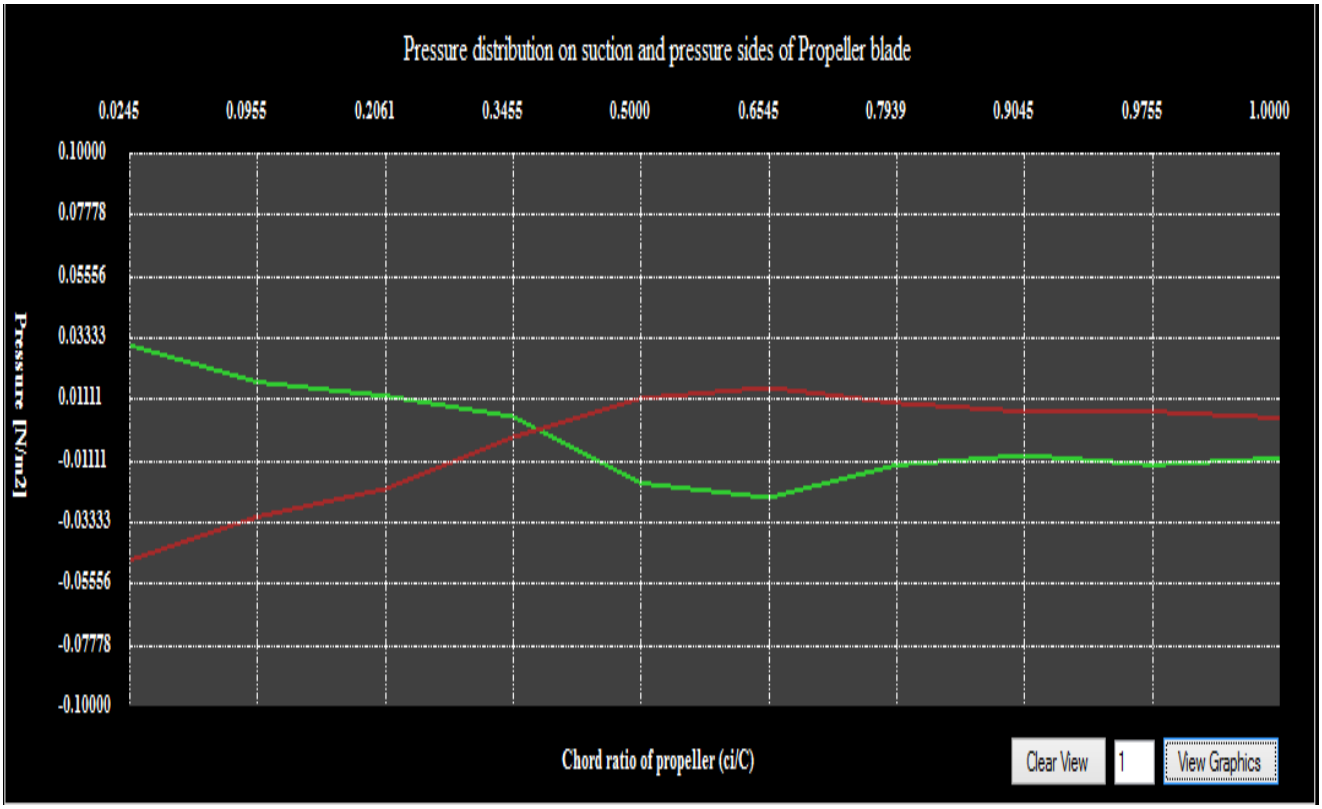

Figutre 3: Pressure distribution on blade r/R=0.18

Table 7: Pressure Distribution on Propeller Blade Surface

	cj/Ci	0.0245	0.0955	0.2061	0.3455	0.5	0.6545	0.7939	0.9045	0.9755	1
r/R= 0.18	Suction +	0.0307	0.0174	0.0125	0.0049	-0.0191	-0.0243	-0.0125	-0.009	-0.0124	-0.01
	Pressure -	-0.0469	-0.0312	-0.0211	-0.0024	0.0116	0.0155	0.0099	0.0068	0.0068	0.0045
r/R= 0.2247	Suction +	0.0223	0.0128	0.0168	0.0179	0.0137	0.0065	0.0025	0.0031	-0.0159	0.0066
	Pressure -	-0.0339	-0.0183	-0.0143	-0.016	-0.0157	-0.013	-0.0102	-0.0083	0.0083	-0.0137
r/R= 0.3001	Suction +	-0.0091	0.0015	0.009	0.0113	0.0087	0.003	-0.0037	-0.0131	-0.0351	0.0081
	Pressure -	0.0064	0.0007	-0.0007	-0.0009	-0.0007	0.0002	0.0031	0.012	0.0347	-0.0083
r/R= 0.4039	Suction +	0.0036	0.0104	0.0149	0.0157	0.0116	0.0035	-0.0067	-0.022	-0.0531	0.0012
	Pressure -	-0.0023	-0.0059	-0.0057	-0.0016	0.0032	0.0069	0.0116	0.024	0.0545	0
r/R= 0.5259	Suction +	-0.0115	0.0042	0.0121	0.0143	0.0118	0.0043	-0.0065	-0.023	-0.057	-0.0003
	Pressure -	0.0159	0.0011	-0.0027	0.0002	0.0055	0.0104	0.0158	0.0282	0.0624	0.0057
r/R= 0.6541	Suction +	0.001	0.0118	0.0177	0.0182	0.0152	0.0089	0.0016	-0.008	-0.0213	-0.0018
	Pressure -	0.002	-0.0105	-0.0135	-0.0077	-0.0012	0.0036	0.0069	0.0126	0.0251	0.0056
r/R= 0.7761	Suction +	0.0227	0.0192	0.0199	0.0201	0.0175	0.012	0.0045	-0.0065	-0.0309	0.0086
	Pressure -	-0.0164	-0.0167	-0.016	-0.0113	-0.0065	-0.0027	0.0021	0.0107	0.0324	-0.0066
r/R= 0.8799	Suction +	-0.0558	-0.0199	-0.0086	-0.0051	-0.0065	-0.0106	-0.016	-0.0239	-0.0487	-0.0032
	Pressure -	0.0745	0.0316	0.0196	0.0209	0.0252	0.0294	0.0346	0.0414	0.0632	0.0175
r/R=	Suction +	0.1857	0.0913	0.0563	0.0344	0.0161	-0.0012	-0.0179	-0.0394	-0.0771	-0.027

0.9553	Pressure -	-0.1759	-0.0894	-0.0548	-0.0287	-0.0087	0.0075	0.0238	0.0452	0.0811	0.0315
r/R= 0.995	Suction +	0.1568	0.0823	0.0596	0.0487	0.0399	0.0308	0.0228	0.0143	0.0061	-0.0061
	Pressure -	-0.1482	-0.0816	-0.06	-0.0455	-0.0354	-0.0281	-0.021	-0.0135	-0.008	0.0045

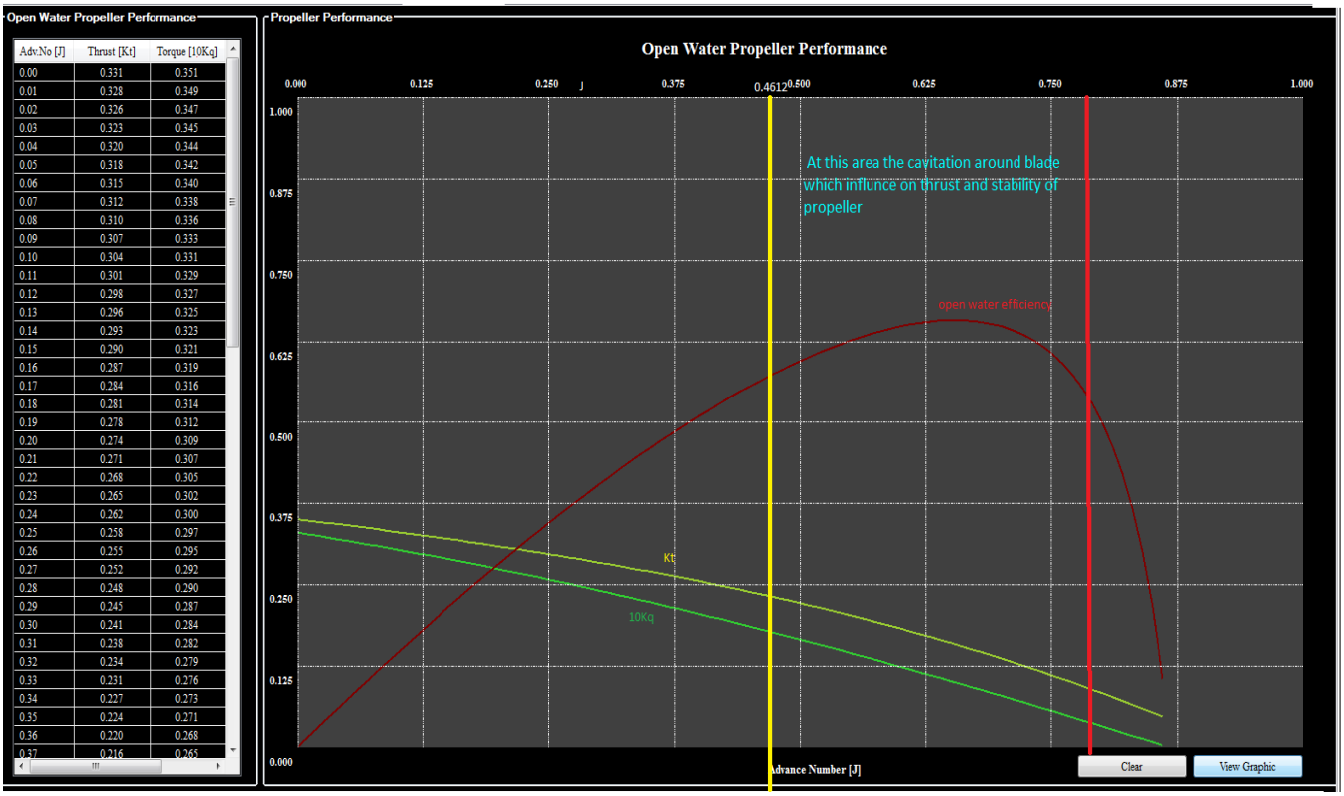

Figure 4: KT-KQ chart

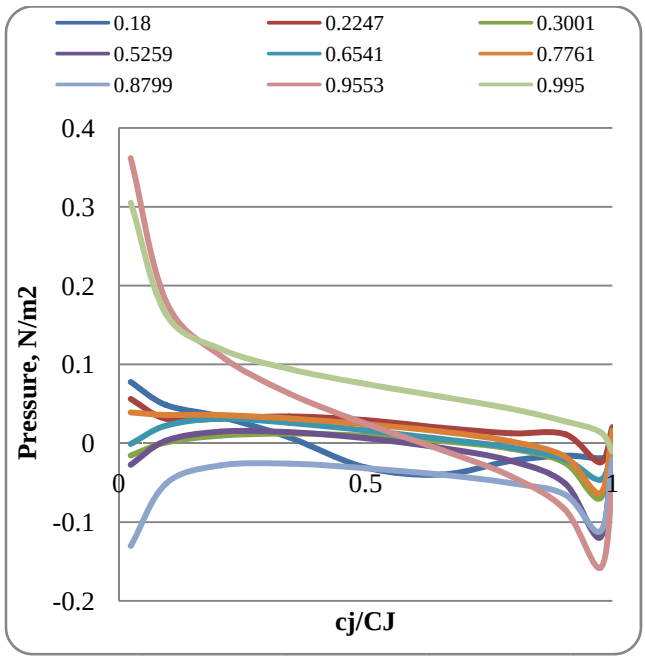

Figure 5: The pressure distribution on blade.

6.0 CONCLUSION

From this research study, the propeller design and optimization process was completed by using the software OcARI S-Power. Besides, the Quasi Continuous Method is also applied in this research. From the study, the open water performance of the designed propeller was predicted by the Quasi Continuous Method, and the data of propeller was designed can be used to analysis the propeller performance and predicted the performance of overall propulsion system. But, the pressure distribution data is useful information can be used for propeller structure analysis. For the future research, the experiments studies are recommended to be done that get the performance of the designed propeller and validate the result from Quasi Continuous Method. Besides, new studies with improving the propulsion performance by rerun the propeller design process by using different geometry of propeller.

ACKNOWLEDGEMENTS

The authors are very grateful to Universiti Teknologi Malaysia, Ocean and Aerospace Research Institute, Indonesia for supporting this study. Authors are also grateful to Mr. C. L Siow for his useful discussions and helps.

REFERENCE

1. Naoto Nakamura. 1985. *Estimation of open-water Charactistics based on Quasi-Continuous Method.* Spring Meeting of The Society of Naval Architects of Japan.
2. Jun Ando and Kuniharu Nakatake. 2001. *Calculation of there-dimensional unsteady sheet cavitations by a simple surface panel method "SQCM".* Kyushu University, Fukuoka 821-8581, Japan.
3. Koichi Koyama, . *On application of the Lifting Surface Theory of Marin Propeller*. Ship Research Tokyo. Japan
4. Takashi Kanemaru and Jun Ando. 2009. *Numerical Analysis of Steady and Unsteady Sheet Cavitation on a Marine Propeller Using a Simple Surface Panel Method "SQCM".* First International Symposium on Marine Propulsors smp'09. Norway.
5. Takashi Kanemaru and Jun Ando. 2012. *Numerical Analysis of Pressure Fluctuation on Ship Stern Induced by Cavitating Propeller Using a Simple Surface Panel Method "SQCM".* Faculty of Engineering, Kyushu University, Fukuoka, Japan
6. Davide Grassi and Stefano Brizzolara. . *Numerical Analysis of Propeller Performance by Lifting Surface Theory*. University Of Genoa, Department of Naval Architecture and Marine Engineering, Genova, Italy.
7. Twenty-Second Symposiums on Naval Hydrodynamics .1999. *Propulsor Hydrodynamics/Hydro acoustics.* Commission on Physical Sciences, Mathematics, and Applications (CPSMA). Page: 110-238.
8. Jun Ando, S. Maita and K. Nakatake. 2000. *A New Surface Panel Method to*
9. *Predict Steady and Unsteady Characteristics of Marine Propeller*. Twenty-Second Symposiums on Naval Hydrodynamics.
10. Koichi Koyama. 2012. *Relation between the lifting surface theory and lifting line theory in the design of an optimum screw propeller*. National Marine Institute, Japan.

Computational Analysis of the influence of Two Circumferential Grooves on Performance of Journal Bearing with Palm Oil as Lubricant

Asral,[a,*] Dodi Sofyan Arief, [a,*] Jamaluddin Md Sherif,[b,*] and Abd Khair Junaidi,[b]

[a)]*Teknik Mesin - Universitas Riau, Kampus Bina Widya Panam 28293 Pekanbaru, Riau Indonesia*
[b)]*Faculty of Mechanical Engineering of Universiti Teknologi Malaysia , 81310, Skudai, Johor, Malaysia*

*Corresponding author: asralst@yahoo.com, dodidarul@yahoo.com, jamal@fkm.utm.my

Paper History

Received: 25-October-2014
Accepted: 13-November-2014

ABSTRACT

This study compares the performance of a bearing with surface waviness liner to a plain bearing. Both bearings are functioned with palm oil as lubricant so that the potential advantages of the journal bearings could be identified. CFD analysis is developed to predict the numerical data for full film lubrication condition. A bearing of 60 mm in diameter with its ratio of length to diameter is 0.5, a clearance 250µm, and 200µm of wave amplitude is simulated. Semi circular wavy surface produces better results in term of load capacity than the plain journal bearing for a small eccentricity. The load carrying capacity is influenced by the increasing in speed of the shaft and the eccentricity ratio.

Keyword: *Load Carrying Capacity; Eccentricity; Wavy; Grooves; Temperature Drop*.

1.0 INTRODUCTION

In designing a bearing system, there are several important aspects that must be considered i.e the method to deliver the lubricant to the bearing, the distribution of the lubricant within the bearing, the quantity of the lubricant which is required and the amount of heat which is generated by the bearing and its effect on the temperature of the lubricant. A good journal bearing is able to support high load with less friction so that it can reduce the losses of energy. In this case, the properties of the lubricant may also be considered as it influences the contact between journal and bearing by a layer of fluid with a certain thickness. As an effort to improve the efficiency of the machine, some modifications on the bearing geometry are highly recommended. On the other hand, the usage of bio-based lubricant will enhance the operation of the machine to be environmental friendly.

In order to minimize the factor of friction, improvements on the surface contour are highly needed. For full film lubrication, the lubricant thickness in the clearance of two or more solid boundaries depends on the loads and fluid viscosity. This will be the main factor to determine the bearing lifespan. Generally, in good practice, lubrication is attempted to maintain the oil inside the bearing so that direct contact that inflicts damage can be prevented. In this paper, the properties of the lubricant at high performance operation of journal bearing are studied. Numerous studies have been done in various ways that involve numerical analysis and experimental investigation. Hargreaves (1991) had investigated the influence of sinusoidal surface waviness on the stationary surface of rectangular slider bearings. Hargreaves found that the surface waviness could enhance the load carrying capacity. Theoretical study of the effect of non linear bearing liner was carried out by Hassan (1998) who then agreed with Hargreaves's findings. Hassan reported that wavy surface liner; both axially and circumferentially, would also increase the load carrying capacity. Gertzos (2008) reported that CFD model by using FLUENT package could solve the journal bearing case study which produced results in a very good agreement between theoretical and experimental. Many studies in non linear surface liner have been investigated such as by Dimofte (2002-2008) which concerning axially three sinusoidal wave journal bearing. Moreover, other researchers also investigated the journal bearing with journal groove shape assorted to achieve a good performance, as mentioned by Hirayama *et al* (2009) and Sahu *et al* (2006).

As the fluid film lubrication for the lubrication between two solids is considered, it is important to understand the influence of the surface topography of these solids on several important parameters in the mechanism of lubrication in order to obtain a journal performance with high performance. Based on the previously-mentioned findings, the aim of this paper is to develop three dimensional CFD models so that the performance

characteristic of semi circular wavy groove journal bearings can be studied. The usage of palm oil lubricants are also included and studied.

2.0 NUMERICAL APPROACH

The presented numerical study here was conducted with the commercial Computational Fluid Dynamics (CFD) code FLUENT. The CFD procedures include the approximation of grid generation technique, turbulence model, boundary conditions, solver scheme and the selection of turbulence model. The software was used to compute the full field pressure distribution and the shear stress information for characteristics inside the journal bearing with semi circular wavy surface conditions. Comparisons were made for smooth surface liner in same conditions.

The first step of simulation was pre-processing, which involved the building of the journal bearing model in Gambit. Then finite-volume-based mesh was applied and all the required boundary conditions and flow parameters were imposed. The numerical model was then ready to be calculated and produced results. The final step in analysis was post-processing, which involves organization and interpretation of the data.

2.1 Computational Meshes

Proper selection of the computational grid is an important aspect in any computational simulation. A suitable grid will provide accurate solution and fast convergence. In this study, geometry and mesh generation are done by using Gambit. For three dimensional (3D) domains, tetrahedral and hexahedral grid types are accepted in Gambit. Tetrahedral and interval size method meshes are chosen to be the type of mesh with 60° of equiangular skewness, which then it will provide smoother meshing that eliminates the highly skewness. In order to obtain a fine grid and reduce the time converging consumption, tetrahedral cells from 223000 up to 320000 of cells are created in the domain.

2.2 Flow Modeling

Turbulence flow is one of the most difficult studies of flow in fluid mechanics. Turbulence take place in eddies in the order of millimetre of size, while the whole flow domain may extend over meters or kilometres. In general, the flow on wavy surface is turbulent. Solving turbulence flow in FLUENT can be divided into two categories as follows:

$$\frac{\partial \rho}{\partial t}+\frac{\partial \rho}{\partial x_i}(\rho u_i)=S_m \qquad (1)$$

Equation (1) is the general form of mass conservation equation and it is valid for incompressible as well as compressible flows. The source S_m is the mass added to the continuous phase from the dispersed second phase (e.g., due to vaporization of liquid droplets) and any user-defined sources. Momentum equation is described by:

$$\frac{\partial}{\partial t}(\rho u_i)+\frac{\partial}{\partial x_j}(\rho u_i u_j) = -\frac{\partial p}{\partial x_i}+\frac{\partial \tau_{ij}}{\partial x_j}+\rho g_i+F_i \qquad (2)$$

where p is the static pressure and ρg_i and F_i are gravitational and external body forces (e.g., forces that arise from interaction with the dispersed phase), respectively.

Two alternative methods can be employed to render the Navier-Stokes equations tractable so that the small-scale turbulent fluctuations do not have to be directly simulated; Reynolds-averaging (or ensemble-averaging) and filtering. Both methods introduce additional terms in the governing equations that need to be modelled in order to achieve a '*closure*' for the unknowns. The Reynolds-averaged Navier-Stokes (RANS) equations govern the transport of the averaged flow quantities, with the whole range of the scales of turbulence being modelled. The RANS based modelling approach greatly reduces the required of computational effort and resources, and it is widely adopted for practical engineering applications. An entire hierarchy of closure models are available in FLUENT. The RANS equations are often used to compute time-dependent flows, which unsteadiness may be externally imposed or self-sustained. The momentum equation for Reynolds Average Naviers-Stokes has been written as:

$$\frac{\partial \rho}{\partial t}+\frac{\partial}{\partial x_i}(\rho u_i)=0 \qquad (3)$$

$$\frac{\partial}{\partial t}(\rho u_i)+\frac{\partial}{\partial x_j}(\rho u_i u_j) = -\frac{\partial \rho}{\partial x_i}+\frac{\partial}{\partial x_j}\left[\mu\left(\frac{\partial u_i}{\partial x_j}+\frac{\partial u_j}{\partial x_i}-\frac{2}{3}\delta_{ij}\frac{\partial u_l}{\partial x_l}\right)\right]+\frac{\partial}{\partial x_j}(-\overline{\rho u_i' u_j'}) \qquad (4)$$

The turbulent kinetic energy, k transport equation for The RNG $k-\varepsilon$ model, is given by:

$$\frac{\partial}{\partial t}(\rho k)+\frac{\partial}{\partial x_i}(\rho k u_i)=\frac{\partial}{\partial x_j}\left(\alpha_k \mu_{eff}\frac{\partial k}{\partial x_j}\right)+G_k+G_b-\rho\varepsilon-Y_M+S_k \qquad (5)$$

and for the dissipation rate, ε is written by:

$$\frac{\partial}{\partial t}(\rho\varepsilon)+\frac{\partial}{\partial x_i}(\rho\varepsilon u_i)=\frac{\partial}{\partial x_j}\left(\alpha_\varepsilon \mu_{eff}\frac{\partial \varepsilon}{\partial x_j}\right)+C_{1\varepsilon}\frac{\varepsilon}{k}(G_k+C_{3\varepsilon}G_b)-C_{2\varepsilon}\rho\frac{\varepsilon^2}{k}-R_\varepsilon+S_\varepsilon \qquad (6)$$

In these equations, G_k represents the generation of turbulence kinetic energy due to the mean velocity gradients. G_b is the generation of turbulence kinetic energy due to buoyancy. Y_M represents the contribution of the fluctuating dilatation in compressible turbulence to the overall dissipation rate. The quantities α_k and α_ε are the inverse effective Prandtl numbers for k and ε, respectively. S_k and S_ε are user-defined source terms. The model constants $C_{1\varepsilon}$ and $C_{2\varepsilon}$ have values derived analytically by the RNG theory. These values, used by default in FLUENT, are $C_{1\varepsilon}$ =1.42, $C_{2\varepsilon}$ = 1.68 C_μ = 0.0845.

2.3 Boundary Conditions

The applied boundary conditions in this simulation are common for an incompressible flow. Figure 1 shows a wavy surface with two grooves semi circular wavy. A bearing of 60mm in diameter

with its ratio of length to diameter is 0.5, a clearance 250 µm and 200 µm of wave amplitude was developed. To represent the study, a set of typical boundary conditions was used in the present work in 3D test section of the journal bearing simulations. The shaft (journal) rotated counter-clockwise whereas the bearing was stationary. The lubricant circulated in the journal bearing clearance circumferentially and followed the groove wavy surface. The boundary conditions of pressure inlet, pressure outlet and wall were developed to the left end, right end, shaft and bearing respectively.

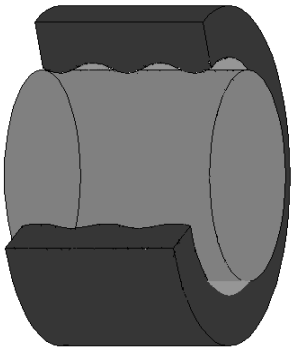

Figure. 1: A-3D open view drawing of two circumferential grooves journal bearing.

Pressure inlet boundary conditions are used to define the fluid pressure at the flow inlets, along with all other scalar properties of the flow. Pressure on the left side in practice is an integral part with respect to direct ambient pressure (here are conditioned to be zero, P_{inlet} = 0 gage), so this condition will result in a calculation which is closer to the actual condition.

Pressure outlet of boundary conditions is assigned at the domain outlet. The use of pressure outlet as the boundary conditions instead of an outflow conditions often results in a higher rate of convergence when backflow occurs during iteration. Pressure outlet which is set to zero, P_{outlet} = 0 gage, is equal to the atmospheric pressure which is typically used as a reference pressure measurement.

Wall boundary conditions are used to bound fluid and solid regions. Journal wavy surface and bearing are treated as wall, moving and stationary wall and no-slip boundary conditions are applied.

2.4 Load Capacity

The load capacity is resulted from the pressure generated in the fluid film. The load capacity is a function of load generated pressure distribution around the journal and surface area due to both the rotation and variation in fluid film thickness along circumference. Therefore, the wave journal bearing load capacity depends on the contact surface shape, amplitude and wave number, which investigated the effect of surface shape as shown in Figure 1 as the scope of this study. Load carrying capacity ratios are plotted in the figure and it is calculated by using the following dimensionless equation load:

$$Wcc = \frac{F}{P\,L\,D} \qquad (7)$$

where *F, P, L, D* are the load on the journal, ambient pressure, length of bearing, and the diameter of the journal respectively.

Eccentricity (*e*) due to the clearance between the shaft and bearing surface is experienced by both external loads and also shaft weight (W), i.e the distance between the axis of the shaft to the bearing as can be seen in Figure 2 while the radial clearance is the difference between the outer radius of journal and the radius of bearing, c = R - r. Consequently the thickness around the circumference of bearing lubrication oil is not the same. The fluid film has a thin film at one end and a thicker film at the other end. As the shaft is rotating at a certain speed, the position of this layer will change. Load and shaft speed are among others that could affect the eccentricity and also the maximum and minimum thickness of lubricant. In this study, eccentricity ratio, ε is set to be 0.107, 0.284, 0.400, 0.568, and 0.632 respectively and also this ensures the minimum thickness of oil lubrication.

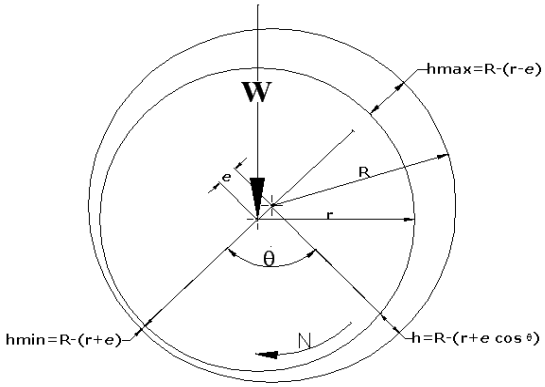

Fig. 2 Schematic of eccentricity

The lubricant properties used in the calculation is based on the palm oil, which subsequently is approached by the nature of the Benzene-Liquid included in FLUENT database where density (ρ) = 887.5 kg/m3, thermal conductivity = 0.1721 w/m-k, heat capacity=1861 kj/kg-K, and viscosity (µ) = 0.07719 kg/m-s.

3.0 RESULTS AND DISCUSSIONS

Figure 3 shows the pressure distribution in the bearing due to the effect of changing surface liner with semi-circular wavy surface. It is shown clearly here that the presence of wavy surface can change the pressure distribution as the vicinity of high pressure becomes more concentrated at the top of the wave. Meanwhile for both bearings, maximum pressure areas are formed at the almost half of the bearings in the direction of shaft rotation.

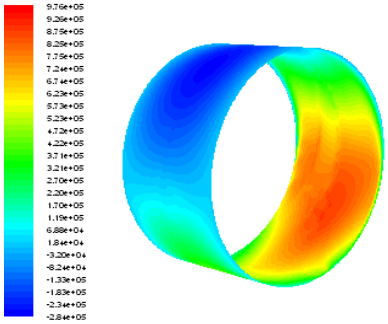

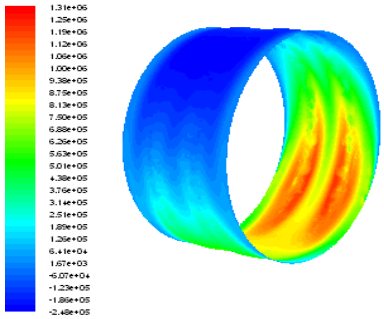

(a)

(b)

Figure. 3:Pressure distribution in the bearing, (a) plain bearing, and (b) semi circular wavy bearing

Then, the effect of the waviness surface shape in dimensionless load carrying capacity in comparison with a linear journal bearing is analyzed. The effects of the shaft speed and eccentricity to the load carrying capacity of the bearing are shown in following Figure 4 to 8. The displayed graphs may provide an explanation that the shaft speed could affect the load capacity, which it is followed by the changes in eccentricity. This provides as an advantage for each changes of the journal bearing inner surface so that the comparison of the characteristics can be obtained. Along with the increasing shaft speed, the characteristics of journal bearings are changed in terms of magnitude load capacity as well as the changes in eccentricity. Plain bearing on a large eccentricity shows a higher performance in load capacity while the wavy bearing seems to be low in performance. This is caused by the fluid pressure that experiences a small clearance around the shaft, as the clearance that serves to support the load on the wavy surface is smaller. Oil can not be forced to be at the peak of the wave so that more are on the valley. The clearance between the surfaces of the shaft with the bearing seems to affect oil pressure. As the semi-circular wavy surface is distinguished by the development of a small groove, it is consequently influenced by the lubrication. By comparing this to the plain bearing, wavy surface seems to have advantage over linear as it increases the load capacity in the small eccentricity. As the shaft speed increases, the characteristics of journal bearings show varied changes in term of magnitude of load capacity and the eccentricity ratio. From these figures, semi circular wavy with the highest value of eccentricity ratio produces the lowest value of load capacity while this event shows contrary in the results of linear journal bearing which it is caused by the development of groove. The trend of curves between semi circular wavy with the plain journal bearing shows a relatively similar behaviour in term of shape.

Best performance in terms of the increasing in load capacity can be achieved by a circular wavy with the eccentricity ratio, ε = 0.4, which if it is accompanied by an increasing in speed of shaft rotations. From these figures, an obvious event of the increasing in load capacity with a small gradient occurs. This is caused by the changes in fluid pressure around the shaft which it simultaneously acts to support the load. To calculate the amount of pressure, the involved significant parameter is the cross-sectional area where the pressure is experienced, where the surface shape that influences the generated pressure forces is also considered.

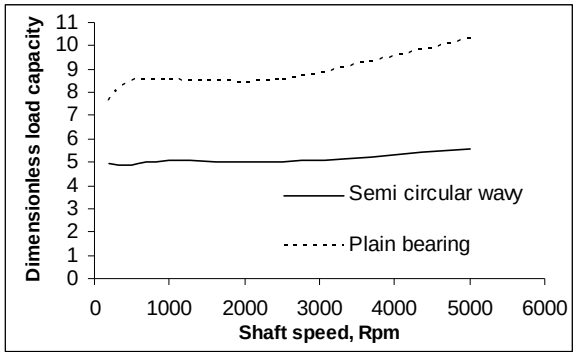

Figure. 4: Shaft rotation speed effects to load capacity at eccentricity ratio, ε = 0.632

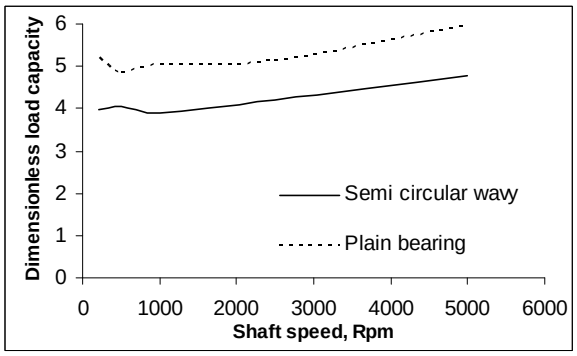

Figure.5: Shaft rotation speed effects to load capacity at eccentricity ratio, ε = 0.568

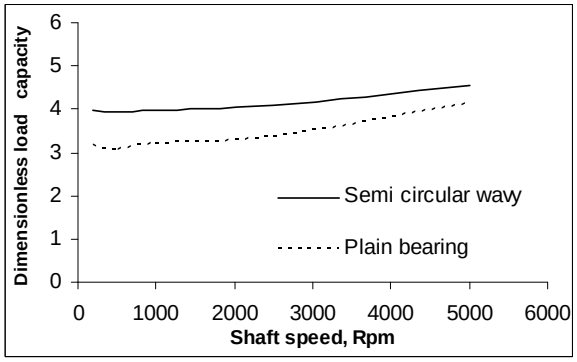

Figure.6: Shaft rotation speed effects to load capacity at eccentricity ratio, ε = 0.4

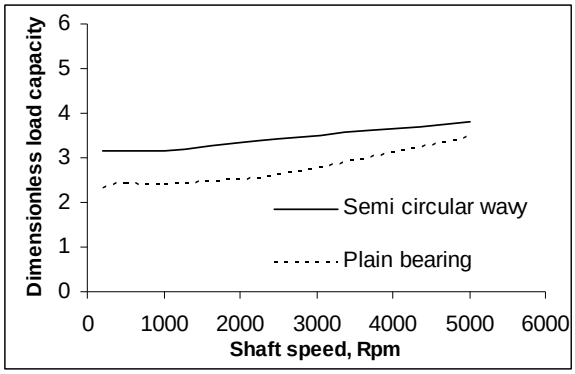

Figure.7: Shaft rotation speed effects to load capacity at eccentricity ratio, $\varepsilon = 0.284$

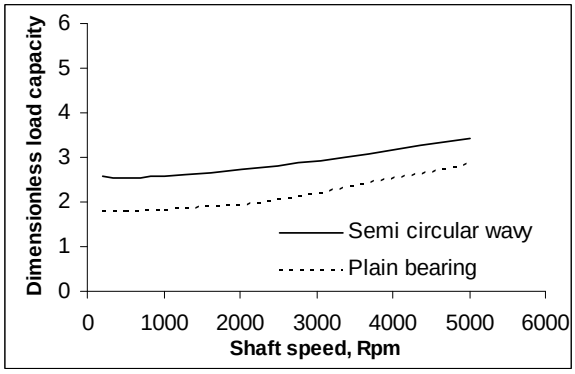

Figure.8: Shaft rotation speed effects to load capacity at eccentricity ratio, $\varepsilon = 0.107$

Drop off in bearing temperature is another function of a lubricant. Lubricant in the bearing is said to work properly when it can reach all parts of the bearing surface, heat can be transferred to the lubricant and subsequently discharged into the ambient. Percentage of temperatures drop which is shown here are plotted from the average temperature of the bearing surface as the thermal equilibrium is achieved. For this study, figure 9 shows the percentage of drop off surface temperature of the bearing on a rate of change in shaft speed at the highest eccentricity. In a large eccentricity, or in a condition where the gap between the bearing and shaft is small, the generated heat becomes high due to the friction. It is required to use a lubricant with properties consist of good thermal conductivity to transfer this heat. From these results, it can be seen that palm oil is able to function properly. Also, it can be seen here that the effect of bearing surface shape as the surface with a semi-circular wavy has a better performance, compared to the plain bearing. This event is caused by the wave bearing surface area as it is larger than the plain bearing in which the heat transfer rate is a function of the area, within a large area of heat transfer rate is increased. For addition, semi-circular wave bearing has much amount of mass lubricant in bearing.

The characteristics of curve change when the eccentricity ratio reduces. As shown in Figure 10, when the shaft rotation reaches about 250 rpm, the temperature drop appears to be the same on both bearings. This is due to the lubricant functions at low speed can not spread uniformly throughout the surface and absorbs heat from the bearings. Along with the increasing in shaft speed, a trend of temperature drop increases for the wave bearing. Significant difference in temperature drop is seen in Figure 11 with the eccentricity ratio is 0.4 where the wave bearing achieves a better performance, compared to plain bearing. Step-up of shaft speed in both types of bearings indicates that the changes in temperature drop are increased. Figure 12 shows an increasing of temperature drop on plain bearing with a small growth on the rotation axis, while the wave bearing equipment shows a significant percentage of increment. Generally, as the shaft speed increases and the eccentricity changes, the wave bearing shows a significant event of temperature drop, compared to the plain bearing.

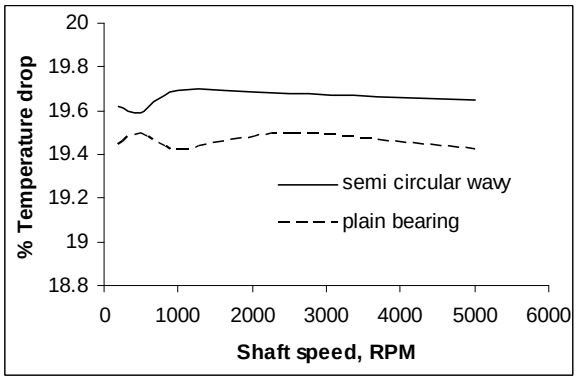

Figure.9: Shaft rotation speed effects to temperature drop at eccentricity ratio, $\varepsilon = 0.632$

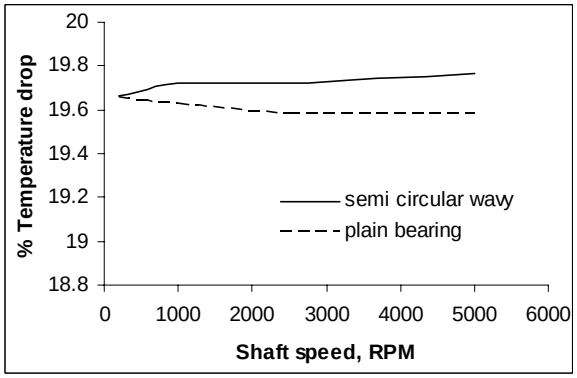

Figure.10: Shaft rotation speed effects to temperature drop at eccentricity ratio, $\varepsilon = 0.568$

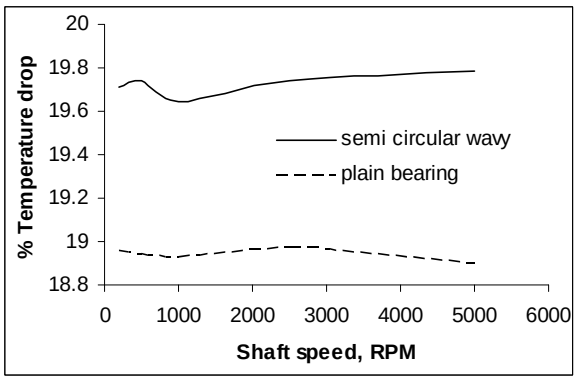

Figure.11: Shaft rotation speed effects to temperature drop at eccentricity ratio, $\varepsilon = 0.400$

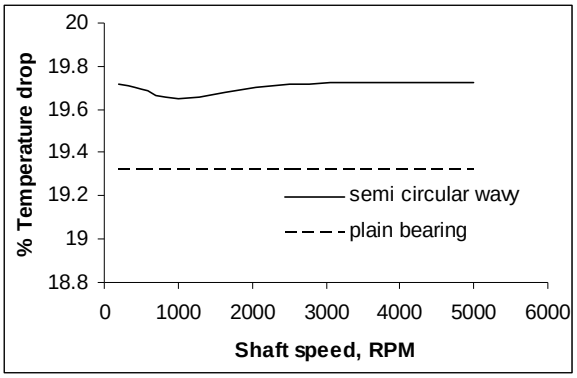

Figure.12: Shaft rotation speed effects to temperature drop at eccentricity ratio, $\varepsilon = 0.284$

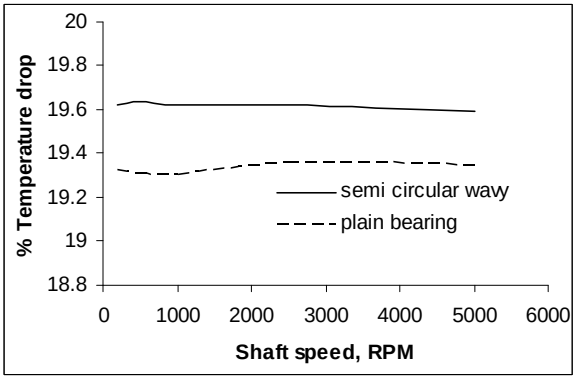

Figure.13: Shaft rotation speed effects to temperature drop at eccentricity ratio, $\varepsilon = 0.107$

4. 0 CONCLUSIONS

In this study, it can be concluded that the presence of surface waviness leads to an increment in bearing load carrying capacity with better results are achieved in semi-circular wavy where improvement remains stable even with the increasing in shaft speed in small eccentricity. Also, a conclusion can be made that the performance of liner journal bearings is generally lower than any other value growth in terms of temperature drop for each changes in shaft speed and eccentricity. Finally, it also can be concluded that palm oil can be used as lubricant.

REFERENCES

1. Habchi,W, Verge, P, Bair,S, Andersson, O, Eyheramendy,D, and Morales-espeje, G.E, 2010, Influence of Pressure and Temperature Dependence of Thermal Properties of a Lubricant on the Behavior of Cicular TEHD Contacts, *Tribology International*, article in press.
2. Mishra, P.C, Pandey, R.K, and Athre,K, 2007, *Temperature Profile of an Elliptic Bore journal Bearing*, Tribology International, 40, 453-458.
3. Chauhan, Amit, Sehgal, Rakesh, and Kumar Sharma, Rajesh, 2010, Thermohydrodynamic Analysis of Elliptical Journal Bearing with Different Grade Oils, *Tribology International*, article in press.
4. Hirayama, Tomoko, Yamaguchi, Naomi, Sakai, Shingo, Hishida, Noriaki, Matsuoka, Takashi, Yabe, Hiroshi, 2009, *Optimization of Groove Dimensions in Herring Bone Grooved* Journal Bearings for Improved Repeatable Run Out Characteristics, Tribology International, 42,675-681.
5. Ene, Nicoleta M, Dimofte, Florin, Keith, Theo. G, 2008, *A stability Analysis for a Hydrodynamic Three Wave Journal Bearing*, Tribology International 41,434-442.
6. Gertzos,K.P,Nikolakopoulos,P.G,Papadopoulos, C.A, 2008, *CFD Analysis of Journal Bearing Hydrodynamic Lubrication by Bingham Lubricant*, Tribology International, 41,1190-1204.
7. Sahu, M, Sarangi, M, Majumdar, B.C, 2006, *Thermo Hydrodynamic Analysis of Herringbone Grooved Journal Bearings*, Tribology International, 39,1395-1404.
8. Dimofte, Florin, 2000, *Wave Journal Bearings Under Dynamic Loads Nasa/Tm*, 212079.
9. E. Rasheed, Hasan, 1998, *Effect of Surface Waviness on the Hydrodynamic Lubrication of a Plain Cylindrical Sliding Element Bearing*, Wear, 223,1-6.
10. [Hargreaves, D.J, 1991, *Surface Waviness Effects on the Load-Carrying Capacity of Rectangular Slider Bearings*, Wear, 145,137-151.

Study on Pitch Motion of Three Floating Structures

Muhammad Farid Abdul Halim,[a] and Jaswar Koto,[a,b,*]

[a)]*Department of Aeronautical, Automotive and Ocean Engineering, Faculty of Mechanical Engineering, UniversitiTeknologi Malaysia*
[b)]*Ocean and Aerospace Engineering Research Institute, Indonesia*

*Corresponding author: jaswar@fkm.utm.my and jaswar.koto@gmail.com

Paper History

Received: 15-October-2014
Accepted: 16-November-2014

ABSTRACT

This paper discuss on the pitch motion due to the hydrodynamic interaction of three floating structures for different gap distances, 25 m and 50 m, and wave directions at 0 degree. In the study, commercial software, ANSYS AQWA software which practices the use of linearized wave theory is used to analyze the added mass, radiation damping and motion responses for the interaction between structures, where a 134 m diameter of round-shaped FPSO is used as a reference structure with a 97.6 m diameter round-shaped FPSO and LNG vessel. From the results, RAO at the gap distance of 50 m produced larger responses compare to RAO at the gap distance of 25 m..

KEYWORDS*: Round-Shape Floating Production Storage Offloading; Hydrodynamic Interaction; Gap Distance; Wave Directions.*

NOMENCLATURE

RAO	Response Amplitude Operator
FPSO	Floating Production Storage Offloading

1.0 INTRODUCTION

Since the demand for oil and gas increased in recent years, there is a huge impact on the growing offshore industry where there are a lot of construction of offshore structures are built and designed not only used to support the exploration of oil and gas, but they are also acting as a base for drilling, production and storage of oil and gas. The exploration for hydrocarbons started from the land to shallow waters (< 350 m) extended to deep water (< 1500 m) and now involves into ultra-deep water (> 1500 m). The development of oil and gas area regarding the offshore structures which considered as a challenge in the past has become a common thing nowadays where the effects of hydrodynamic interaction on the motion of the offshore structures have to be carefully taken into consideration for their safe operation.

There are many situations where it is important to understand the hydrodynamic interaction that occurs as a result of the motion between the multiple bodies of offshore structures. As an example, in general, there are many offshore operations involving the use of two or more floating structures in which they are placed close to each other to transfer the oil and gas during offloading. From this activity, the motions of each other are affected due to the hydrodynamic interaction in waves. As a result of the large motions between the two floating bodies can cause disturbance to the offloading system and collision to each body. It is important to understand, study and analyze the hydrodynamic interaction effect that occur due to the motion of the multiple bodies of offshore structure in order to trace the problem and minimize the serious implications that may be occurring.

There are many methods that have been used in order to analyze the motion of the floating structures due to the hydrodynamic effect. A common method that is usually has been performed to study the motion of the structure is by conducting an experiment using the model test in towing tank. In this research, three types of analysis are conducted; single body of offshore structure, two bodies of offshore structures and three bodies of offshore structures. The models which consist of two different rounds-shaped floating, productions, storage and offloading (FPSO) and liquefied natural gas (LNG) vessel from the previous research are used for the hydrodynamic analysis. The use of

commercial software which is ANSYS Hydrodynamic Diffraction (AQWA) is utilized in order to predict the effect of the gap or distance between the bodies of offshore structures on the wave forces.

2.0 LITERATURE REVIEW

There are many researches have been done regarding to hydrodynamic interaction effect on multiple bodies of offshore structures. The researches have been done analytically and numerically in order to solve the problems regarding the hydrodynamic analysis between multiple bodies. Some previous researches have been used as a guideline to the present researches.

For the hydrodynamic behavior of a single body of offshore structure, Saad et al. (2009) [18] used a mono-hull production platform in real environmental conditions which is in Brazilian waters. They also compared the data obtained from the field measurements with the results from the numerical simulations as well as the results acquired from model tests performed during the design phase. The hydrodynamic behavior of the mono-column showed satisfactory results and valid even though there are quite conservative to those related to the higher period amplitude. Cueva et al. (2010) [7] presented the numerical and experimental models for motion evaluation by using a circular shaped floater which is also a mono-column structure. The results for both numerical and experimental evaluations are presented in terms of Response Amplitude Operators (RAOs) for heave and pitch/roll motions. The results obtained for both numerical and experimental models are quite satisfactory except that there are slight differences and they are still valid.

There are many researches have been done regarding the problem of hydrodynamic interaction between multiple bodies and strip theory and potential theory are normally used to analyze the motions of the floating structures. Ohkusu (1974) [17] adopted strip theory to analyze the ship's motion around large floating structure. The results described clearly the effects of position of a smaller body in opposition to a large body. Ohkusu's method is extended by Kodan (1984) [14] to investigate the hydrodynamic interaction between two parallel structures in oblique waves. In order to support the validity of strip theory, he compared his investigation with model experiment but neglecting the speed effect and the results obtained are satisfactory with the experimental results. Fang and Kim (1986) [8] also utilized the strip theory to predict the motion between two ships due to hydrodynamic effect in oblique sea. Their method is different with previous researcher where the speed effects are taken into account, however, some deficiencies popped up due to the assumptions of two-dimensional.

Van Oortmerssen (1979) [22] solved the hydrodynamic interaction problem between two floating structures in waves by using the three-dimensional linear diffraction theory to solve. The results obtained for the numerical calculation achieve an agreement with the data obtained from the experiment but the speed effects are not considered as well as he did not applied his method to the ship configuration. Loken (1981) [15] used three-dimensional sink-source method to investigate the wave-induced motion and wave-drifting forces and moment on several close vessels in waves and the results obtained were satisfactory but the results for resonance region were quite unsatisfactory. Wu et al. (1997) [23] reviewed numerically and experimentally on the motion of a moored semi-submersible in regular waves and the wave-induced internal forces in the semi-submersible. For numerical method, the linearized equations of motions of the semi-submersible which is modelled as an externally constrained floating body are obtained in a common reference system fixed on the body. The results between the numerical and experiment in the practical wave-frequency range achieved very good agreement.

As the ability to compute is evolved, three-dimension approach to solve the hydrodynamic problems has become popular. Choi and Hong (2002) [5] employed a higher-order boundary element method (HOBEM) or wave Green function to analyze numerically the hydrodynamic interactions of multi-body system for twin barges and FPSO-shuttle systems. The results obtained show that there are rapid changes in hydrodynamic loads and responses along the wave frequencies caused by the hydrodynamic interaction. M. Kashiwagi and Q. Q. Shi (2010) [12] investigated numerically the wave interaction theory of four identical box-shaped floating bodies to compute the pressure distribution and integrated forces on body surfaces using the separation distance between the multiple floating bodies. The results obtained from the wave interaction theory are compared to HOBEM because the results obtained from HOBEM are accurate with respect to the separation distance between bodies. Clauss et al. (2002) [6] analyzed numerically and experimentally the sea keeping behavior of a semi-submersible in rogue wave. A panel-method program is used for wave or structure interactions in time-domain which is TiMIT (Time-domain investigation developed at the Massachusetts Institute of Technology) to evaluate the motions of the semi-submersible. The results showed good agreement with model test despite the fact that TiMIT theory is strictly linear and applicable for moderate sea conditions only.

Zhou Xianchu et al (1997) [24] applied the linear potential theory to investigate the hydrodynamic interaction between two vertical cylinders in water waves where the diffraction wave and radiation waves are considered. It is found that the incident angle which is the angle between the incident wave direction and the line joining two cylinder centers is depended on the magnitude of wave excited forces on cylinders. M.S. Kim and M. K. Ha (2002) [13] studied the motion responses between two offshore floating structures due to hydrodynamic interaction by using linearized three-dimensional potential theory with various heading waves. They used three-dimensional source distribution method for twelve coupled linear motion responses and elative motions of the barge and the ship in oblique waves to solve the numerical calculation. The results obtained provide a good correlation with the experimental results. Zhu et al. (2008) [9] applied time domain method to research the influence of the separation distance on the wave forces for hydrodynamic resonance of three-dimensional multiple floating structures. The results obtained from the time domain method for the peak force response on each floating body show similar resonant phenomena and hydrodynamic interaction when compared with frequency domain method, thus the time domain method is said as practically efficient.

M. T. Ali et al (2010) [1] investigated the first order wave exciting forces and motion responses due to hydrodynamic interaction between two unequal-sized freely floating three-dimensional rectangular boxes in regular waves using 3-D source

distribution method through different wave headings angles and separation distances (gaps). The results obtained show that the magnitude of the amplitude of motion responses and wave exciting forces for the smaller box can be increased or decreased depending on the wave heading while high peak frequencies is obtained as the gaps between two floating rectangular boxes is reduced. Z. Tajali et al. (2011) [21] carried out the hydrodynamic analysis of a floating multiple bodies of floating pier interacting with incident waves in the frequency domain. They used three-dimensional diffraction theory to predict the dynamic response of modules in irregular waves. The pier is modeled as a rigid body platform and pontoons are connected to each body of the floating piers by hinge. The results showed that for a fixed length of the pier, the amplitude of heave and pitch motions increased as the number of pontoons increased.

Siow et al (2013) [20] study the hydrodynamic interaction between Tension Leg Platform (TLP) and semi-submersible and the characteristics of multiple floating bodies when placed near to each other in regular waves. The experiment tests were carried out to find out the effect of hydrodynamic interaction to the motions of the structures. They applied Fourier Transform method to get the data in frequency domain by converting the data in time domain. The result shows that the hydrodynamic interaction will occur due to the scattering wave and radiation wave generated by another floating body which can cause the increase to the magnitude of the motions of the structures.

Siow et al. (2013) [21] proposed the method of three-dimensional diffraction potential methods to predict the motion response of multiple hulls semi-submersible structures as well as the use of three-dimensional green functions to estimate the wave velocity potential at each panel on semi-submersible surface. They only modified the meshing system in order to make it able to be applied to multiple hull structures. Good agreement between numerical and experimental results is obtained even though the numerical result obtained is slightly under-predicted compared to experimental results in most cases.

Siow et al. (2014) [22] included the viscous damping in the calculation to improve the heave damping magnitude in the motion equation due to over-estimated in heave motion from the previous study. The total damping is revised with the addition of viscous damping to the linear damping from diffraction theory. As a result of this revision, the involvement of viscous damping helps in correcting a part of heave motion response and reducing over-predicted error of heave damping magnitude.

Siow et al. (2014) [23] did another improvement by involving the drag effect in the calculation of diffraction potential theory and viscous damping. In order to correct the insufficient of diffraction potential theory, the nonlinear drag term in Morrison equation that is linearized using Fourier series linearization method is inserted in the motion equation. Hence, a satisfied result of heave response especially in damping is obtained.

3.0 PRINCIPAL THEORY

3.1 Motions of Floating Body

At sea, a floating structure experienced the motions responses due to waves where the motions are divided into 6 degrees-of-freedom in which three of them are linear while the other three are rotational about the three principal axes as in Figure 1.

The linear motions are surge (x-axis), sway (y-axis) and heave (z-axis) while the rotational motions are roll (x-axis), pitch (y-axis) and yaw (z-axis). From the six motion responses, heave, roll and pitch are considered as oscillatory motions since they are moving about a neutral point while for surge, sway and yaw, they do not return to their original equilibrium unless they are forced by exciting forces or moments.

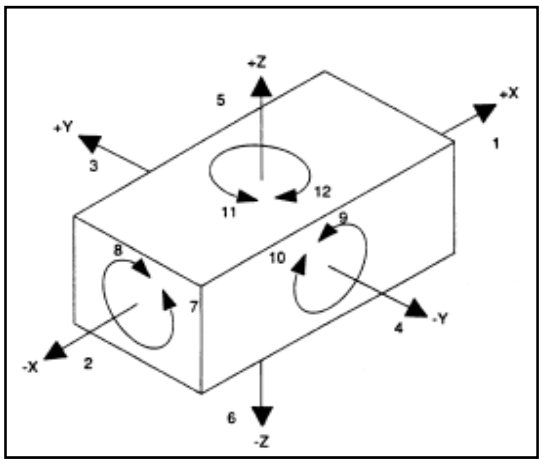

Figure 1: Six Degree-of-Freedom of a Floating Body

The equation of motion of a floating body can be expressed as

$$(m_j + a_{jj})\ddot{x}_{j(t)} + b_{jj}\dot{x}_{j(t)} + c_{jj}x_{j(t)} = f_{j(t)} \quad (1)$$

where x is displacement, $\dot{x}$ is velocity, $\ddot{x}$ is acceleration and f is exciting force. The displacement can be expressed as

$$x_{j(t)} = x_{jo}\cos(\omega t - \varepsilon_j), \quad (2)$$

the velocity, can be expressed as

$$\dot{x}_{j(t)} = -x_{jo}\omega \sin(\omega t - \varepsilon_j), \quad (3)$$

the acceleration can be expressed as

$$\ddot{x}_{j(t)} = -x_{jo}\omega^2 \sin(\omega t - \varepsilon_j), \quad (4)$$

and the exciting force can be expressed as

$$f_{j(t)} = f_{jo}\cos(\omega t) \quad (5)$$

where; m_j is the mass of the system, a_{jj} is the hydrostatic reaction in phase with acceleration (added mass), b_{jj} is the hydrostatic reaction in phase with velocity (damping coefficient), c_{jj} is the stiffness, x_{jo} is the amplitude of the motion, f_{jo} is the amplitude of the force and ε_j is the phase angle.

3.2 Concept of Interaction of Floating Bodies

3.2.1 Diffraction Wave Potential

Based from potential flow theory, the fluid flow around the bodies can be described by velocity potential by satisfying the conservation of mass and momentum equations using Laplace's equation. It is assumed that the fluid flow around bodies as

incompressible, inviscid which is frictionless and irrotational where the fluid particles are not rotating due to the viscous effects which are limited to the boundary layer. The velocity potential can be defined as$\Phi(x,y,z)$. The velocity potential can be divided into three parts; incident wave Φ^I, scattered wave Φ^S and radiation waveΦ^R.

$$\Phi(x,y,z) = \Phi^I(x,y,z) + \Phi^S(x,y,z) + \Phi^R(x,y,z) \quad (6)$$

Eq. 6 can be simplified as

$$\Phi(x,y,z) = \frac{gA}{i\omega}\{\emptyset_I(x,y,z) + \emptyset_S(x,y,z)\} + \sum_{k=1}^{6} \omega X_k \emptyset_R(x,y,z) \quad (7)$$

where, g is the gravitational acceleration (9.81 m/s^2), A is the amplitude of the incident wave, $\emptyset_I$ is the incident wave potential, $\emptyset_S$ is the scattering wave potential, $\emptyset_R$ is the radiation wave potential due to the motions, X_k is the amplitude of the motions and k is the direction of the motion.

The diffraction wave is the scattered wave from the fixed body caused by the incident wave. The radiation wave represents the wave propagated by the oscillating body in calm water. The diffraction wave and radiation wave can cause a significant effect on the bodies of floating structure in deep water.

It is assumed that the phase and amplitude for both the incident wave and diffraction wave are the same but the radiation wave is affected by each type of motions of each single floating body in the system. As a result, the total potential for radiation wave for a single body is the summation of the radiation waves generated by each type of motions of body which are surge, sway, heave, roll, pitch and yaw.

$\emptyset_I$ which is the incident wave potential can be written as

$$\emptyset_I(x,y,z) = -\frac{igA}{\omega}\frac{\cosh[k_0(z+h)]}{\cosh kh} e^{ik_0(x\cos\alpha + y\sin\alpha)} \quad (8)$$

where, α is the angle where the incident waves propagate relative to x-axis.

The scattering wave potential, $\emptyset_S$, due to the continuous surface of fluid can be represents as

$$\emptyset_S(x,y,z) = \frac{1}{4\pi}\iint_S \sigma_S(a,b,c)\, G(x,y,z;a,b,c)\, ds \quad (9)$$

$$\emptyset_S(x,y,z) = -4\pi u_n(x,y,z) \quad (10)$$

where, $\sigma_S(a,b,c)$ is the source of the strength function, $G(x,y,z;a,b,c$ is the Green's function, (x,y,z) is the coordinates of the field and (a,b,c) is the coordinates for thesource point

Diffraction wave potential $\emptyset_D$ can be obtained from the sum of incident wave potential and scattering wave potential.

$$\emptyset_D(x,y,z) = \emptyset_I(x,y,z) + \emptyset_S(x,y,z) \quad (11)$$

The diffraction wave potential $\emptyset_D$ must be satisfied with the boundary conditions:

- Laplace's equation:

  $\nabla^2\emptyset_D = 0$ for $0 \le z \le h$

- Free-surface condition:

  $\frac{\partial\emptyset_D}{\partial z} + K\emptyset_D = 0$ at $z = 0$ where $K = \frac{\omega^2}{g}$

- Bottom boundary condition:

  $\frac{\partial\emptyset_D}{\partial z} = 0$ at $z = h$

- Radiation condition:

  $\emptyset_D \sim \frac{1}{\sqrt{r}} e^{-ik_0 r}$ should be 0 if r is ∞

- Body boundary condition:

  $\frac{\partial\emptyset_D}{\partial n} = -\frac{\partial\emptyset_I}{\partial z}$ on the boundary

Thus,

$$\emptyset_D(x,y,z) = Re\left[\frac{gA}{i\omega}\{\emptyset_I(x,y,z) + \emptyset_S(x,y,z)\}e^{-i\omega t}\right] \quad (12)$$

The boundary conditions for the radiated wave potential are the same with the boundary conditions for incident wave potential. For radiated wave potential which is related to the motions of the body can be given as

$$\emptyset_R(x,y,z) = \sum_{k=1}^{6} \omega X_k \emptyset_R(x,y,z) \quad (13)$$

The radiated wave potential due the motions of the body can be obtained from as shown below

$$2\pi\emptyset_R(x,y,z) + \sum \emptyset_R(a,b,c) \iint_{S_B} \frac{\partial G(x,y,z,a,b,c)}{\partial n} dS = \sum \emptyset_R(a,b,c) \frac{\partial\emptyset_R(a,b,c)}{\partial n} \iint_{S_B} G(x,y,z,a,b,c) dS \quad (14)$$

where, S_B is the wet body surface of the floating body

3.2.2Green Function and Wave Potential

The wave potential at any point can be shown by eq. (15) in consideration of the wave potential can only be affected by structure surface, S_H:

$$\emptyset(P) = \iint_{S_H} \left\{\frac{\partial\emptyset(Q)}{\partial n_Q} G(P;Q) - \emptyset(Q)\frac{\partial G(P;Q)}{\partial n_Q}\right\} dS(Q) \quad (15)$$

where, $P = (x,y,z)$ is the fluid flow pointed at any coordinate and $Q = (\xi,\eta,\zeta)$ is any coordinate, (x,y,z), on the structure surface, S_H.

In order to estimate the strength of the wave flow potential, the Green function in eq. (15) can be utilized as follows:

$$G(P;Q) = \frac{1}{4\pi\sqrt{(x-\xi)^2 + (y-\eta)^2 + (z-\zeta)^2}} + H(x-\xi, y-\eta, z-\zeta) \quad (16)$$

where, is the effect of the free surface.

3.2.3Added Mass and Damping

For each motion, the added mass, and damping, can be obtained by using the integration of the radiation wave due to each motion along the surface of the structure as shown as following:

(17)

(18)

where, is the normal vector for each direction of motion, and , is the direction of motions and is the type of motions.

4.0 SIMULATION SETUP

Simulation of hydrodynamic interaction of three floating bodies was arranged as shown in Figure.2. The simulation was carried out at different wave directions as follows: 0^0, 45^0, 90^0, 135^0 and 180^0 headings using parameters of environmental conditions at Kikeh field as shown in Table.1.

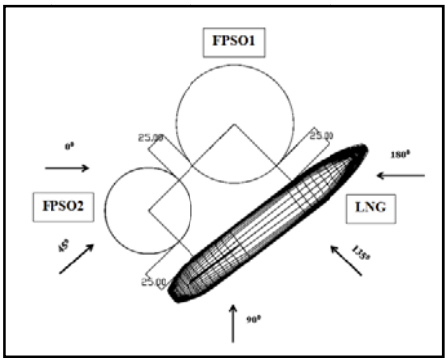

Figure 2: Wave Direction at 0^0, 45^0, 90^0, 135^0 and 180^0 headings

Table 1: Environmental Condition in Kikeh Field

Description	Value	Unit
Sea Water Characteristics		
Water Depth	1320	m
Water Density	1025	kg/m^3
Wave Characteristics		
Type	Range of Directions, No Forward Speed	
Wave Range	-180^0 to 180^0 (-PI to PI)	
Interval	45^0	
Number of Intermediate Directions	7	

The FPSO's and ship are analyzed using commercial software which is Rhinoceros for design and ANSYS AQWA Hydrodynamic Diffraction and ANSYS AQWA Hydrodynamic Time Response. Figure.3 shows drawn of FPSO-1, FPSO-2 and ship by Rhinoceros viewed from top, front, and right sides. Table.2 and Table.3 show principal dimensions of FPSO and ship, respectively.

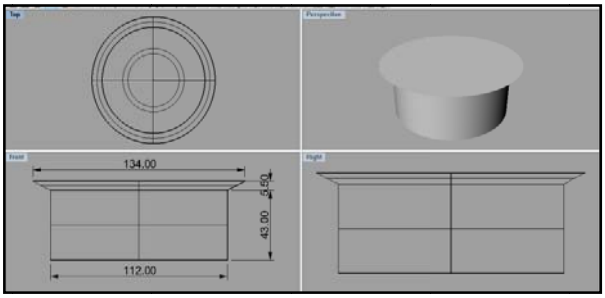

Figure 3.a: View of FPSO-1 from top and front

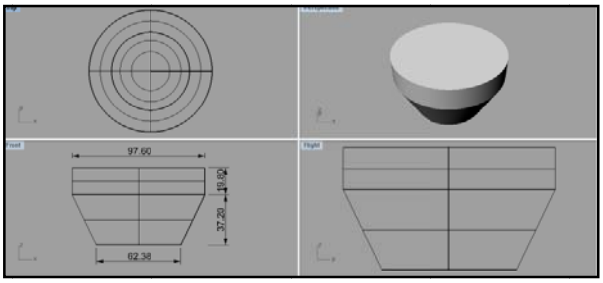

Figure 3.b: View of FPSO-2 from top and front

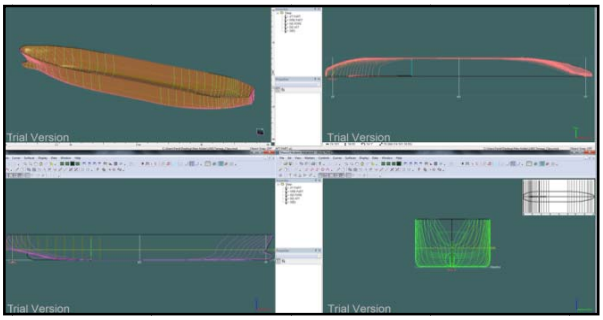

Figure 3.c: View of ship from top, front and side

Table 2: Principal Dimensions of FPSO

Parameter	FPSO-1	FPSO-2
Diameter at Upper Deck (m)	134.00	97.60
Diameter at Base (m)	112.00 m	62.38
Draught (m)	32.00	37.20

Table 3: Principal Dimensions of LNG ship

Parameter	LNG
Length	270.70 m
Breadth	44.30 m
Draught	11.13 m

5.0 RESULTS AND DISCUSSION

The results in relation to the hydrodynamic analysis of single body, two bodies and three bodies of offshore structures for added mass, damping coefficients and RAO are analyzed for every added mass, damping coefficients and RAO for each direction are presented by using graphical method the data that has been extracted from ANSYS AQWA Hydrodynamic Diffraction and ANSYS AQSA Time Response. These results will be discussed on the differences between the motion of single body, two bodies and three bodies of offshore structures due to hydrodynamic interaction.

5.1Added Mass

Figure 4 shows the results of added mass on pitch motion against frequency for FPSO-1 with FPSO-1 with FPSO-2, FPSO1 with LNG and FPSO-1 with FPSO-2 and LNG for two different gap distances which are 25 m and 50 m respectively. The figure show that the added mass has the same trend despite there are small differences in between due to more interaction between numbers of floating structures are involved in smaller gap distance. The trends for the added mass at 25 m gap distance is different with the trend for the added mass at 50 m gap distance where the values of added mass decreases rapidly at the resonant frequency as the gap distance increases. As a result, this shows that gap distance and presence of other structures can give different effects to the values of added mass for the hydrodynamic interaction between two and three floating structures.

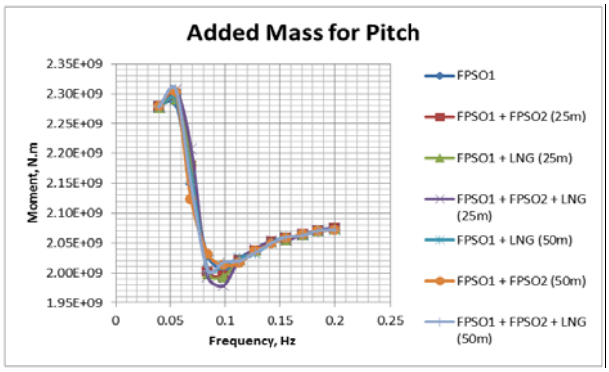

Figure 4: Added mass on pitch motion

5.2 Radiation Damping Coefficient

Figure 5 shows the results of radiation damping on pitch motion against frequency for FPSO-1 with FPSO-1 with FPSO-2, FPSO-1 with LNG and FPSO-1 with FPSO-2 and LNG for two different gap distances which are 25 m and 50 m respectively.

From the figures, all the radiation damping pitch motion have experienced same trend though there are small differences in the values obtained. Apart from that, the radiation damping for three floating structures have the highest values on pitch motion compare to others especially at the gap distance 25 m due to the motion effects of two other structures experienced by one structure. The trends for the radiation damping at 25 m gap distance are slightly different compare to the trend for the radiation damping at 50 m gap distance in which the radiation damping values drop down rapidly at the resonant frequency as the gap distance increases. Therefore, gap distance and presence of other structures plays important roles in affecting the radiation damping values for the hydrodynamic interactions between two and three floating structures.

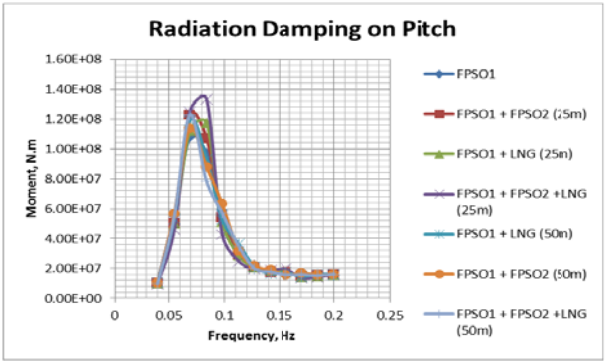

Figure 5: Radiation Damping on Pitch Motion

5.3 Response Amplitude Operators (RAO)

Figure 6 shows the results of RAO on pitch motion against frequency at 0° heading for FPSO-1 related to FPSO-1 and FPSO-2, related to FPSO1 and LNG and related to FPSO-1, FPSO-2 and LNG for two different gap distance which are 25 m and 50 m respectively. The pitch motion, there are slight differences between the motion responses of the structures at 25 m and 50 m in which the motion responses at 50 m are higher than the motion responses at 25 m. Although there are small differences on pitch motion with the presence of neighboring structures, there are slight motion responses between multiple floating structures for the direction of wave at 0° heading and it is proved there are hydrodynamic interactions between multiple floating structures.

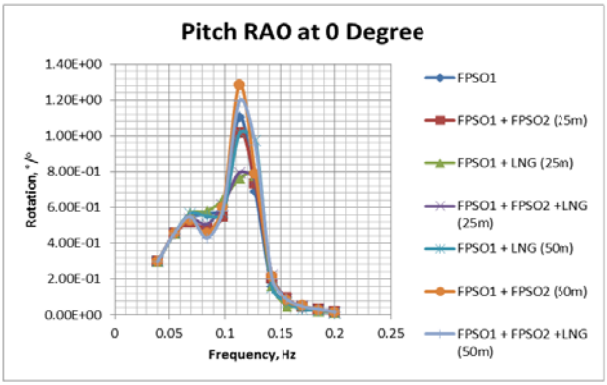

Figure 6: Pitch RAOs at 0 Degree

6.0 CONCLUSION

In this study, the simulation of three floating bodies of offshore structures has been conducted interaction using ANSYS AQWA

software in order to investigate the effect of hydrodynamic interaction for different gap distances, 25 m and 50 m, and wave directions at 0 degree.

For the results of added mass and radiation damping, more reactions have been experienced by the structure at the gap distance of 25 m where the values of added mass and radiation damping are large compare to the results of added mass and radiation damping at the gap distance of 50 m. The wave directions do not affect the added mass and radiation damping since all the results at every direction are the same. RAO at the gap distance of 50 m produced larger responses compare to RAO at the gap distance of 25 m.

REFERENCES

1. Ali, M. T., Rahman, M. M. and Anan, T., 2010. *A Numerical Study on Hydrodynamic Interaction for a Small 3-D Body Floating Freely Close to a Large 3-D Body in Waves*. Proc. of Int'l Conference on Marine Technology, Dhaka, Bangladesh.
2. ANSYS, Inc., 2012. *AQWA User Manual*. ANSYS, Inc. Canonsburg, PA.
3. Azmi, M. F., 2012. *Conceptual Design on Round Shaped FPSO*. Undergraduate Project Thesis. Universiti Teknologi Malaysia, Johor, Malaysia.
4. Brown, P. A., Rooduijn, E. and Lemoël, M, 2008. *Kikeh Development: Design of the World's 1st Gravity Actuated Pipe (GAP) Fluid Transfer System*. Offshore Technology Conference, Houston, Texas, U.S.A.
5. Choi, Y. R. and Hong, S. Y., 2002. *An Analysis of Hydrodynamic Interaction of Floating Multi-Body using Higher-Order Boundary Element Method*. Proc. of 12th Int'l Offshore and Polar Engineering Conference, Kitakyushu, Japan.
6. Clauss, G. F., Schmittner, C. and Stutz, K., June 23-28, 2002. *Time-Domain Investigation of a Semi-Submersible in Rogue Waves*. Proc. of 21st Int'l Conference on Offshore Mechanics and Arctic Engineering, Oslo, Norway.
7. Cueva, M., Faria, F., Voogt, A. and Vandenworm, N., 2010. Model Tests and Simulations on Circular Shaped FPSO with Dry Three Solutions. Proc. of 16th Offshore Symposium, Houston, Texas, USA.
8. Fang, M. C. and Kim, C. H., 1986. *Hydrodynamically Coupled Motions of Two Ships Advancing in Oblique Waves*. Journal of Ship Research.
9. H-R. Zhu, R-C. Zhu and G. P. Miao, 2008. *A Time Domain Investigation on the Hydrodynamic Resonance Phenomena of 3-D Multiple Floating Structures*. Journal of Hydrodynamics, 20(5), 611-616.
10. Jaswar, 2013. *Marine Hydrodynamic Lecture Note*. Universiti Teknologi Malaysia, Johor, Malaysia.
11. Kanbua, W. *Motion in the Sea Waves*. Thai Marine Meteorological Centre, Bangkok, Thailand.
12. Kashiwagi, M. and Shi, Q., 2010. *Pressure Distribution Computed by Wave-Interaction Theory for Adjacent Multiple Bodies*. 9th Int'l Conference on Hydrodynamics, Shanghai, China.
13. Kim, M. S. and Ha, M. K., 2002. *Prediction of Motion Responses between Two Offshore Floating Structures in Waves*. Journal of Ship and Ocean Technology, 6(3), pp. 13-25.
14. Kodan, N., 1984. *The Motions of Adjacent Floating Structures in Oblique Waves*. Proc. of 3rd Offshore Mechanics and Arctic Engineering, OMAE, New Orleans.
15. Loken, A. E., 1981. *Hydrodynamic Interaction between Several Floating Bodies of Arbitrary Form in Waves*. Proc. of Int'l Symposium on Hydrodynamics in Ocean Engineering, NIT, Trondheim.
16. MIT., 2001. *Marine Hydrodynamics Lecture 19*. Department of Ocean Engineering, Massachusetts Institute of Technology, Cambridge, MA
17. Ohkusu, M., 1974. *Ships Motion in Vicinity of a Structure*. Proc. of Int'l Conference on Behavior of Offshore Structure, NIT, Trondheim.
18. Saad, A. C., Vilain, L., Loureiro, R. R., Brandao, R. M., Machado Filho, R. Z., Lopes, C. and Gioppo, H., 4-7 May, 2009. *Motion Behavior of the Mono-Column FPSO Sevan Piranema in Brazilian Waters*. Offshore Technology Conference, Houston, Texas, USA.
19. Shaiful, M., 2013. *Analysis of Motion on FPSO in Shallow Water with a Non Collinear Environment*. Undergraduate Project Thesis. Universiti Teknologi Malaysia, Johor, Malaysia.
20. Siow, C. L., Jaswar, Afrizal, E., Abyn, H., Maimun, A. and Pauzi, M., 2013. *Comparative of Hydrodynamic Effect between Double Bodies to Single Body in Tank*. The 8th Int'l Conference on Numerical Analysis in Engineering: 64 - 73, Pekanbaru, Riau.
21. Siow, C.L., Abby, H. and Jaswar. 2013. *Semi-Submersible's Response Prediction by Diffraction Potential Method*. The International Conference on Marine Safety and Environment: 21 – 28. Johor, Malaysia.
22. Siow, C.L., Jaswar, K, and Abby, H. 2014. *Semi-Submersible Heave Response Study Using Diffraction Potential Theory with Viscous Damping Correction*. Journal of Ocean, Mechanical and Aerospace Science and Engineering 5: 23-29.
23. Siow, C.L., Jaswar, K., Abby, H. & Khairuddin, N.M. 2014. *Linearized Morison Drag for Improvement Semi-Submersible Heave Response Prediction by Diffraction Potential*. Journal of Ocean, Mechanical and Aerospace Science and Engineering 6: 8-16.
24. Tajali, Z. and Shafieefar, M., 2011. *Hydrodynamic Analysis of Multi-Body Floating Piers under Wave Action*. Ocean Engineering, 38(17-18), 1925-1933.
25. Van Oortmerssen, G., 1979. *Hydrodynamic Interaction between Two Structures of Floating in Waves*. Proc. of BOSS '79. 2nd Int'l Conference on Behavior of Offshore Structures, London.
26. Wu, S., Murray, J. J., and Virk, G. S., 1997. *The Motions and Internal Forces of a Moored Semi-Submersible in Regular Waves*. Ocean Engineering, 24(7), 593-603.
27. Xianchu, Z., Dongjiao, W. and Chwang, A. T., 1997. *Hydrodynamic Interaction between Two Vertical Cylinders in Water Waves*. Applied Mathematics and Mechanics, 18(10), 927-940.

Numerical Analysis and Experimental Tests about Water Entry of Trimaran Vessels

M. Nikfarjam,[a,*] O. B. Yaakob,[a] M. S. Seif,[b] J. Koto,[c, d] and A. Aref,[b]

[a)]*Marine technology centre, Universiti Teknologi Malaysia*
[b)]*Centre of excellence in hydrodynamic & dynamic of marine vehicles, Sharif University of Technology, I.R.Iran*
[c)]*Department of Aeronautics, Automotive and Ocean Engineering, Universiti Teknologi Malaysia, Malaysia*
[d)]*Ocean and Aerospace Research Institute, Indonesia*

*Corresponding author: nmooud2@live.utm.my

Paper History

Received: 25-October-2014
Accepted: 13-November-2014

ABSTRACT

Investigation about water entry problem is one of the basic methods for simulation of impacts due to "Slamming" on high-speed crafts. Those impacts can be considered as a main source for structural damages on hull, equipments and on top of that for crew and passengers. This subject has more importance for multi-hull crafts because their intermediate structure, which connects the main hulls, should have enough strength under the slamming loads and waves forces. For optimum design of structure and achieving the minimum weight as an important parameter of performance for high-speed crafts, the pressure distribution around this area and the impact velocity should be determined in various loading conditions. In current paper, numerical analysis of a typical section for Trimaran hull had done by ANSYS-CFX software for determination of peak pressures and followed by experimental tests for validation. The results of current research can be used as a way for determination of loads on structure of these types of vessels particularly in a basic design phase beside the guidelines, which has proposed, by the rules of classification societies.

KEY WORDS: *Pressure, Water entry, Trimaran*

NOMENCLATURE

P	Pressure (Kpa)
V	Velocity (m/sec)
C_p	Pressure coefficient (-)
h_D	Drop height (m)
W_C	Width of channel (m)
h_w	Height of water (m)
t	time (msec)

1.0 INTRODUCTION

The application of high-speed crafts spreads in recent decays for different uses. Research fields, which are related to these vessels, are very complicated because of their performance condition with high speed in rough seas and one of these challenges is determination of loads on structure in various cases for optimum structural design. Extreme conditions for calculation of loads should be considered when the vessel moves in huge waves with large motions, which exert large impact loads that called "Slamming". This phenomenon is a limit state for design of structure and the rules of classification societies offer some formula for calculation of pressure distribution based on accelerations of hull in various sea states.
Trimaran hulls are effective platforms that because of their large deck area can be used for transportation with high speed in long-range routs. For these vessels, structural strength has more importance because of their special configuration of hulls and so, some classification societies try to propose new rules for these types of crafts as a special issue. For example, Lloyd's Register (LR) published a technical paper for introducing the development of Trimaran rules for calculation of global loads such as bending and torsional moments and shear forces. [1] As mentioned, these

researches are generally about the global loads on large-scale vessels and for small-sized high-speed trimarans, the effect of local loads, as an important issue needs more studies by reviewing the published references.
In this paper, the process of construction of a setup for drop test of Trimaran hulls was introduced and the results of experimental measurements were compared with numerical analysis to use as a guideline for future investigations.

1.1 Research background

When a trimaran's hull smashed to the water surface, the impact loads cause a dynamic force which may lead to damage on structure particularly for the connecting structure of them.
For crafts with special hull-form or novel designs such as unconventional Trimarans, classification societies emphasized that performing numerical analysis or experimental tests to determination of slamming loads is necessary. These loads act on structure in short period of time with large domain and so the structure should strength enough to withstand under them.
This field of study, which is known as "water entry problem", was investigated by Von-Karman [2] in 1929 to analyzing the pressure on seaplanes during the landing process. After him, many researchers conducted analytical, numerical and experimental works in this field such as Wagner in 1932 [3], Stravory and Chung in 1976 [4], Faltinsen in 2002 [5], Vorus in 2004 [6] and others. However, a large number of these studies are about the pressure distribution around simple geometries such as wedges, cones and etc. and the effect of dead-rise angle, weight, and impact velocity were determined for them.
In addition, some numerical methods such as CFD had been used for the evaluation of slamming loads. Tahara et al were conducted a research on high-speed multi hull catamaran ship with forward speed using CFD code which employed RANS equation solvers [7]. Besides, simulation of fluid flow characteristic around rounded-shape FPSO was also conducted by A. Efi et.al using RANS Method [8]. Jaswar et al were also developed an integrated CFD simulation software to analyse hull performance of VLCC tanker. The integrated CFD simulation tool was developed based on potential theory and possess the capability to simulate wave profile, wave resistance and pressure distribution around a ship hull [9]. C.L Siow has developed the CFD using multi core engine to increase the speed simulation [10] and has been tested using VLCC ship.
However, about multi-hull vessels there are only few references such as the simulations of slamming for catamaran hulls by Whelan et al. [11] and Davis et al. [12] at the University of Tasmania which experimental tests to measure the pressure during free falling process for catamaran hulls was done by them.
Besides that, some different approaches were used to simulate the water entry of catamaran crafts with boundary element method (BEM). For example, Wu [13] conducted the simulation of twine wedges with constant speed based on potential theory. Mei [14] analyzed the similar problem with a simple analytical method and derived pressure coefficients. Yousefnezhad et al. [15] performed analysis of water entry problem for double wedges at constant vertical speed and the effect of dead-rise is considered in comparison with the distance between the hulls. Recently, some other researchers analyzed a similar problem with conventional finite element method software for determination of pressure distribution around a typical double-wedge hull. [16]
About the numerical and experimental evaluation of pressures on Trimaran hulls, there are few references. Peng et al. [17] did one of studies in this field by experimental tests on a Trimaran hull which followed by numerical analysis for validation of results to determination of relation between pressure and impact velocity.

1.2 Water entry of typical Trimaran hull

The impact process takes very short time and lasting only few milliseconds. Figure-1 shows the quantity and position of peak pressure, the maximum pressure coefficient and other paremeters which affect the hull during water entry process.

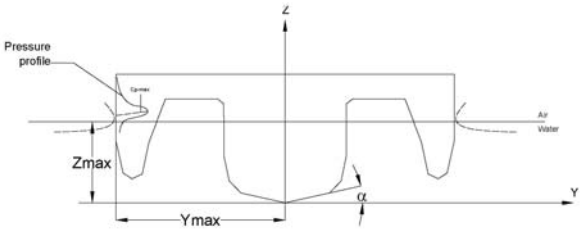

Figure 1: Slamming pressure's parameters during water entry of Trimaran hulls

In this paper for a typical Trimaran section with 12° deadrise and 30 kg weight, the pressure distribution was discussed in a specific drop height. A configuration of experimental test setup which designed for testing of hydrodynamic loads on multi-hull sections during water entry was explained that can be used in future researches of similar problems.

2.0 NUMERICAL ANALYSIS

2.1 Problem definition

After modeling of geometry, numerical analysis was started when the hull were in contact with the water surface. Fine mesh was used near the borders of hull and coarse ones were used for other areas. Figure-2 shows the geometry and meshing of model for analysis.

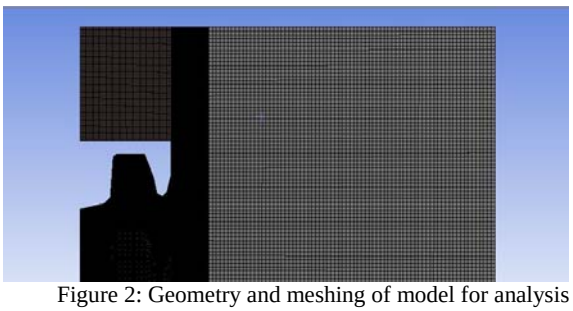

Figure 2: Geometry and meshing of model for analysis

Figure 3 illustrates the modeling of water entry process for the hull in first moments of contact. It can be seen that at first the main hull enter the water and after few time two side hull contact the water. If the height of water is large enough then water touches the cross structure too.

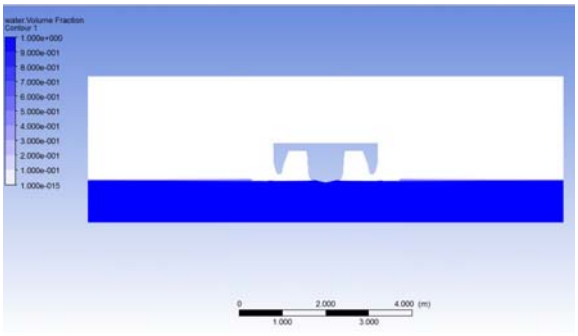

Figure 3: The modeling of water entry process for the selected hull in first moments of contact

3.0 EXPERIMENTAL TESTS

3.1. Geometry of model

The model of midship section for a typical Trimaran hull was constructed with fiber reinforced plastic (FRP) material and wood Figure-4 depicts it.

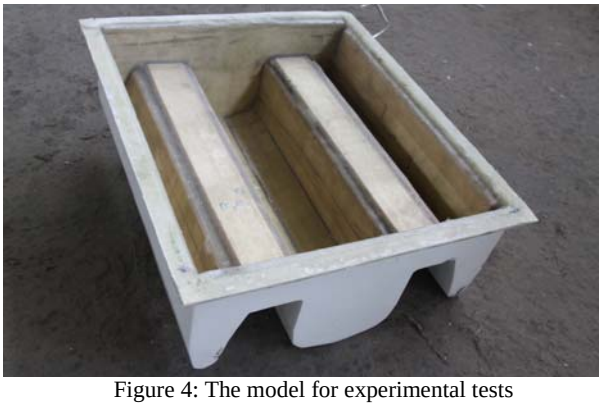

Figure 4: The model for experimental tests

The Geometry of model and position of sensors is shown in Figure-5.

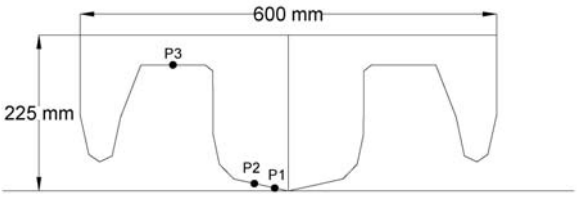

Figure 5: The Geometry of model and position of sensors

3.2 Experimental test setup

For conducting the tests for measurement of pressure on the section of hull during the drop process, a structure according to Figure-6 was installed in the tank of marine laboratory of Sharif University of Technology. The length of basine is 25 m and the width and height of it are 2.5 m and 1.5 m respectively.

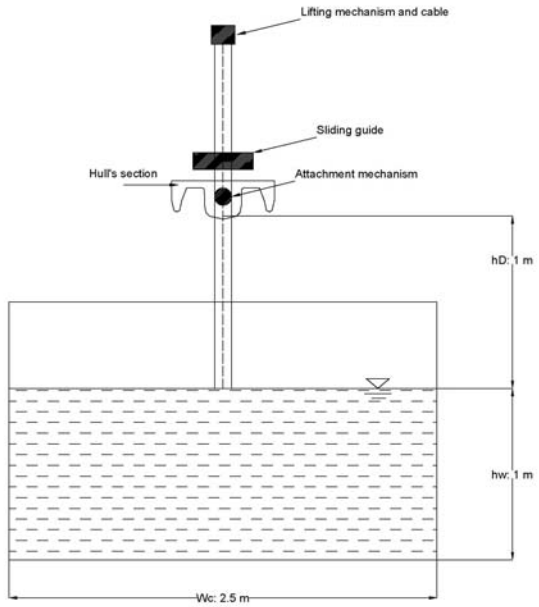

Figure 6: Illustration of test set-up main elements and basic dimensions

The test set-up's configuration is shown in Figure-7. A vertical guide is fixed to the wall of channel for both side of hull section and it can move freely with two sliding guides. The water level was considered at 1 m and maximum height of drop was set to 1-1.3 m.

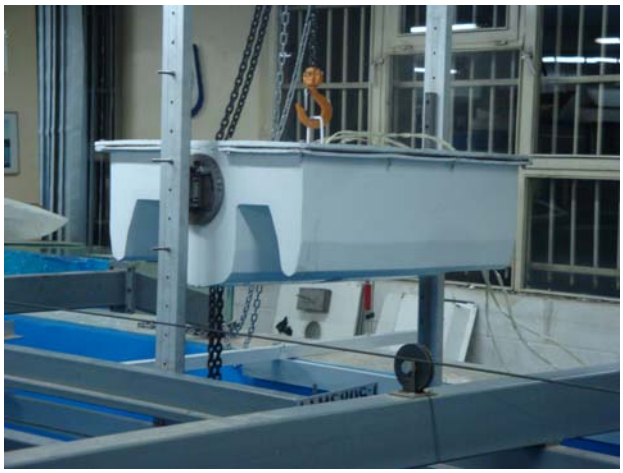

Figure 7: General view of test set-up after installation in channel

Three pressure transducers were installed on bottom and cross structure of hull. These sensors can measure the pressure up to 1000 psi with accuracy range of 0.001 psi. In addition, a suitable data acquisition system with three channels was constructed for receiving of data from sensors and transfer of them to computer. Sensors have the capability of measuring the 25000 data in second. Also an appropriate software for analyzing and filtering of data was developed. Figure-8 shows the collection of above

equipments.

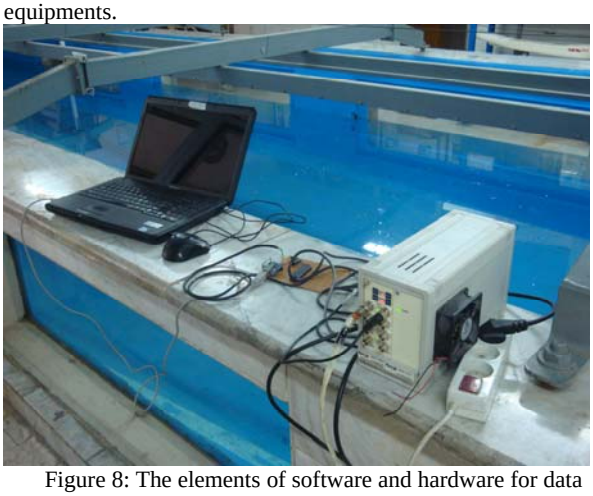

Figure 8: The elements of software and hardware for data collection process

The tests were done for specific drop height. The parameters of test are shown in Table-1.

Table 1: The parameters of tests

Deadrise (Degree)	Weight (Kg)	Drop height (m)
12	30	0.5

The hull was dropped vertically under effect of its weight, each test was repeated five times, and the average of results was used as final data. When the wedge contacts the water surface, sensors can register the pressure changes over time and with having data, the pressure coefficient can be calculated with following equation:

$$C_p = \frac{P}{\frac{1}{2}\rho V^2} \quad (1)$$

4.0 RESULTS AND DISCUSSION

Figure-9 shows the pressure trend at defined points of the hull during water entry according the results of numerical simulation.

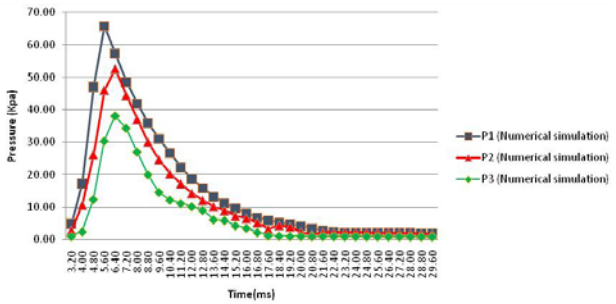

Figure 9: Illustration of pressure trend at defined points of the hull according to numerical simulation

It can be seen that the pressure had an increasing trend with the addition of submergence height and it reached a maximum value of about 65 kpa. Table-2 depicts the range of Cp in this case that can be used as a guide for pressure estimation for real model.

Table 2: The range of Cp according to numerical simulation

Pressure sensor number	Maximum pressure (Kpa)	Quantity of Cp
P1	65.7	0.84
P2	52.5	1.72
P3	38.1	1.24

Regarding to pressures measured during the experimental tests, Figure-6 shows the value in similar points.

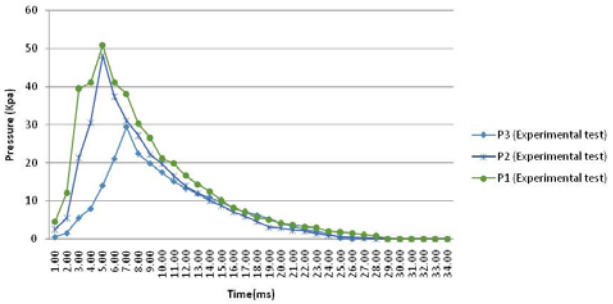

Figure 10: The value for pressures during the experimental tests

It can be seen that the pressures follows a similar trend in comparison with results of numerical simulation but the values are different a bit. For comparison of results the data was compared for each sensor and the results are shown in Figure 7 to 9 for the sensors P1 to P3 respectively.

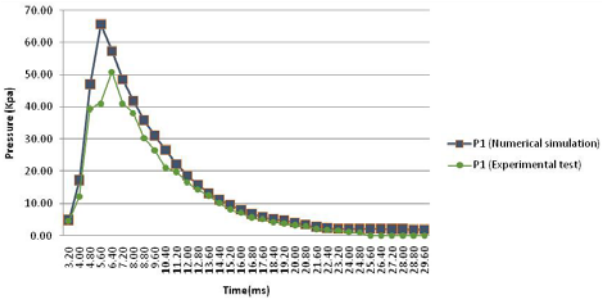

Figure 11: The comparison of results of numerical simulation and experimental data for point P1

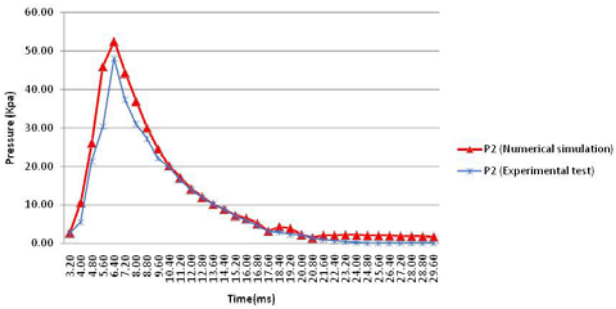

Figure 12: The comparison of results of numerical simulation and experimental data for point P2

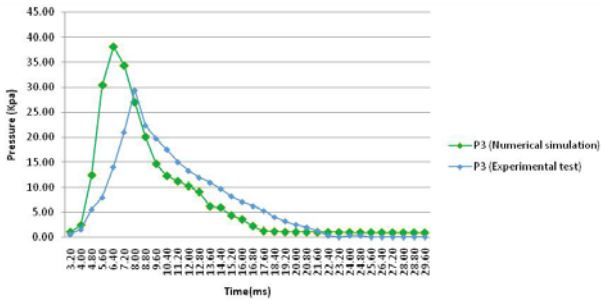

Figure 13: The comparison of results of numerical simulation and experimental data for point P3

Regarding the differences between results of numerical simulation and experimental tests, an error between 10-30 percent can be found which may be occurred because of some reasons such as the differences between models, initial conditions and also for the method of modeling of air entrapped in tunnel in simulation and real condition. It should be mentioned that conventional software uses assumption of ideal gases for analysis. The next item that can be assumed as a source of errors is the effects of non-linearity in the real condition and situation of tests.

5.0 CONCLUSION

In this paper the numerical analyses of water entry for a typical trimaran section was done and the results were compared with data from experimental tests. The results are evident of effect for position of measurement's points on the quantity of pressure, which can affect the peak value of it on hull and should be considered in design phase.

As a conclusion, it can be said that selecting the best configuration and distance of side hulls, which has the minimum effect on main hull's peak pressure can be one of the applications of analyzing the water entry problem for Trimaran hulls.

ACKNOWLEDGEMENTS

The authors would like to convey a great appreciation to Marine Laboratory of Mechanical Faculty of Sharif University of Technology for supporting the experimental test's facilities.

REFERENCE

[1] Cheng, F., Mayoss, C., Blanchard, T., (2006), The development of Trimaran Rules, Lloyd's Register Technical Papers, Lloyd's Register, 71 Fenchurch Street, London EC3M 4BS, England.

[2] Von Karman, T., (1929), The impact on seaplane floats during landing, National Advisory Committee for Aeronautics: NACATN321. p. 2–8.

[3] Wagner, H., (1932), Landing of sea planes, NACA Tech Memo.

[4] Stavovy, A.B, Chuang, S-L(1976). Analytical determination of slamming pressures for high-speed vehicles in waves. Journal of Fluid Mechanics:20(4), 190-198.

[5] Faltinsen, O.M(2002) Water entry of a wedge with finite dead-rise angle. Journal of Ship Research:46(1), 39-51.

[6] Vorus, W.S. (2004). A compliant-hull concept for planing craft wave-impact shock reduction.Journal of Engineering Mathematics 48, pp. 253–277.

[7] Y.Tahara et al., Development and Demonstration of CAD-CFD-Optimizer Integrated Simulation- Based Design Framework by Using High-Fidelity Viscous Free-Surface RaNS Equation Solver, Journal of the Japan Society of Naval Architects and Ocean Engineers, Vol. 7 (2008), pp. 171-184

[8] E.Afrizal, F.M. Mufti, C.L.Siow, Jaswar Study of Fluid Flow Characteristic Around Rounded-Shape FPSO Using RANS Method, The 8th International Conference On NumericalAnalysis In Engineering, Pekanbaru, Indonesia (2013)

[9] Jaswar et al, An integrated CFD simulation tool in naval architecture and offshore (NAO) engineering, The 4th International Meeting of Advances in Thermofluids (IMAT 2011), 3–4 October, Melaka, Malaysia, AIP Conf. Proc. 1440 (2011), pp. 1175-1181.

[10] C.L Siow, Jaswar, Efi Afrizal, Computational Fluid Dynamics (CFD), Parallel Computing, Reynolds Average Navier-Stokes, Round-Shaped FPSO, Advances in Applied Mechanics and Materials,Volume 493, pp.80-85.

[11] Whelan JR (2004) Wetdeck slamming of high speed catamarans with a centrebow. Ph.D. Thesis, University of Tasmania

[12] Davis MR, Whelan JR (2007) Computation of wet deck bow slam loads for catamaran arched cross sections. Ocean Eng 34(17–18):2265–2276

[13] Wu GX (2006) Numerical simulation of water entry of twin wedges. J Fluids Struct 22:99–108

[14] Mei X (1998) On the impact of arbitrary two-dimensional sections. M.Sc. Thesis, Massachusetts Institute of Technology

[15] Yousefnezhad R., Zeraatgar H., (2014) A parametric study on water-entry of a twin wedge by boundary element method. J Mar Sci Technol. DOI 10.1007/s00773-013-0250-1.

[16] Nikfarjam M., Yaakob O. B., Seif M. S., Aref a., Koto J., (2014) Numerical Analysis of Pressure Distribution on Double Wedges During Water Entry, In proceeding of 9TH international on marine technology (MARTEC 2014), Surabaya, Indonesia

[17] Sheng P., Weiguo W., Huangxiang S., Jin P., Ziyu X., (2011) Experimental Study and Numerical Simulation on Slamming of Trimaran, Proceedings of the Twenty-first (2011) International Offshore and Polar Engineering Conference Maui, Hawaii, USA, June 19-24.

Publishing

ISOMAse
Resty Menara Hotel
Jalan Sisingamangaraja No.89
Pekanbaru-Riau, INDONESIA
http://www.isomase.org/

Editing

Building P-23, Room: 314
Department of Aeronautics,
Automotive & Ocean Engineering,
Faculty of Mechanical, Universiti
Teknologi Malaysia, MALAYSIA
http://web1.fkm.utm.my/

ISSN: 2443-1710

Publication

Teknik Mesin
Fakultas Teknik,
Universitas Riau, INDONESIA
http://www.unri.ac.id/en

Organizing

Ocean & Aerospace Research
Institute, Indonesia
Pekanbaru-Riau, INDONESIA
http://isomase.org/OCARI.php/

Supporting

Mechanical Chapter of the
Institution of Engineers,
INDONESIA

Malaysian Joint Branch Royal
Institution of Naval Architects &
Institute of Marine Engineering,
Science and Technology
-Southern Chapter (MJB RINA
&IMarEST – SC)-